UNIVERSITY OF SOUTHAMPTON

THE ACTIVE CONTROL OF RANDOM NOISE IN AUTOMOTIVE INTERIORS

by
Trevor John Sutton

A thesis submitted for the degree of Doctor of Philosophy

Institute of Sound and Vibration Research

April 1992

UNIVERSITY OF SOUTHAMPTON

ABSTRACT

FACULTY OF ENGINEERING AND APPLIED SCIENCE

INSTITUTE OF SOUND AND VIBRATION RESEARCH

Doctor of Philosophy

THE ACTIVE CONTROL OF RANDOM NOISE IN AUTOMOTIVE INTERIORS

by Trevor John Sutton

The problem of actively attenuating random sound inside cars using loudspeakers is considered. A feedforward control approach is adopted, the FIR control filters being adapted to minimise the sum of squared pressures at a number of microphone locations in the enclosure. An expression is developed which defines the optimum coefficients of finite-length, causal filters for the case with multiple reference signals, multiple secondary sources and multiple microphones. In addition it is shown that the maximum possible sound reduction using causally unconstrained filters can be expressed simply in terms of the multiple coherence function.

The active control of random sound in the idealised case of a rectangular enclosure bounded by a vibrating plate is examined and it is seen that the degree of attenuation is highly sensitive to delays of a few milliseconds in the control signals. However, lightly-damped low-frequency modes of the plate introduce almost-periodic components into the sound which are more predictable and make the system less susceptible to time-delays.

A central part of the work is a prediction of the sound reductions which could be obtained in two widely-used family cars based on measurements of vehicle vibration and noise. It is shown that sound reductions of the order of 5 dB can be expected at a point inside the car (*eg* at the driver's head) at frequencies in the range 90-140 Hz using six accelerometers attached to the vehicle structure as reference signals. It is found that accelerometers attached to the vehicle suspension give adequate time-advance for a practical system but many accelerometers are needed to detect all the contributions to interior noise. On the other hand, accelerometers attached to the vehicle floor are more coherent with interior noise (so less are needed) but they give less time-advance and hence poorer sound reduction.

A preliminary study was carried out of the possibility of using a neural network to model the nonlinear elements in the transmission path from the suspension to the vehicle interior. Tests with simple idealised dynamic nonlinear elements showed some success, but it appeared that the backpropagation algorithm had the effect of excluding some hidden-layer neurons from the model.

CONTENTS

3 STRUCTURAL-ACOUSTIC SIMULATIONS

4 VEHICLE TESTS

Acknowledgements

The work presented here has been entirely funded by Lotus Engineering and forms part of a collaboration with the University of Southampton on active sound control. Their generous support is warmly appreciated. Specific thanks are due to Malcolm McDonald and to the NVH team at Lotus Engineering for providing equipment and technician support for the vehicle measurements.

Dr Steve Elliott has supervised the project and it is a pleasure to acknowledge his valuable advice, encouragement and support at all stages of the work. I have also benefited from many useful discussions with Dr Phil Nelson, who has maintained a close interest in the project.

1 INTRODUCTION

1.1 Introduction

Consumer choice in the domestic car market has produced a demand for vehicles which are responsive, fuel-efficient, and low in cost. These pressures have resulted in a trend towards lighter vehicles, with increased power/weight ratios and lower drag. The use of light structures has however created another problem for the designer: increased structural vibration and consequent interior noise. It is necessary for the designer to find ways of maintaining a quiet environment inside the car without adding substantially to its mass. Active noise control offers the possibility of achieving this objective. In active noise control, secondary loudspeakers inside the car introduce an additional sound which is similar to the vehicle noise but is maintained to be out of phase with it, creating zones of quiet inside the car. The subject of this Thesis is the active control of noise inside cars, and in particular the control of random noise such as the broadband rumble which is created as the tyres meet irregularities in the road surface.

Three features of active noise control make it attractive for use inside vehicles:

(1) Active sound cancellation is most effective at low frequencies (*eg* up to a few hundred Hertz) where conventional passive methods of noise control are least effective. This is because at low frequencies (long wavelengths) the spatial distribution of the sound in the enclosure can be described in terms of a few modes only and it is possible to generate a matching sound-field for cancellation using a small number of loudspeakers.

(2) Vehicles constructed by the same production line often show large variations in noise characteristics. Noise levels inside nominally identical cars driven at the same speed may vary by 10-15 dB [Wood,1984]. An adaptive electronic system can in principle adjust itself to cater for vehicle-to-vehicle variations.

(3) Two or possibly four loudspeakers and associated amplifiers are normally fitted as standard as part of the in-car entertainment system. The inclusion of a (mass-produced) active noise cancellation system need not involve great additional expense.

The aim of the project has been to examine the use of active noise control techniques to reduce random noise inside vehicles. Specific objectives were:

(1) to identify the basic sources of noise and examine the mechanisms of transmission and radiation of random sound into the passenger cabin;
(2) to establish the performance limits which would constrain an active noise control system;
(3) to assess the possible control schemes by computer simulation;
(4) to design, implement and test an appropriate control strategy.

Early in the project it was decided that the design and implementation of a working controller should go ahead as soon as possible, alongside the other work rather than being left to the end. This design and development was handled at Lotus Engineering by Mr IM Stothers. The resulting broadband active noise controller has yielded promising results, which are discussed in Chapter 4.

The remainder of this Introductory chapter is divided into four sections. Section 1.2 introduces the subject of active sound control and reviews its application to one-dimensional problems, specifically noise control in ducts. Section 1.3 discusses the control of harmonic sound inside three-dimensional enclosures. This has previously been applied to the control of harmonic engine noise in cars. Section 1.4 briefly reviews some of the literature on random noise inside cars, with particular emphasis on low-frequency sources and the mechanisms of transmission to the vehicle interior. Finally Section 1.5 summarises the rest of the Thesis chapter by chapter.

1.2 Feedforward active sound control

1.2.1 Control strategy

The idea of a device to control unwanted sound by introducing an additional, interfering sound field was patented by Paul Lueg as long ago as 1936 [Lueg,1936]. The patent described the control of sound in a duct using a microphone to detect the unwanted sound and a loudspeaker as the interfering sound source. However the idea had to wait for the development of fast digital signal processors before reliable, practical active sound control devices could be realised.

There are two basic strategies for the active control of sound: feedback and feedforward. They are illustrated in Figure 1.1. In the feedback approach, introduced by Olsen and May [1953], the signal received at the microphone is taken directly to a nearby loudspeaker via a high-gain inverting amplifier. The microphone detects the superposition of the primary (unwanted) sound and the secondary sound from the loudspeaker. The action of the feedback loop is to drive this combined sound signal to zero, creating a zone of quiet. This can be seen by considering the complex amplitude of the sound pressures. The total acoustic pressure at the microphone $p_t(\omega)$ consists of the sum of the pressure due to the primary source $p_p(\omega)$ and the pressure due to the secondary speaker $p_s(\omega)$:

$$p_t(\omega) = p_p(\omega) + p_s(\omega)$$

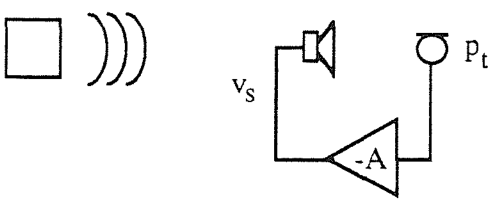

(a) feedback system

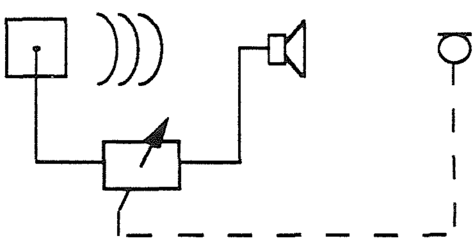

(b) feedforward system

Figure 1.1: Two control strategies for active sound control

If the frequency response between loudspeaker voltage $v_s(\omega)$ and resulting microphone pressure $p_s(\omega)$ is taken to be $B(\omega)$, we have:

$$p_s(\omega) = B(\omega)\, v_s(\omega)$$

Also:

$$v_s(\omega) = -Ap_t(\omega)$$

so that

$$p_t(\omega) = p_p(\omega) - AB(\omega)p_t(\omega)$$

$$p_t(\omega) = \frac{p_p(\omega)}{1 + AB(\omega)}$$

Thus if A is large the sound level at the microphone due to the primary source is much reduced. The system is effective for broadband sound up to a frequency which is limited to maintain loop stability. The frequency response $B(\omega)$ between the loudspeaker and microphone depends on the acoustic delay between them and (in an enclosed space) on their surroundings [Wheeler,1986; Carme,1987]. This response introduces a phase lag which increases with frequency. For loop stability the amplifier A needs to be bandlimited so that the loop gain is less than unity at higher frequencies where the phase lags in the loop approach 180°.

This idea was originally put forward by Olsen and May as a way of reducing noise at the seat positions in aircraft and cars. Its use in vehicle cabs has been investigated by Berge [1983]. Two drawbacks of this approach in a vehicle application are:

(1) for closed-loop stability it is essential to have the loudspeaker close to the microphone (and therefore to the listener). If they are separated, the acoustic delay results in a large phase lag in $B(\omega)$ rendering the system unstable. In a vehicle this would appear to rule out using the existing in-car entertainment speakers unless these were moved to the headrests.

(2) In principle the controller would attenuate all incoming sound unless it were deliberately introduced electronically into the circuit. This would include speech from other passengers and warning sounds from outside the car.

Active systems using this strategy have however been successfully applied to reduce intruding ambient noise in the headsets of aircraft pilots [Wheeler,1987]. The earpiece itself is used as a secondary source, generating a small zone of quiet at the ear. In this application the microphone is placed only a centimetre or so away from the earpiece.

The other approach to active control shown in Figure 1.1 is feedforward control, proposed by Conover [1956] as a means of reducing transformer noise. A feedforward control system requires a reference signal which is closely related to the primary sound. This reference signal may be taken from the source itself or by measurement of the primary sound field. The signal is passed through a suitable filter and on to the secondary loudspeaker. A monitor (error) microphone measures the resulting sound field due to the primary and secondary sources combined. The filter is adjusted (manually or automatically) to obtain the best sound reduction at the microphone.

The advantage of this approach is that the loudspeaker does not need to be placed next to the error microphone. Any adjustment of the filter coefficients can happen slowly and so the stability problem with feedback systems is avoided. The drawback with a feedforward approach is the need to obtain a reference signal which is well correlated with the primary sound field. This turns out to be an important problem in the control of road noise in cars and is discussed in Chapter 4.

Feedforward control has been applied to the reduction of periodic noise at a diesel exhaust by Chaplin [1983] and has been developed commercially for the reduction of broadband noise in ducts [Goodman *et al*,1990]. The feedforward approach to active control has been adopted throughout this Thesis in considering the attenuation of road noise in vehicles; feedback methods are not considered further.

1.2.2 Active sound control in ducts

Active control of random sound has been demonstrated in one-dimensional applications, particularly in ducts. At frequencies up to the cut-on frequency of a duct, only plane waves will propagate. Therefore in practical systems only a single secondary speaker is needed to cancel the sound, and a single-channel system can be used for control.

The theoretical basis for the active control of sound propagation in ducts was set out by Swinbanks [1973]. He showed that two ring sources were required to generate a unidirectional plane wave for control of broadband sound over a limited frequency range. He went on to propose a feedforward active control scheme.

Ross [1982a] reported the successful attenuation of noise inside a wind tunnel. The source of noise was the fan generating the air flow. The flow was piped over some distance and then passed through a passive silencer followed by a diffuser, opening out to the wind-tunnel. A single secondary loudspeaker was used, mounted on the diffuser section (Figure 1.2). A feedforward strategy was used for control. The primary noise was detected by a microphone in the flow path upstream of the silencer. It was necessary to build a nose-cone for the microphone to avoid additional pressure disturbances due to the turbulent flow around the microphone. The microphone signal was passed through a digital filter and then on to the secondary speaker.

An attenuation of 11.2 dB was achieved in the range from 40 to 160 Hz as shown in Figure 1.3. The maximum possible reduction (also shown in the Figure) was 12.9 dB, limited by coherence. Section 2.2 below discusses in detail the coherence of reference signals and their effect on performance.

Roure [1985] achieved attenuations of around 20 dB in a commercial air-conditioning

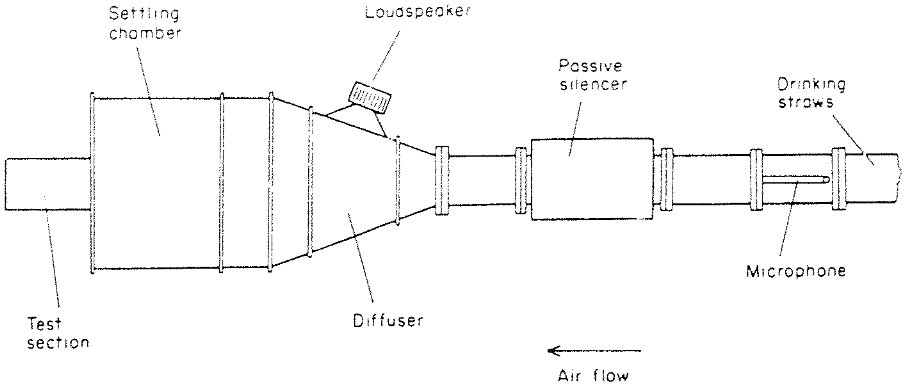

Figure 1.2: Layout of the wind tunnel (from [Ross,1982a])

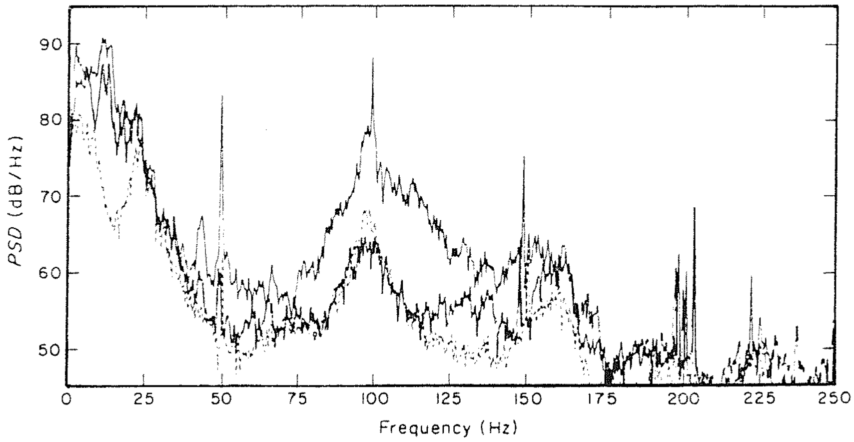

Figure 1.3: PSD of sound in the settling chamber of the wind tunnel (from [Ross,1982a]) Top trace: no active control; centre trace: measured sound level with active control; dotted trace: minimum possible sound level, calculated from coherence

duct for the frequency range 200-600 Hz. The primary sound was detected by a unidirectional microphone to minimise unwanted feedback from the secondary source. In this application the filter calculations were carried out using a microprocessor while the filter coefficients themselves were adapted at intervals by a host computer.

An important requirement for feedforward control of random sound (compared with periodic sound) is that because the primary sound is unpredictable, the reference signal must be received early enough for the digital processing to be carried out, along with any analogue filtering, so that the secondary sound can be generated simultaneously with the primary noise it is to cancel. In Roure's application the microphone detecting the primary source was located 1.5 m upstream of the secondary speaker, giving 4.4ms time advance as the sound travelled down the duct. This consideration does not apply when the primary sound consists of periodic, repetitive waveforms.

Active sound control in ducts has been developed to the point where equipment is now commercially available [Goodman *et al*,1990]. However, the control of distributed sources of broadband sound in three-dimensional enclosures is less straightforward. In particular, it is necessary to find reference signals which detect all the significant contributions to the noise. The simpler problem of controlling *harmonic* sound in enclosures such as aircraft and car interiors has already been examined and demonstrated in practice, as discussed in the next Section. In this case there is only the need for one reference signal, representing the frequency of the periodic sound.

1.3 Active control of harmonic sound in enclosures

1.3.1 Rectangular enclosure, low modal density

Bullmore *et al* [1987] have reported a computer simulation of active sound control in a rectangular enclosure. The primary source was a single piston generating harmonic sound. Up to four secondary piston sources were located at various positions on the walls in order to compare the available reductions in acoustic potential energy. The secondary source strengths were found by minimising the acoustic potential energy inside the enclosure.

The acoustic potential energy E_p at frequency ω in an enclosure of volume V is given by:

$$E_p(\omega) = \frac{1}{4\rho_0 c_0^2} \int_V |p(\mathbf{x},\omega)|^2 \, dV \qquad (1.3.1)$$

where

$p(\mathbf{x},\omega)$ is the complex amplitude of acoustic pressure at each point $\mathbf{x}$ inside the enclosure

ρ_0, c_0 are the density of air and the speed of sound in air respectively

If it is assumed that the enclosure is hard-walled, then the pressure can be expressed at low frequencies as the finite sum of N orthogonal modeshapes $\psi_n(\mathbf{x})$:

$$p(\mathbf{x},\omega) = \sum_{n=0}^{N-1} \psi_n(\mathbf{x})\, a_n(\omega) \qquad (1.3.2)$$

where $a_n(\omega)$ is the complex amplitude of the nth mode. Expressing $\psi_n(\mathbf{x})$ and $a_n(\omega)$ as Nth order vectors $\underline{\psi}$ and $\mathbf{a}$:

$$p(\mathbf{x},\omega) = \underline{\psi}^T \mathbf{a}$$

Using the orthogonality property of the modeshapes the potential energy then becomes:

$$E_p = \frac{1}{4\rho_0 c_0^2} \mathbf{a}^H \mathbf{a} \qquad (1.3.3)$$

(Superscript H denotes the Hermitian transpose of the vector, *ie* the complex conjugate of the transpose) In general the amplitude of each mode is affected by all the secondary sources. If the modal amplitudes due to the primary source are defined to be $\mathbf{a}_p$, then the total modal amplitude vector is

$$\mathbf{a} = \mathbf{a}_p + \mathbf{B}\mathbf{q}_s \qquad (1.3.4)$$

where $\mathbf{q}_s$ is an Mth order vector of secondary source strengths (*ie* assuming M secondary sources). $\mathbf{B}$ is an NxM matrix of modal excitation coefficients, giving the excitation of the nth mode due to the mth secondary source. It can be seen from eqn. (1.3.3) and (1.3.4) that the potential energy is a quadratic function of the secondary source strengths. It is shown in [Nelson *et al*,1987a] that this function has a unique minimum value corresponding to a single set of secondary source strengths. The minimum potential energy is given by:

$$E_{p0} = E_{pp} - \frac{1}{4\rho_0 c_0^2} \mathbf{a}_p^H \mathbf{B}[\mathbf{B}^H\mathbf{B}]^{-1}\mathbf{B}^H \mathbf{a}_p \qquad (1.3.5)$$

where E_{pp} is the value of E_p without active control. E_{p0} thus depends on matrix $\mathbf{B}$, the matrix of modal excitation coefficients. The individual elements B_{nm} of $\mathbf{B}$ give the degree of coupling of the mth secondary source into the nth mode and depend strongly on where the secondary source is located. The minimum potential energy is therefore heavily dependent on the location of the secondary sources in the enclosure.

Bullmore presents the reduction in potential energy for various arrangements of secondary sources in a flat rectangular enclosure. Figure 1.4 shows the reduction when there is one secondary source

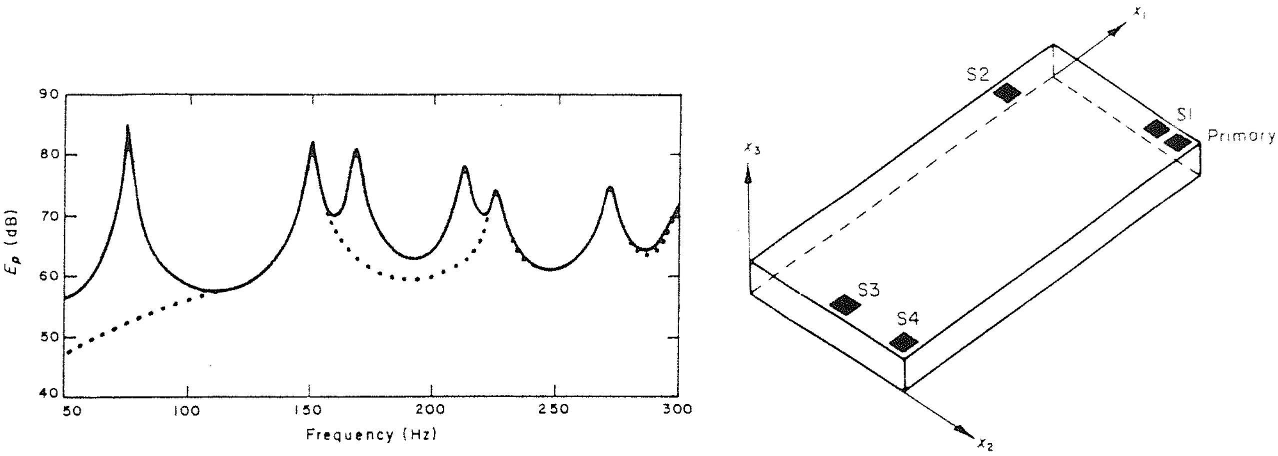

Figure 1.4: Acoustic potential energy E_p when minimised using secondary source S2 alone (from [Bullmore *et al*,1987])
——— no control; ······· with active control

(designated S2), located as shown, on the opposite side of the enclosure from the primary source. The primary source is driven at each frequency in Figure 1.4 separately and the amplitude and phase of the secondary source adjusted at that frequency to minimise E_p. It is apparent that only three of the six resonant peaks are attenuated. The reason for this is clear from Figure 1.5, which shows the nodal planes for the first six modes of the enclosure. Source S2 is located near the nodal plane of one of the two resonances at 150.6Hz, also on nodal planes for the resonances at 225.9Hz and 271.5Hz. Because of its location the secondary source does not couple into these modes and so fails to attenuate the sound field at these frequencies. When one secondary source is placed in a corner of the enclosure it couples into all the modes and attenuates all the resonances (Figure 1.6).

These results contrast with those for active control of harmonic sound in the free field [Nelson *et al*,1987a]. Nelson examined the sound power due to point sources in a free field and showed that no significant reduction in acoustic power output could be achieved if the secondary sources were located more than half a wavelength from the primary source. In the second case considered above, the secondary source was more than half a wavelength from the primary for all frequencies above 75Hz. Thus the internal reflections inside a hard-walled enclosure make it possible to achieve global reductions in acoustic potential energy even when the secondary sources are not located close to the primary sources.

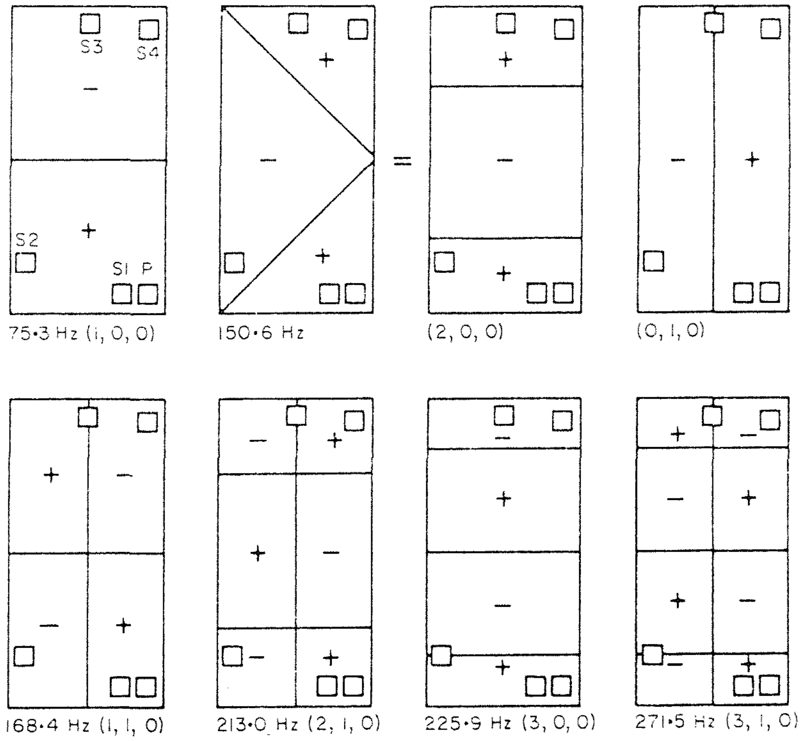

Figure 1.5: Distribution of nodal planes for the first six resonances of enclosure of Fig. 1.4 (from [Bullmore *et al*,1987])

Bullmore's paper [1987] shows that the main effect of the secondary sources is to alter the impedance conditions seen by the primary source. The primary source is made to drive into a reduced and more reactive impedance and so the power it imparts is sharply reduced. The secondary sources may either introduce or absorb small amounts of power but their direct contribution is small even when compared with the reduced primary

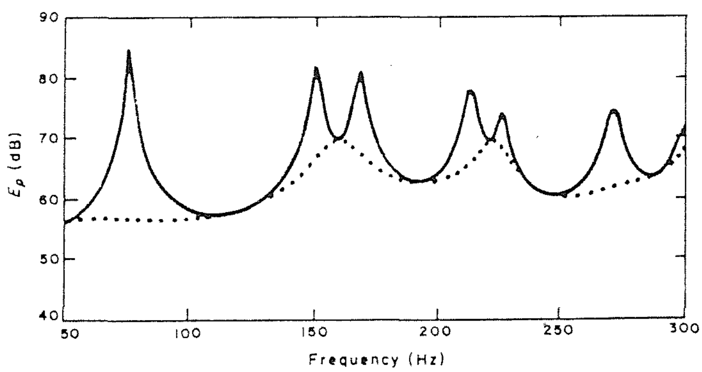

Figure 1.6: Acoustic potential energy E_p when minimised using secondary source S4 alone (from [Bullmore *et al*,1987])

source output. The paper goes on to consider minimising the sum of squared pressure measurements at discrete locations (*ie* microphone signals) rather than the total acoustic potential energy. It shows that the resulting acoustic potential energy reductions are virtually unchanged provided the microphones are located in the corners of the enclosure, at the peaks of the modeshapes.

1.3.2 Rectangular enclosure, high modal density

The number of acoustic modes with natural frequencies within the bandwidth of any one mode in an enclosure increases roughly as the square of the frequency. When the resonant peaks of the spectrum become much closer together than the bandwidth of any one peak, the sound field is said to be diffuse. In a diffuse field it is no longer possible to contemplate global control by coupling secondary sources into all the modes. The transition to a diffuse field is generally considered to take place when the separation between modes is 1/3 of the 3 dB modal bandwidth. This transition is quantified by the Schroeder frequency [Pierce,1981], which in SI units is given approximately by the expression:

$$f_{sch} = 2000 \left(\frac{T_{60}}{V}\right)^{0.5}$$

where T_{60} is the reverberation time of the enclosure and V is its volume. For a small family hatchback car with $V = 4.9\ m^3$ and $T_{60} = 90$ ms, the Schroeder frequency is about 270 Hz. (The transition is actually less clear-cut than this figure implies. As the width and height of a car have similar dimensions there is 'bunching' of the modes giving diffuse field conditions at some frequencies but not at other higher frequencies.)

At high modal densities, well above the Schroeder cut-off frequency, the modes are closely spaced and when calculating acoustic potential energy it is possible to replace the modal summations by integrations [Nelson *et al*,1987b]. In particular, the quantities $\mathbf{B}^H\mathbf{B}$ and $\mathbf{B}^H\mathbf{a}_p$ in eqn (1.3.5) take the form of arrays whose elements are functions of the form $\frac{\sin kr}{kr}$, where k is wavenumber and r is distance between the primary and secondary sources, or from one secondary source to another. The result is that the optimal secondary source strengths (for minimum acoustic potential energy) are exactly the same as those required to minimise radiated power in the free field. As in the free field case it is found that no significant reductions are available unless the secondary source (or sources) are less than half a wavelength from the primary source. For 10 dB reductions the separation needs to be less than 1/10 wavelength. This would be impractical in a car at frequencies above 270 Hz because the primary source is not compact. The 1/10 wavelength criterion would require the secondary sources to be placed within 13 cm of all possible primary sources.

Where the secondary source is remote from the primary, Joseph [1990] has shown that above the Schroeder frequency it is only possible to create small zones of quiet close to the error microphones, of the order of 1/10 wavelength in diameter. These must be created close to the secondary sources to avoid increasing the sound field elsewhere in the enclosure. Thus it is clear from this work that global control of the sound field in the car is limited to low frequencies below about 270 Hz, and that active sound control above this frequency is limited to small zones close to the secondary sources.

1.3.3 Active control of engine noise in cars

The work on control of harmonic sound in enclosures showed that substantial global reductions in sound levels could be achieved at low frequencies in idealised situations. It was expected that a number of secondary sources would be required, and so equipment was developed for the feedforward multi-channel control of harmonic sound for investigation of such control in practice. Firstly a system was built to control periodic interior noise in aircraft caused by propellor rotation [Elliott *et al*,1990a]. Later a smaller device was developed for reduction of engine noise in cars [Elliott *et al*,1988]. Rapid filter adaptation was required to enable the system to track changes in vehicle speed. In each case the equipment implemented a set of adaptive filters relating a single reference signal (*eg* derived from the engine ignition circuit) to an array of secondary loudspeakers. The systems were fully adaptive, using a multi-channel extension of the Widrow-Hoff stochastic gradient algorithm to update the control filter coefficients. This extension was published by Elliott *et al* [1987] and is described in Sect. 2.4 below.

A demonstration of active control of engine noise in cars first was reported in 1986 [Elliott *et al*,1986]. Development work has continued since then in association with Lotus Engineering and Figure 1.7 shows a typical result: the reductions obtained in a small family hatchback car for a range of engine speeds up to 6000 rpm (200 Hz engine firing frequency) [Elliott *et al*,1990b]. The Figure shows reductions of 10-15 dB or more at engine firing frequency. The first longitudinal mode (~80Hz, 2400 rpm) is not seen in the front of the car because the driver's head is roughly in the nodal plane of this mode; however it is apparent at the rear of the car. The multichannel control system used eight

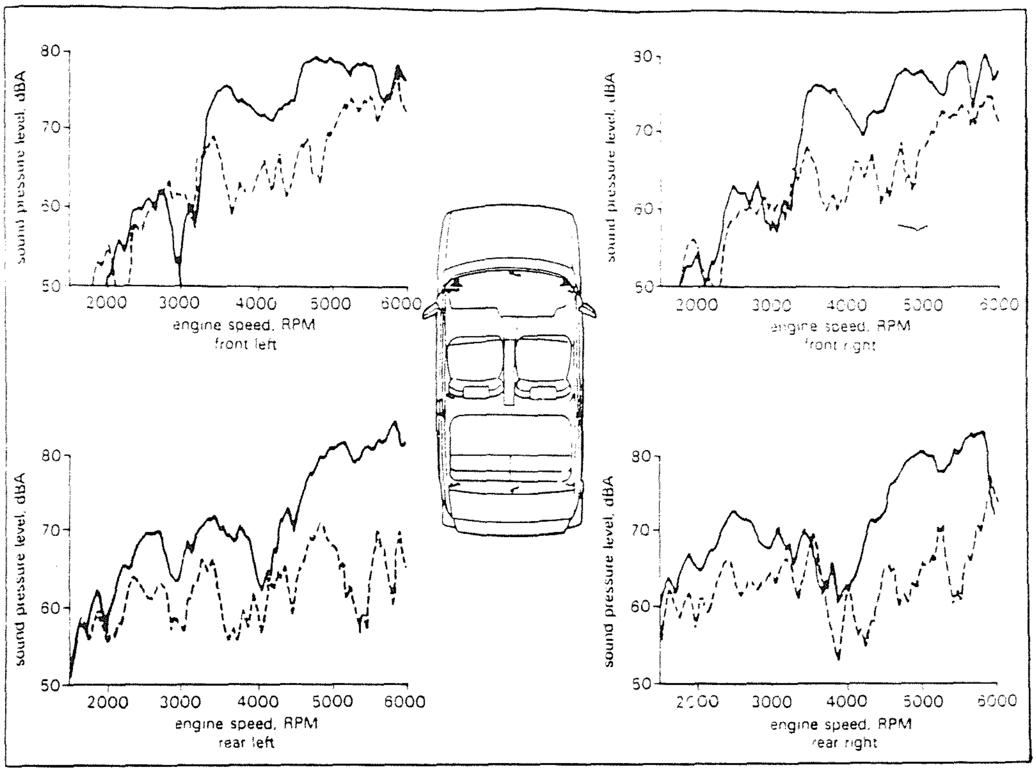

Figure 1.7: A-weighted SPL due to engine firing frequency at head height in a small hatchback car (from [Elliott *et al*, 1990b])

microphones in the roof lining to detect the sound field and four secondary loudspeakers, two at the front and two at the rear of the car.

1.4 Random noise in cars

1.4.1 Sources of road noise

In order to attempt feedforward control of random noise in a car, it will be necessary to provide reference signals which detect all the significant sources of noise. These might be direct measurements of, for example, road roughness; or indirect, perhaps from accelerometers attached to the vehicle structure. The following Sections summarise the main sources of random noise in cars and the means by which this noise is transmitted to the vehicle interior.

There are three principal sources of the noise heard inside a car:

(1) periodic noise due to the engine, drive train, air intake and exhaust;

(2) road noise;

(3) wind noise.

The first of these sources is periodic rather than random, repeated at mainly the engine firing frequency and other related frequencies. As mentioned above, active control techniques have already been applied successfully to the reduction of periodic sound in enclosures, including engine noise in cars.

Road noise arises as the tyre treads meet random irregularities in the road surface. The resultant vibration and noise depends on both the tread structure of the tyres and on the road surface itself. Measurements of the road surface roughness have been reported by Dodds and Robson [1973] and others [*eg* Captain *et al*,1979]. The road-surface wavelengths of interest for active control are in a range from about 74 mm (corresponding to 300 Hz at 50 mph) up to 630 mm (50 Hz at 70 mph). This is at the short-wavelength extreme of the published data. Using data published by the Motor Industries Research Association, Dodds and Robson found that measured road surface

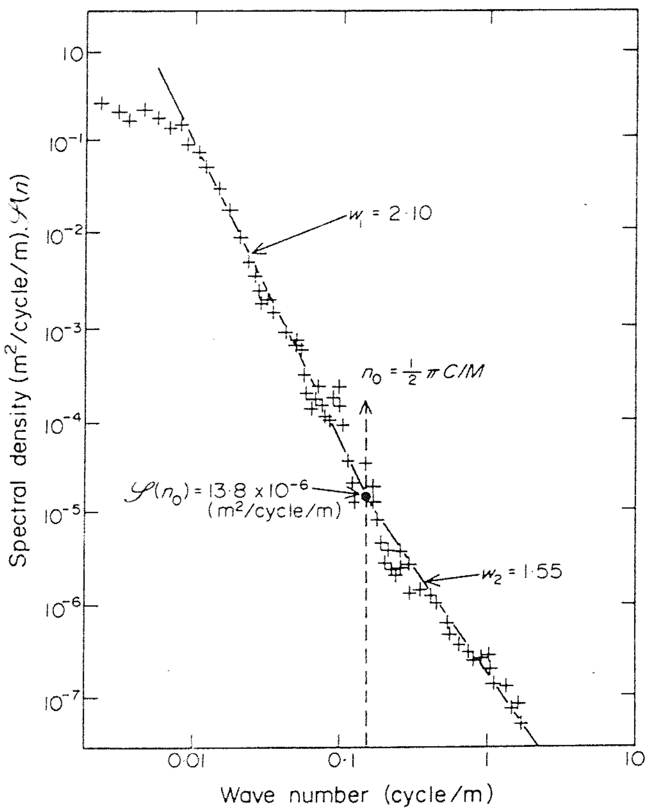

Figure 1.8: Road roughness spectrum of a typical principal road (from [Dodds *et al*,1973])

spectra can be fitted to a reasonable approximation by:

$$S(n) = S(n_0)\left(\frac{n}{n_0}\right)^{w2} \qquad n \geq n_0$$

where:

- n is wavenumber (cycles/m)
- n_0 1/6.3 cycle/m (ie 6.3 m wavelength)
- w_2 ~ 1.4 (calculated separately for each principal road; standard deviation 0.3)
- $S(n_0)$ spectrum of the particular road surface at $n=n_0$ (m^3/cycle)

The spectrum of surface displacement against wavenumber is thus a straight line of gradient $-w_2$ on a log-log scale. For long-wavelength disturbances (λ>6.3 m) a different straight line approximation is used. Figure 1.8 shows the road roughness spectrum for a typical principal road [Dodds *et al*,1973]. It should be noted that only at the highest frequency of interest and at low vehicle speeds are appropriate road-surface wavelengths comparable with the patch of tyre in contact with the road.

On a smooth road the tyre motion is periodic rather than random, the wheel rotation rate at 70 mph being typically 18 Hz. In order to avoid generating tones, the tyre treads are not evenly spaced around the tyre: instead the spacing is varied by at least +/-20% around a mean value [Heckl,1986].

Walker and Evans [1988] showed that for heavy goods vehicles it is possible to separate out the noise which is excited by the road surface from that due to the tyre tread pattern. The truck was driven over a rolling road with various replica road surfaces. To measure the tyre contribution, a time history of exterior noise was recorded once per revolution of the wheel. Successive time histories were added together. The road-excited noise averaged out while the tyre-excited noise accumulated. Similarly the average was taken once per revolution of the rolling road to give the road surface excited noise. Applied to the exterior noise of trucks the method showed that on an asphalt motorway surface the road-excited noise substantially exceeded the tread pattern excited noise for most types of tyre.

1.4.2 Tyre characteristics

There are two routes by which road/tyre interactions create sound inside the car: (1) tyre vibration creates sound outside the car which is transmitted to the interior through the panels making up the car body; (2) the tyres transmit vibration to the suspension system and so to the car body and interior.

Heckl [1986] reviews the dynamics of tyres and the mechanisms by which tyres generate sound. He reports that the main contributors are the outer circular ring and the individual tread blocks. The tyre side-walls are not considered to be important radiators of sound. At lower frequencies (up to about 800 Hz) the tyre can be modelled as a circular ring using two coupled linear differential equations which express radial and tangential displacement of the ring material as functions of angle and time [based on Boehm,1966]. Radial and tangential motions depend on the radial and tangential bedding stiffnesses respectively, quantities which depend on the elastic properties of the side-walls and also the tyre pressure. A third wave motion is also possible: longitudinal (compressive) waves through the ring material.

Heckl calculates that for a typical tyre the fundamental frequency of longitudinal waves (when one wavelength equals the circumference) is around 400 Hz; however the corresponding frequencies for radial and tangential waves are lower, at around 112 Hz and 40 Hz respectively. Kropp [1989] presents comparisons of this linear ring model with measurements on a smooth tyre. It turns out that the coupled system has about 10 predominantly radial modes in the range up to 400 Hz. In addition the circular air passage inside the tyre is resonant at around 250Hz [Walker *et al*,1988b]. Loss-factors η vary from 0.05 below 250 Hz to 0.3 towards 400 Hz. Rigid-body motion of the wheel against the elasticity of the tyre creates a further mode at around 140 Hz [Kung *et al*,1986]. The wavelengths of the radial and tangential modes are smaller than the corresponding wavelengths in air, so they are poor radiators of sound. However they can be expected to affect the force transmitted to the wheel axle. Figure 1.9 shows a calculation by Kung *et al* [1986] of vertical displacement at the wheel axle due to harmonic input displacement at the ground contact point. The calculation assumes a single suspension comprising an ideal spring and damper.

At higher frequencies the tyre tread blocks contribute to sound generation due to [Heckl,1986]:

- resonances of air-filled channels (800-3000 Hz)
- horn amplification effects. The tyre and road surfaces form a megaphone, increasing noise radiation by 10 dB or more (1.6 - 6 kHz).

At the low frequencies of interest for active noise control, it appears that the tyre can be considered as a linear resonant system which transmits vibration to the axle and to a small extent radiates noise by its own vibration. It is possible that small variations in tyre pressure could give an indication of the force transmitted to the wheel hub and thus provide a reference signal related to vehicle interior noise, but no measurements of this have come to light.

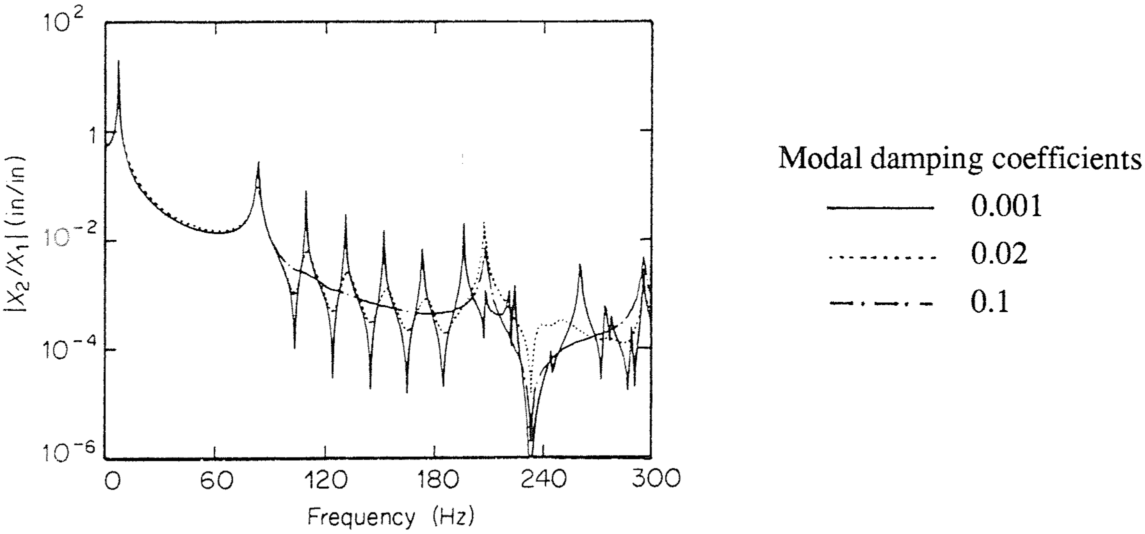

Figure 1.9: Displacement response at the wheel axle per unit harmonic excitation at the ground contact point (from [Kung *et al*,1986])

1.4.3 Transmission to interior

Vibration of the wheels is transmitted to the body of the vehicle through the suspension mounting points. There are typically two or three suspension mounting points per wheel and at each mounting point the applied forces and moments can act in the vertical, fore/aft and lateral directions. This represents a large number of potential inputs.

Walker and Evans [1987] have attempted to rank the various paths to find the main contributors to interior noise. They first applied a shaker to a number of mounting points in turn and measured the transfer functions between measured acceleration (not force) at the mounting point (each direction) and the corresponding interior noise. They then ran the vehicle over a rolling road and measured the actual accelerations at each mounting point. Using the transfer functions it was then possible to calculate the contribution of each mounting point to the interior noise. The main drawback with this approach (as noted in their paper) is that it assumes that there is no cross-coupling between mounting points, whereas in fact the acceleration at any one mounting point will depend partly on forces applied elsewhere.

For the particular car tested, the results indicated that at 80Hz the main contribution was due to lateral motion of one of the rear spring-damper mounting points. However it is clearly not a simple task to assess and rank the vibration transmission paths to the vehicle interior. Furthermore any results will be specific to the model of vehicle tested. This will present a problem in finding suitable locations to measure vibration as a reference for feedforward control. The 'best' location can be expected to vary from car to car.

1.4.4 Vibration of the car body

The vibration characteristics of the car body have been extensively studied [Priede *et al*,1970; Jha *et al*,1976]. There are typically more than 40 distinct modes of vibration in the frequency range up to 200Hz. In the audible range the main effects are:

	Hz
- bending and torsional vibration of the body as a whole	25 - 40
- 'ring-mode' vibration of the passenger compartment (see below)	50 - 150
- bending modes of the drive line (engine/transmission)	50 - 150
- acoustic resonances of the passenger cavity	~90,140,160..
- plate modes of individual panels	150 upwards

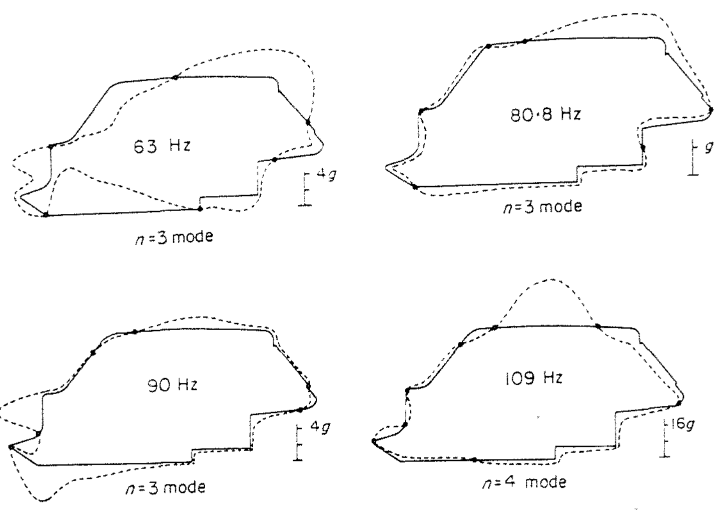

Figure 1.10: Ring-mode vibration of the passenger compartment of a car body shell (from [Jha *et al*,1976])

Ring modes are circumferential modes around the passenger compartment (Figure 1.10). In these modes the vibration is generally uniform across the width of the car. The roof and floor tend to vibrate with greatest amplitude. In each mode the panels may vibrate in phase or out of phase with each other so that their contributions to interior noise may reinforce or cancel. At higher frequencies (*eg* above 150 Hz) the central parts of the roof and floor panels are subject to individual plate mode vibrations.

The first longitudinal acoustic mode of the passenger cavity is typically at 80-90Hz. An unpleasant 'boom' will often occur in the rear of the car at particular speeds when this mode is excited by the engine. If the acoustic modes also coincide with major structural resonances of the car body, serious noise problems are likely.

The vibration of the body panels can be expected to correlate closely with the interior noise. Therefore, measurements of this vibration may well form a suitable set of reference signals for control. Drawbacks would be: (1) the measurement is far removed from the original source of the disturbance (the road) and may not have sufficient time advance; and (2) there are many panels so many measurements may be required.

1.4.5 Wind noise

The interior noise levels of many vehicles are significantly affected by wind noise at speeds above about 60 mph. Turbulence and vortex-shedding create unsteady pressures around the outside surface of the car. These unsteady pressures give rise to noise inside the car either indirectly by acoustic transmission through body panels and windows, or directly through leaks such as imperfect door seals. AR George has published a comprehensive review of the mechanisms of wind noise in cars [George,1989].

The various aerodynamic phenomena create noise over a wide range of frequencies, including:

	Hz
-turbulence due to large-scale flow separation over rear of car	6 - 100
-vortex shedding, front A-pillar (prediction)	100 - 500
-flow separation/turbulence associated with accessories and small features of scale 10mm - 100mm	300 - 3000
-vortex shedding, car aerial (pure tones)	~ 1000
-leaking window seal (monopole source, efficient radiator)	1000-8000
-air flow/turbulence over gap between doors and bodywork	2000-4000

The paper reports a calculation by Dobrynski [1986] which compared the interior noise contributions from different parts of the vehicle body when the vehicle was travelling at high speed (119 mph). The result is shown in Figure 1.11. The largest contributions on an A-weighted basis turn out to be the front vent windows and front side windows in the range 100 - 500 Hz.

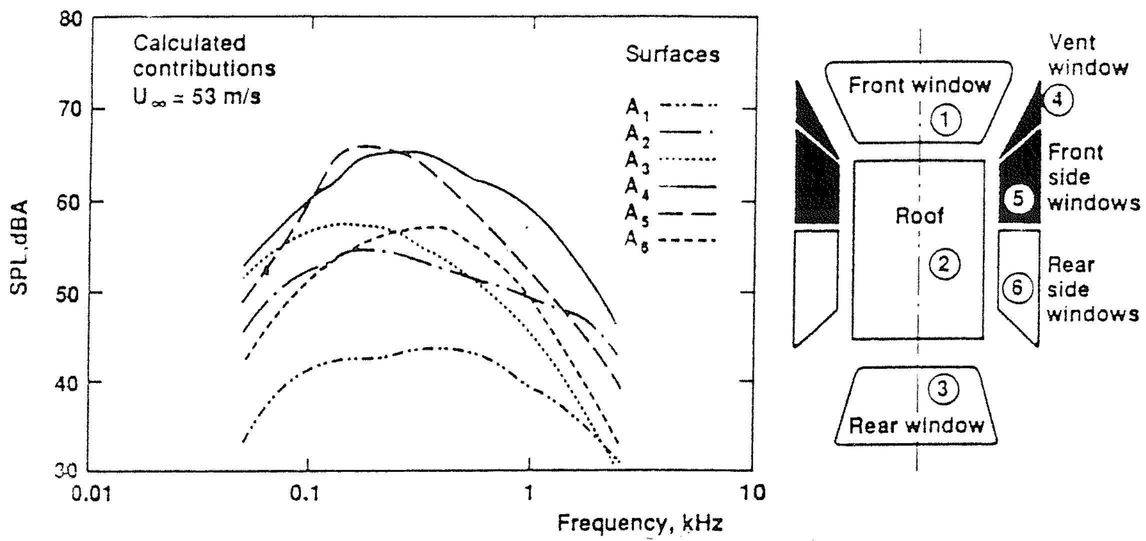

Figure 1.11: Calculated interior noise contributions from different parts of the car body (from [George,1989])

This contribution arises because:

(1) vortex shedding at the front A pillars (structural members between the windscreen and side windows) creates large unsteady pressures over the surface of the side windows; and

(2) the windows, as single panels, have relatively poor transmission loss.

Possible reference signals to detect wind noise would be microphones to detect the exterior pressure variations, or simply a measurement of the resulting panel (or window) vibrations.

1.5 Scope of project

The Thesis is divided into four main chapters. Chapter 2 sets out the theory of active control of random sound in enclosures where there are several primary sources. It is shown how the performance depends on adequate detection of the primary sources of the noise: specifically, on the coherence between the reference signals and the acoustic pressure in the car. The Chapter goes on to show how to calculate the optimal causal filters for random noise control. An analysis in the frequency domain is set out, followed by a multichannel time-domain analysis from which the optimal finite-length causal control filters are obtained. This theory forms the basis of a suite of computer programs to calculate the required optimal filters. The programs predict the noise reduction which would be achieved by a controller in an enclosure with given (or measured) characteristics.

Chapter 3 considers the model problem of a hard-walled rectangular box bounded on one side by a thin plate. Random vibration of the plate creates sound inside the box. Up to four secondary sources are positioned at various locations inside the box and the performance of an active sound control system is assessed. Point acceleration measurements on the plate simulate the use of accelerometers as reference signals in a practical vehicle structure. The calculations examine the required number and locations of the secondary sources along with the effects of plate thickness, location of accelerometers and controller delays. Close examination of this model problem gives insight into the mechanisms of active sound control inside cars.

Vehicle test results are given in Chapter 4. The calculation methods described in Chapter 2 are used to predict the available noise reduction in two test vehicles on the basis of measured noise and vibration data. The vehicle tests examine the number of reference signals required, the effect of different locations and possible delays in the data acquisition and signal processing equipment. One limit to performance is the existence of nonlinear transmission paths through the vehicle structure. Chapter 5 looks at the possibility of using neural network techniques to model nonlinear transmission paths with a view to the possible use of neural networks in a nonlinear active sound control system.

The material presented in this thesis is the original work of the author except where otherwise acknowledged. Preliminary accounts of parts of this work have already been presented [Sutton *et al*, 1990a,1990b,1991].

2 CONTROL OF RANDOM SOUND IN ENCLOSURES

2.1 Introduction

This Chapter sets out the theoretical basis for the active control of random sound in enclosures. It was shown in Section 1.3 that for harmonic sound the acoustic potential energy in an enclosure can be expressed as a quadratic function of the secondary source strengths. It followed that the potential energy had a single minimum value corresponding to a single value of all the secondary source strengths. In this Chapter the same approach will be used to identify the filters required for the control of *random* sound in enclosures. To start with this optimisation will be carried out in the frequency domain, yielding useful and reasonably simple expressions both for the frequency response of the filters themselves and for the reduction in acoustic potential energy. It will be seen that the available reductions are directly related to the coherence between the reference signals and the field to be cancelled. However the optimal filters may not be realisable in practice because of the additional constraint of causality: they cannot respond to input signals before those signals have been received. To include this constraint it is necessary to frame the problem in the time domain. The Chapter goes on to present in Sect. 2.3 expressions for the optimal causal filters for multiple-channel active control of random sound.

2.2 Frequency domain analysis for random signals

2.2.1 Single channel case

The earlier work on harmonic sound [Bullmore *et al*,1987] used as a cost function the total acoustic potential energy in the enclosure (E_p). The work showed that global reductions of acoustic potential energy are possible for harmonic sound in enclosures at low frequencies, *ie* when a sufficiently small number of acoustic modes are excited. For practical applications it is necessary to minimise a cost function which can actually be measured, based for example on signals from microphones placed in the enclosure. Therefore in calculating the optimal filters for control of random sound the sum of the squares of a number of microphone signals (designated J_p) will be used in this Chapter as a practical cost function. As noted in Section 1.3.1 above, Bullmore found that when J_p is minimised, the acoustic potential energy E_p may also be minimised if the microphones are located at peaks of the modeshapes, for example in the corners of a hard-walled rectangular box. For the single-channel case just one microphone is used to detect the sound field.

Figure 2.1 shows the block diagram of a single-channel feedforward control system with a single source of primary excitation $p(\omega)$; ω is radian frequency. The signal at the microphone due to the primary sound, $d(\omega)$, is related to primary excitation by frequency response $A(\omega)$; the reference signal $x(\omega)$ is also related to $p(\omega)$ by $B(\omega)$. Signals $p(\omega)$, $d(\omega)$, *etc* are the Fourier transforms a finite length T seconds of stationary time-series data. Measurement noise $n(\omega)$ (uncorrelated with p) also contributes to the reference signal as shown. $H(\omega)$ is the transfer function of the control filter; $C(\omega)$ is a transfer function representing the secondary loudspeaker, the acoustic path and the microphone.

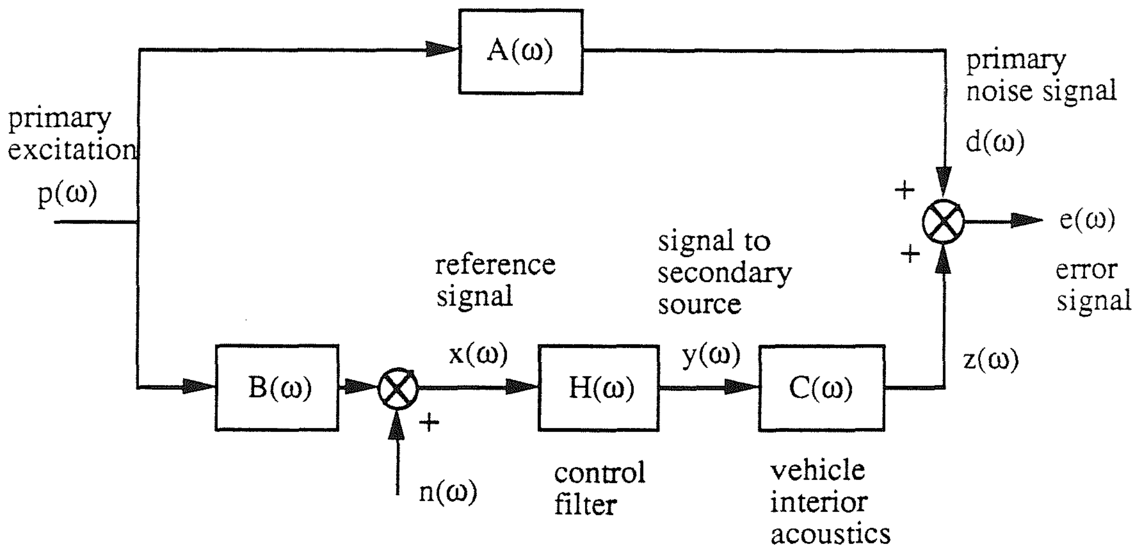

Figure 2.1: Single-channel feedforward active control system

The problem is stated in the frequency domain and in this Section we develop the expression for the sound reduction at a single microphone when the control filter $H(\omega)$ is not constrained to be causal.

From Figure 2.1 we can see that the microphone (error) signal is:

$$e(\omega) = d(\omega) + C(\omega)H(\omega)x(\omega) \qquad (2.2.1)$$

Defining a cost function J_p as the spectrum of acoustic pressure at the microphone:

$$J_p = \lim_{T\to\infty} E\left[\frac{1}{T} e^*(\omega)e(\omega)\right] = S_{ee} \qquad (2.2.2)$$

where E denotes expected value and T is the duration of the data record. S_{ee} is thus the auto-spectral density of the microphone signal and it is this which is to be minimised. Substituting for e(ω) we have

$$J_p = \lim_{T\to\infty} E[\frac{1}{T}(d + CHx)^*(d + CHx)]$$

$$= \lim_{T\to\infty} E\,[\frac{1}{T}(d^*d + C^*H^*x^*d + CHd^*x + H^*|C|^2x^*xH)]$$

$$= S_{dd} + C^*S_{xd}H^* + CS_{xd}^*H + H^*S_{xx}|C|^2H \tag{2.2.3}$$

where S_{dd}, S_{xd} and S_{xx} are the auto- and cross-spectral densities between x(ω) and d(ω). J_p is thus a quadratic function of the complex transfer function H(ω) of the control filter at each frequency. The quantity $S_{xx}|C|^2$ is both real and positive, ensuring that J has a unique minimum value corresponding to a single value of the real and imaginary parts. This minimum (J_{p0}) is given by [Nelson *et al*,1987a]:

$$J_{p0} = S_{dd} - \frac{(S_{xd}^*C)(S_{xd}C^*)}{S_{xx}|C|^2} \tag{2.2.4}$$

corresponding to a filter frequency response:

$$H_0 = -\frac{S_{xd}}{C\,S_{xx}} \tag{2.2.5}$$

The cost function with no control is simply

$$J_d = S_{dd} \tag{2.2.6}$$

so that the reduction can be written

$$\frac{J_{p0}}{J_d} = 1 - \frac{|S_{xd}|^2}{S_{dd}S_{xx}}, \quad \text{or}$$

$$\frac{J_{p0}}{J_d} = 1 - \gamma^2{}_{xd}(\omega) \tag{2.2.7}$$

where $\gamma^2{}_{xd}(\omega)$ is the ordinary coherence function between the reference signal x(ω) and the primary noise signal d(ω) as noted by Ross [1982b]. If the reference signal x(ω) were fully coherent with the primary sound d(ω), *ie* if n(ω) = 0, then $\gamma^2_{xd}(\omega) = 1$ and the primary sound at the microphone could be cancelled completely. In practice $\gamma^2_{xd}(\omega)$ is between 0 and 1 and Equation (2.2.7) gives the reduction which could be achieved with the given reference signal using a control filter H(ω) which is independently specified at each frequency ω (and so has an unconstrained impulse response).

The frequency response of the filter required to minimise the cost function is given by (2.2.5). The impulse response of this filter is found by using the inverse Fourier transform. There is no constraint in this analysis which prevents the filter impulse response from starting before time zero. If this happens, the filter is said to be non-causal because the impulse response begins before the impulse which causes it. Such a filter is not realisable in practice, and in a practical system with a causal filter the sound reduction predicted by Eqn. (2.2.7) would not be achieved: the actual reduction would be less.

Eqn. (2.2.7) is a simple and useful expression giving the maximum reduction which could possibly be achieved with the given reference signal x(ω). In decibels the reduction Δ(ω) can be written:

$$\Delta(\omega) = -10\log(1 - \gamma_{xd}^2(\omega)) \qquad (2.2.8)$$

The sound reduction achieved by a practical system may be less than this because of the causality problem discussed above. However the reduction cannot be greater than this limit in a stationary environment [Nelson *et al*,1991].

2.2.2 Multiple reference signals

In this Section the analysis of the previous Section is extended to cover control systems which use multiple reference signals to detect the primary excitation but still considering a single error signal e(ω). The block diagram is shown in Figure 2.2. The calculation procedure is due to Nelson *et al* [1990].

In this case **p**(ω) is a vector of the spectra of P primary excitations which may be correlated with each other and **x**(ω) is a vector of the spectra of K reference signals. **A**(ω) is a vector of transfer functions between the primary excitations and the primary sound at the microphone d(ω). **B**(ω) is a KxP matrix of transfer functions. **H**(ω) is a

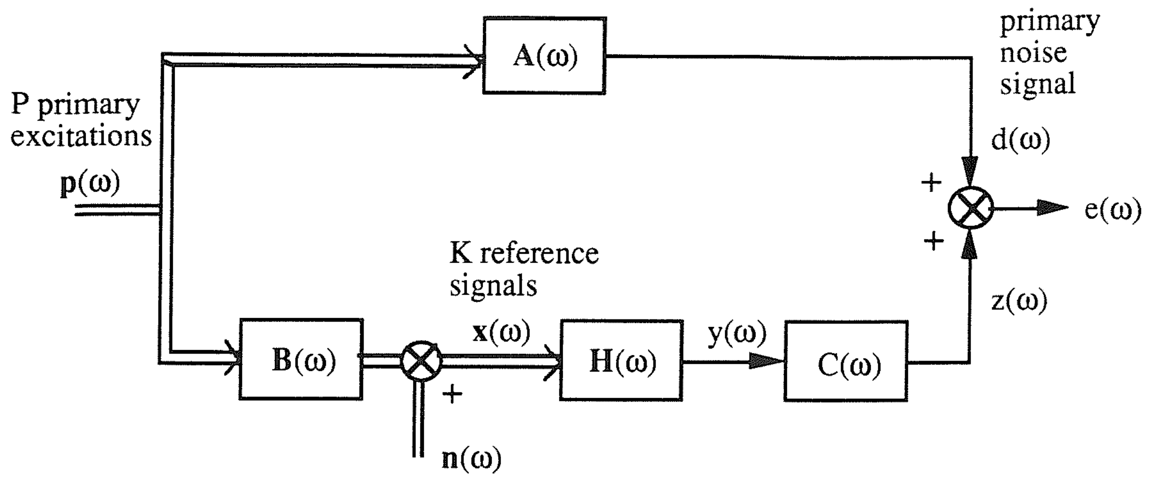

Figure 2.2: Feedforward active control system with multiple reference signals

vector of control filters such that

$$y(\omega) = \mathbf{H}^T\mathbf{x} \qquad (= \mathbf{x}^T\mathbf{H}) \tag{2.2.9}$$

As before we seek to minimise a cost function J_p

$$J_p = \lim_{T\to\infty} E\,[\tfrac{1}{T}\, e^*(\omega)e(\omega)]$$

$$= \lim_{T\to\infty} E\,[\tfrac{1}{T}\,(d + \mathbf{x}^T\mathbf{H}C)^*(d + \mathbf{x}^T\mathbf{H}C)]$$

$$= \lim_{T\to\infty} E\,[\tfrac{1}{T}(d^*d + d^*\mathbf{x}^T\mathbf{H}C + C^*\mathbf{H}^H\mathbf{x}^*d + \mathbf{H}^H\mathbf{x}^*C^*C\mathbf{x}^T\mathbf{H})]$$

$$= S_{dd} + C\mathbf{S}_{xd}{}^H\mathbf{H} + C^*\mathbf{H}^H\mathbf{S}_{xd} + \mathbf{H}^H|C|^2\mathbf{S}_{xx}\mathbf{H} \tag{2.2.10}$$

where $\mathbf{S}_{xd}$ is the vector given by $\lim_{T\to\infty} E[\frac{1}{T}\mathbf{x}^*d]$ and $\mathbf{S}_{xx}$ is the KxK matrix given by $\lim_{T\to\infty} E[\frac{1}{T}\mathbf{x}^*\mathbf{x}^T]$.

The vector $\mathbf{H}(\omega)$ is chosen to minimise this quadratic function, giving [Nelson *et al*,1987a]:

$$J_{p0} = S_{dd} - \mathbf{S}_{xd}{}^H\mathbf{S}_{xx}{}^{-1}\mathbf{S}_{xd} \tag{2.2.11}$$

The reduction compared with J_d (cost function with no control, $J_d = S_{dd}$) is

$$\frac{J_{p0}}{J_d} = 1 - \frac{S_{xd}^H S_{xx}^{-1} S_{xd}}{S_{dd}} \qquad (2.2.12)$$

This expression can be further simplified by introducing the multiple coherence function [Bendat *et al*,1986]

$$\frac{J_{p0}}{J_{dd}} = 1 - \eta^2_{d:\mathbf{x}}(\omega) \qquad (2.2.13)$$

where $\eta^2_{d:\mathbf{x}}(\omega)$ is the multiple coherence between the K reference signals $\mathbf{x}(\omega)$ and the primary sound $d(\omega)$ at the microphone. The multiple coherence takes values between 0 and 1 and represents the fraction of power in the primary sound signal $d(\omega)$ which can be expressed by a linear combination of the reference signals $x_1(\omega)$ ... $x_k(\omega)$.

Equation (2.2.13) is a useful expression when assessing prospective reference signals for multiple-channel control. As in the single-channel case it gives the maximum available sound reduction which may be obtained with a given set of reference signals.

2.2.3 General multichannel case

The analysis of the previous two Sections is here extended to the general frequency-domain case where there are K reference signals, M signals to secondary sources and L error sensors (microphones). In Figure 2.3 **H** is an MxK array of control filter frequency responses and **C** is an LxM array of frequency responses between the secondary sources and microphones.

We follow Nelson *et al* [1990] and define a set of filtered reference signals $r_{lmk}(\omega)$. The basic matrix equations are:

$$\mathbf{e}(\omega) = \mathbf{d}(\omega) + \mathbf{z}(\omega) \qquad (2.2.14)$$

$$\begin{aligned} \mathbf{z}(\omega) &= \mathbf{C}\mathbf{y} \\ &= \mathbf{C}\mathbf{H}\mathbf{x} \qquad (2.2.15) \end{aligned}$$

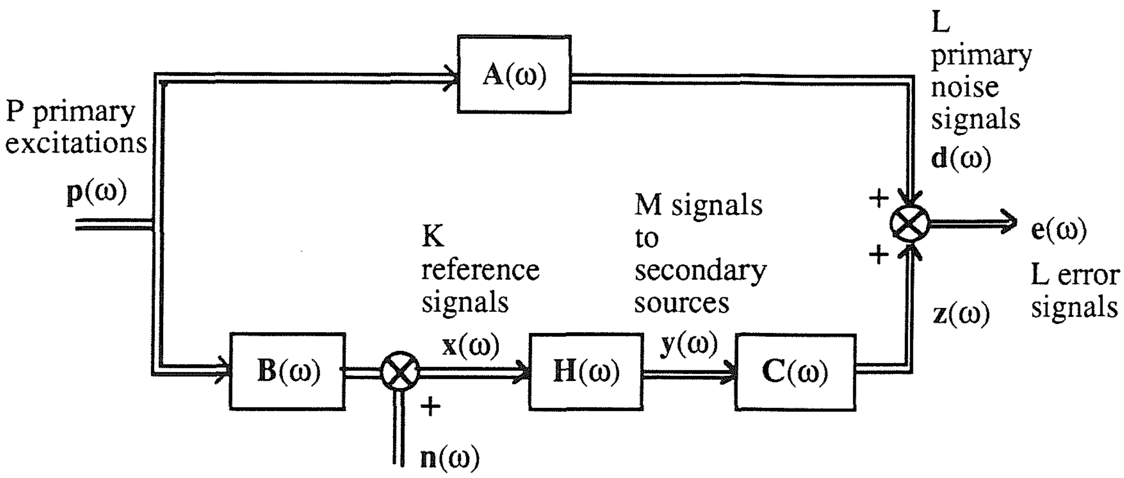

Figure 2.3: Feedforward active control system: full multichannel case

Considering just the lth error signal:

$$e_l(\omega) = d_l(\omega) + z_l(\omega) \tag{2.2.16}$$

$$z_l(\omega) = \sum_{m=1}^{M} c_{lm} \sum_{k=1}^{K} h_{mk} x_k(\omega) \tag{2.2.17}$$

The filtered reference signal $r_{lmk}(\omega)$ is defined as the response of filter $c_{lm}(\omega)$ to signal $x_k(\omega)$:

$$r_{lmk}(\omega) = c_{lm}(\omega) x_k(\omega) \tag{2.2.18}$$

so that

$$z_l(\omega) = \sum_{m=1}^{M} \sum_{k=1}^{K} h_{mk}(\omega) r_{lmk}(\omega) \tag{2.2.19}$$

The vector of error signals can then be expressed as:

$$\mathbf{e}(\omega) = \mathbf{d}(\omega) + \mathbf{r}(\omega)\mathbf{w}(\omega) \tag{2.2.20}$$

where $\mathbf{w}(\omega)$ contains the elements $h_{mk}(\omega)$ of the control filter array but rearranged as a composite vector:

$$\mathbf{w}(\omega) = \begin{bmatrix} h_{11}(\omega) \\ h_{12}(\omega) \\ \dots \\ h_{1K}(\omega) \\ h_{21}(\omega) \\ \dots \\ h_{MK}(\omega) \end{bmatrix} \qquad \text{(vector, length MK)} \qquad (2.2.21)$$

In addition the filtered reference signals are arranged in an LxMK array:

$$\mathbf{r}(\omega) = \begin{bmatrix} r_{111}(\omega) & r_{112}(\omega) & \dots & r_{1MK}(\omega) \\ r_{211}(\omega) & r_{212}(\omega) & \dots & \\ \dots & & & \\ r_{L11}(\omega) & \dots & & r_{LMK}(\omega) \end{bmatrix} \qquad \text{(LxMK array)}$$

$$(2.2.22)$$

It is now possible to obtain an optimum value of $\mathbf{w}(\omega)$ by expressing the cost function J_p in Hermitian quadratic form. In this multiple-error case the cost function is defined to be

$$J_p = \lim_{T\to\infty} E[\tfrac{1}{T}\mathbf{e}^H\mathbf{e}]$$

$$= \lim_{T\to\infty} E[\tfrac{1}{T}(\mathbf{d}^H\mathbf{d} + \mathbf{w}^H\mathbf{r}^H\mathbf{d} + \mathbf{d}^H\mathbf{r}\mathbf{w} + \mathbf{w}^H\mathbf{r}^H\mathbf{r}\mathbf{w})] \qquad (2.2.23)$$

Eqn. (2.2.23) can be expressed in terms of spectral density functions, defined as follows:

$$S_{dd} = \lim_{T\to\infty} E[\tfrac{1}{T}\mathbf{d}^H\mathbf{d}] \qquad \text{(scalar)} \qquad (2.2.24)$$

$$S_{rd} = \lim_{T\to\infty} E[\tfrac{1}{T}\mathbf{r}^H\mathbf{d}] \qquad \text{(vector, length MK)} \qquad (2.2.25)$$

$$S_{rr} = \lim_{T\to\infty} E[\tfrac{1}{T}\mathbf{r}^H\mathbf{r}] \qquad \text{(MKxMK matrix)} \qquad (2.2.26)$$

so that

$$J_p = S_{dd} + \mathbf{w}^H S_{rd} + S_{rd}^H\mathbf{w} + \mathbf{w}^H S_{rr}\mathbf{w} \qquad (2.2.27)$$

This is recognised to be in Hermitian quadratic form. The vector of optimum filters is given by:

$$w_0(\omega) \quad = \quad - S_{rr}^{-1} S_{rd} \tag{2.2.28}$$

The minimum value of the cost function is

$$J_{p0} \quad = \quad S_{dd} \; - \; S_{rd}^H S_{rr}^{-1} S_{rd} \tag{2.2.29}$$

The fractional reduction in cost function compared with the case with no active control is given by:

$$\frac{J_{p0}}{S_{dd}} \quad = \quad 1 \; - \; \frac{S_{rd}^H S_{rr}^{-1} S_{rd}}{S_{dd}} \tag{2.2.30}$$

This result is similar in form to eqn. (2.2.12), the case with a single secondary source and single microphone. For the special case of one error signal (L=1) but M secondary sources and K reference signals, this result shows that the minimum cost function depends on the multiple coherence between the MK filtered reference signals defined above and the single primary noise signal $d(\omega)$.

This Section (2.2) has examined the problem of defining the optimum frequency response of the filters for active sound control. In the following Section the practical case of realisable filters is addressed. For this analysis the problem needs to be framed in the time domain.

2.3 Sampled time-domain analysis for random signals

2.3.1 Single channel control

The optimal filter transfer functions $\mathbf{H}(\omega)$ which were presented in the previous Section may have impulse responses which are non-causal and therefore physically unrealisable. In order to cancel the sound field, they are required to anticipate a primary excitation which has not yet happened. When the filters are constrained to be causal, the problem becomes one of predicting future random signals on the basis of their present and past values. This prediction/estimation problem was addressed by Wiener in 1942.

Wiener's work resulted in the well-known Wiener-Hopf integral equation in which the optimal causal filter was expressed in terms of correlation functions between the 'received signal' and the 'desired signal' to be predicted. This continuous-time formulation was extended to cover the discrete-time case by Levinson [1947]. The discrete-time formulation of Wiener's work can be readily applied using digital computers because the required optimal filters are obtained by matrix inversion rather than by solving integral equations. Furthermore Levinson devised a recursive method for inverting the matrices which took advantage of their special (Toeplitz) form and involved a huge saving in time.

The remainder of this Section summarises the Wiener/Levinson method of optimal filter design and applies it to a single-channel active sound control system. In the following Section the calculation method for the more complicated multiple-channel case is developed.

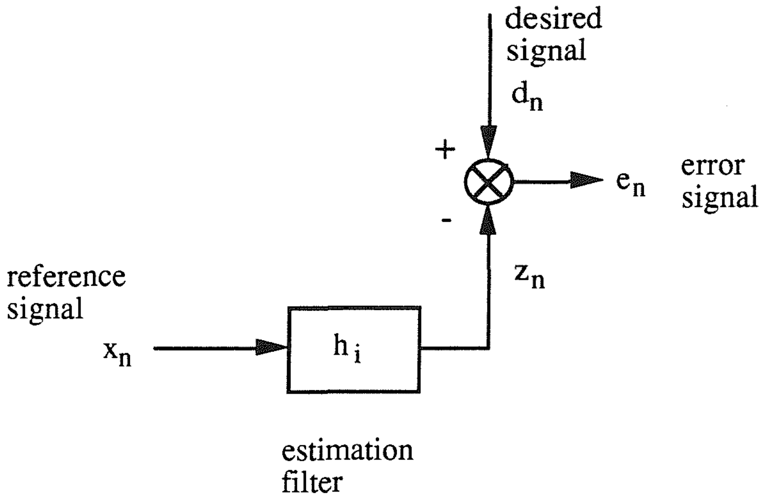

Figure 2.4: Single-channel estimation problem

The basic estimation problem is shown in Figure 2.4. It is required to calculate the coefficients h_0, h_1, ...h_{I-1} of the FIR filter such that the filter output z_n is as close as possible to the desired signal d_n. The cost function J to be minimised is chosen to be mean squared error:

$$J = E[(d_n - z_n)^2] \tag{2.3.1}$$

The filter output is defined by:

$$z_n = \sum_{i=0}^{I-1} h_i x_{n-i} \tag{2.3.2}$$

so that

$$J = E[d_n^2] - 2\sum_{i=0}^{I-1} h_i E[d_n x_{n-i}] + \sum_{i=0}^{I-1}\sum_{j=0}^{I-1} h_i h_j E[x_{n-i}x_{n-j}] \qquad (2.3.3)$$

The expected-value terms are recognised to be autocorrelation and crosscorrelation functions and are denoted by R_{xx}, R_{xd} and R_{dd}:

$$\begin{aligned} E[d_n^2] &= R_{dd}(0) \\ E[d_n x_{n-i}] &= R_{dx}(-i) \\ &= R_{xd}(i) \\ E[x_{n-i}x_{n-j}] &= R_{xx}(i-j), \text{ so that} \end{aligned}$$

$$J = R_{dd}(0) - 2\sum_{i=0}^{I-1} R_{xd}(i) + \sum_{i=0}^{I-1}\sum_{j=0}^{I-1} h_i h_j R_{xx}(i-j) \qquad (2.3.4)$$

Differentiating J with respect to each filter coefficient h_i and setting $\frac{\partial J}{\partial h_i} = 0$ reveals that the filter coefficients h_i which minimise the cost function are given by the solution to the equation:

$$\sum_{i=0}^{I-1} h_i R_{xx}(n-i) = R_{xd}(n) \qquad n = 0, 1, 2,... \qquad (2.3.5)$$

Equation (2.3.5) is known as the Wiener equation. It can be written in the form of a set of simultaneous equations which can be solved for the I filter coefficients h_i, $i = 0, 1,...I-1$. The autocorrelation and crosscorrelation functions can be estimated from records of past data and, provided the random process is stationary, the filter h_i can be used to estimate the current values of the d_n. Future values can also be estimated using this techinque: the crosscorrelation term in (2.3.5) becomes $R_{xd}(n+s)$ for a time-advance of s time-steps.

Writing (2.3.5) out in matrix form shows the structure of the autocorrelation matrix which is to be inverted:

$$\begin{bmatrix} R_{xx}(0) & R_{xx}(1) & R_{xx}(2) & \dots & R_{xx}(I-1) \\ R_{xx}(1) & R_{xx}(0) & R_{xx}(1) & \dots & \\ R_{xx}(2) & R_{xx}(1) & R_{xx}(0) & \dots & \\ \dots & & & & \\ R_{xx}(I-1) & \dots & & & R_{xx}(0) \end{bmatrix} \begin{bmatrix} h_0 \\ h_1 \\ h_2 \\ \dots \\ h_{I-1} \end{bmatrix} = \begin{bmatrix} R_{xy}(0) \\ R_{xy}(1) \\ R_{xy}(2) \\ \dots \\ R_{xy}(I-1) \end{bmatrix} \quad (2.3.6)$$

The autocorrelation matrix has the characteristic that the elements of each diagonal are the same within that diagonal and the matrix is symmetric. This is termed a Toeplitz structure. Levinson [1947] devised a recursive method for solving matrices of this form which is described clearly by Clarkson [1983].

This formulation of the Wiener equation can be applied to the active attenuation of random sound using a single-channel system. The error signal for a practical single-channel active sound control system is the electrical output of one microphone in the sound field. The microphone detects the superposition of the primary sound to be cancelled and the secondary sound generated by the controller. Figure 2.5 shows a single-channel system in which a single reference signal x_n passes through a control filter h_i to create a signal y_n to a secondary source (loudspeaker) in the enclosure. The FIR filter c_j $j = 0,1,...J-1$ represents the transfer function of the loudspeaker, acoustics of the enclosure and the response of the single microphone. z_n is the microphone signal due to the secondary speaker while d_n is the signal due to the primary sound.

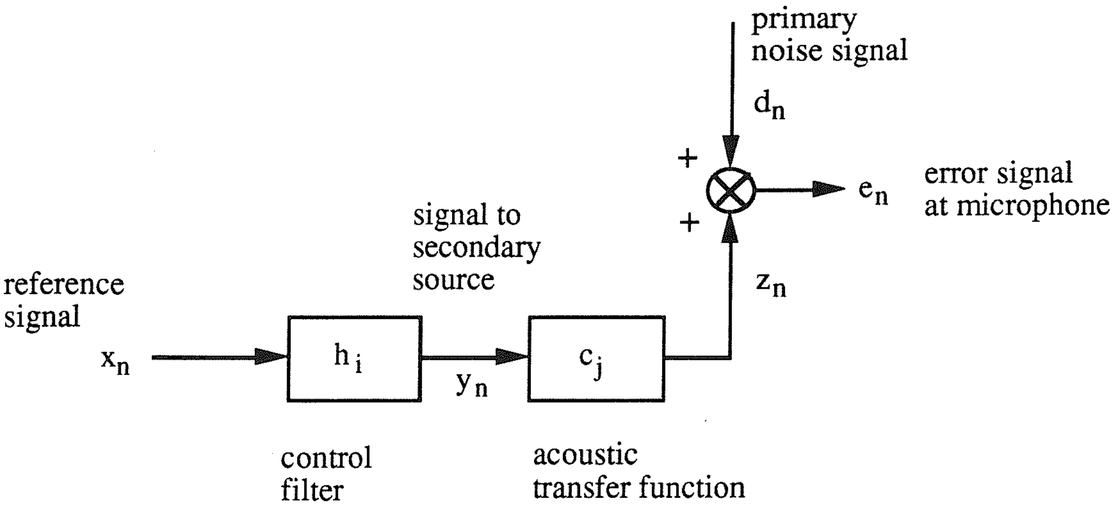

Figure 2.5: Single-channel active control system with acoustic transfer function after control filter

The calculation of the coefficients h_i is complicated by the fact that filter c_j is interposed between the control filter and the error signal. In this single-channel case it is only necessary to interchange h_i and c_j (both filters being linear and time-invariant) as shown in Figure 2.6. The signal r_n is termed the *filtered reference signal.* The coefficients h_i can now be calculated using the Wiener equation (2.3.5) noting that the contributions to the microphone error signal e_n are added by superposition rather than subtracted:

$$\sum_{i=0}^{I-1} h_i R_{rr}(n-i) = -R_{rd}(n) \qquad (2.3.7)$$

where

$$R_{rr}(i) = E[r_n r_{n+i}]$$
$$R_{rd}(i) = E[r_n d_{n+i}]$$

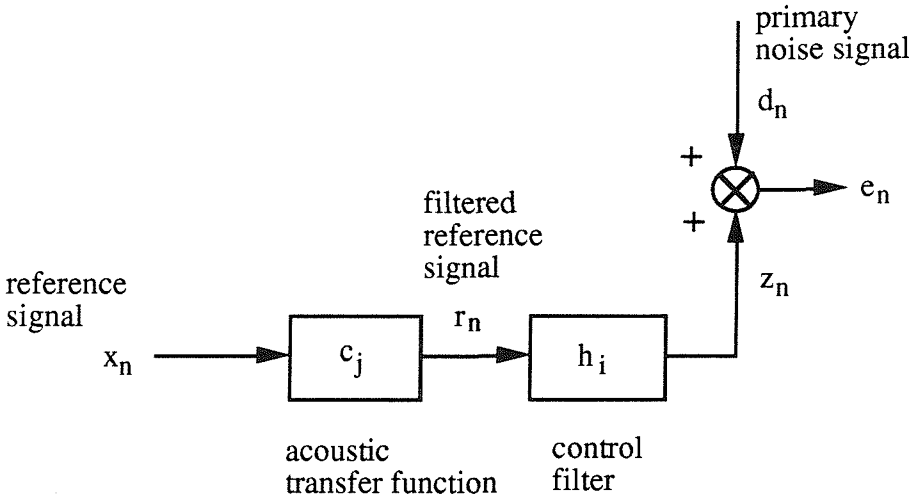

Figure 2.6: Single-channel active control system with control filter and acoustic transfer function interchanged

The interior acoustics (contained in the coefficients c_j) are thus allowed for when calculating the correlation functions R_{rr} and R_{rd}.

2.3.2 Multiple-channel control

In this Section the above single-channel analysis is extended to cover the situation where there are multiple reference signals, multiple secondary sources and the sound field is detected by multiple microphones. As in the previous Section, we consider first the basic multiple-channel estimation problem and go on afterwards to apply it to active sound control.

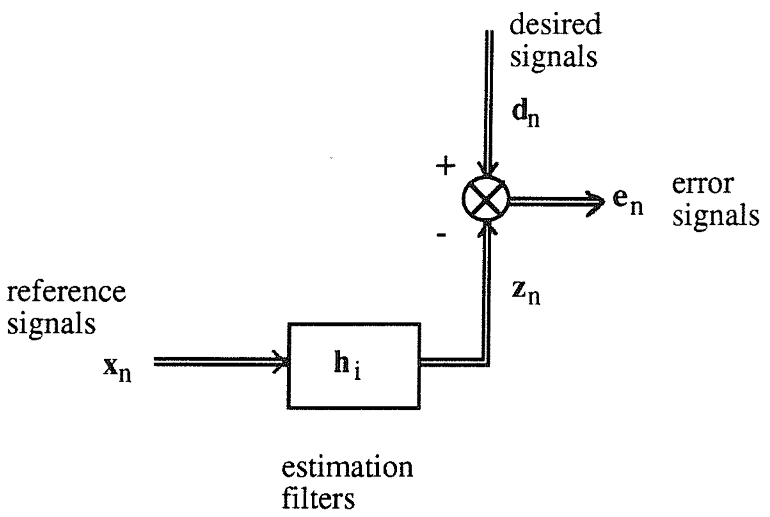

Figure 2.7: Multiple-channel estimation problem

The multiple-channel optimal filtering problem was first introduced for problems in geophysical data processing with multiple reference signals and multiple desired signals [Schneider *et al*,1964; Wiggins *et al*,1965; Galbraith *et al*,1968]. Efficient methods for the solution of the resulting normal equations were also developed at that time [Wiggins *et al*,1965; Robinson,1978].The basic block diagram is shown in Figure 2.7 where this time $\mathbf{x}_n$ is a vector of K reference signals; $\mathbf{z}_n$, $\mathbf{d}_n$ and $\mathbf{e}_n$ are vectors of L controller outputs, desired signals and error signals respectively; and $\mathbf{h}_i$ is an LxK array of I-point FIR filters, with i = 0,1,...I-1.

The cost function to be minimised is chosen to be the mean value of the sum of squares of the error signals:

$$J_p = E[e_1^2(n) + e_2^2(n) + \ldots e_L^2(n)] \tag{2.3.8}$$

where $e_1(n)$, $e_2(n)$,... are individual elements of $\mathbf{e}_n$. The cost function is expressed as the trace of a mean-square error matrix (in order to facilitate the matrix manipulations):

$$J_p = \mathrm{tr}\, E[\mathbf{e}_n\mathbf{e}_n^T] = E[e_1^2(n) + e_2^2(n) + \ldots e_L^2(n)] \tag{2.3.9}$$

where the trace of a square matrix is defined as the sum of entries along its principal diagonal. From Figure 2.7 we have

$$\mathbf{e}_n = \mathbf{d}_n - \sum_{i=0}^{I-1} \mathbf{h}_i \mathbf{x}_{n-i} \qquad (2.3.10)$$

so

$$\mathbf{e}_n\mathbf{e}_n^T = (\mathbf{d}_n - \sum_{i=0}^{I-1} \mathbf{h}_i\mathbf{x}_{n-i})(\mathbf{d}_n - \sum_{j=0}^{I-1} \mathbf{h}_j\mathbf{x}_{n-j})^T$$
$$= \mathbf{d}_n\mathbf{d}_n^T - \mathbf{d}_n \sum_{j=0}^{I-1} \mathbf{x}_{n-j}^T\mathbf{h}_j^T - \sum_{i=0}^{I-1} \mathbf{h}_i\mathbf{x}_{n-i}\mathbf{d}_n^T + \sum_{i=0}^{I-1}\sum_{j=0}^{I-1} \mathbf{h}_i\mathbf{x}_{n-i}\mathbf{x}_{n-j}^T\mathbf{h}_j^T \qquad (2.3.11)$$

Taking the ensemble average:

$$E[\mathbf{e}_n\mathbf{e}_n^T] = E[\mathbf{d}_n\mathbf{d}_n^T] - \sum_{j=0}^{I-1} E[\mathbf{d}_n\mathbf{x}_{n-j}^T]\mathbf{h}_j^T - \sum_{i=0}^{I-1} \mathbf{h}_iE[\mathbf{x}_{n-i}\mathbf{d}_n^T] + \sum_{i=0}^{I-1}\sum_{j=0}^{I-1} \mathbf{h}_iE[\mathbf{x}_{n-i}\mathbf{x}_{n-j}^T]\mathbf{h}_j^T \qquad (2.3.12)$$

The ensemble averages can be expressed as arrays of autocorrelation and crosscorrelation functions:

$$E[\mathbf{d}_n\mathbf{x}_{n-j}^T] = \mathbf{R}_{dx}(-j) \qquad \text{LxK matrix}$$
$$E[\mathbf{x}_{n-i}\mathbf{d}_n^T] = \mathbf{R}_{xd}(i) \qquad \text{KxL matrix}$$
$$E[\mathbf{x}_{n-i}\mathbf{x}_{n-j}^T] = \mathbf{R}_{xx}(i-j) \qquad \text{KxK matrix}$$
$$E[\mathbf{d}_n\mathbf{d}_n^T] = \mathbf{R}_{dd}(0) \qquad \text{LxL matrix}$$

Note that $\mathbf{R}_{dx}$ and $\mathbf{R}_{xd}$ are related by:

$$\mathbf{R}_{dx}^T(-j) = E[\mathbf{x}_{n-j}\mathbf{d}_n^T] = \mathbf{R}_{xd}(j)$$
$$\mathbf{R}_{xx}^T(p) = E[\mathbf{x}_{n+p}\mathbf{x}_n^T] = \mathbf{R}_{xx}(-p)$$

It is now possible to write $E[\mathbf{e}_n\mathbf{e}_n^T]$ in terms of the correlation function matrices:

$$E[\mathbf{e}_n\mathbf{e}_n^T] = \mathbf{R}_{dd}(0) - \sum_{j=0}^{I-1} \mathbf{R}_{dx}(-j)\mathbf{h}_j^T - \sum_{i=0}^{I-1} \mathbf{h}_i\mathbf{R}_{xd}(i) + \sum_{i=0}^{I-1}\sum_{j=0}^{I-1} \mathbf{h}_i\mathbf{R}_{xx}(i-j)\mathbf{h}_j^T \qquad (2.3.13)$$

Differentiating the trace of $E[e_n e_n^T]$ with respect to each filter coefficient, Robinson [1978] obtains a set of simultaneous matrix equations in the $\mathbf{h}_i$:

$$\begin{array}{lllll}
\mathbf{h}_0\mathbf{R}_{xx}(0) & + \mathbf{h}_1\mathbf{R}_{xx}(-1) & + \ldots & + \mathbf{h}_{I-1}\mathbf{R}_{xx}(-I+1) & = \mathbf{R}_{xd}(0) \\
\mathbf{h}_0\mathbf{R}_{xx}(1) & + \mathbf{h}_1\mathbf{R}_{xx}(0) & + \ldots & + \mathbf{h}_{I-1}\mathbf{R}_{xx}(-I+2) & = \mathbf{R}_{xd}(1) \\
\ldots & \ldots & \ldots & \ldots & \ldots \\
\mathbf{h}_0\mathbf{R}_{xx}(I-1) & + \mathbf{h}_1\mathbf{R}_{xx}(I-2) & + \ldots & + \mathbf{h}_{I-1}\mathbf{R}_{xx}(0) & = \mathbf{R}_{xd}(I-1)
\end{array} \quad (2.3.14)$$

We can rewrite these equations in *block matrix* form, noting that each element of a block matrix is itself a matrix:

$$[\mathbf{h}_0\ \mathbf{h}_1\ \ldots\ \mathbf{h}_{I-1}] \begin{bmatrix} \mathbf{R}_{xx}(0) & \mathbf{R}_{xx}(-1) & \mathbf{R}_{xx}(-2) & \ldots & \mathbf{R}_{xx}(-I+1) \\ \mathbf{R}_{xx}(1) & \mathbf{R}_{xx}(0) & \mathbf{R}_{xx}(-1) & \ldots & \\ \mathbf{R}_{xx}(2) & \mathbf{R}_{xx}(1) & \mathbf{R}_{xx}(0) & \ldots & \\ \ldots & & & & \\ \mathbf{R}_{xx}(I-1) & \ldots & & & \mathbf{R}_{xx}(0) \end{bmatrix}$$

$$= [\mathbf{R}_{xd}(0)\ \mathbf{R}_{xd}(1)\ \ldots\ \mathbf{R}_{xd}(I-1)] \quad (2.3.15)$$

The matrix of autocorrelation functions is a block Toeplitz matrix, having identical matrices along its diagonals. The individual submatrices $\mathbf{R}_{xx}(i)$ are not themselves of Toeplitz form. Each filter coefficient matrix $\mathbf{h}_i$ is an LxK array as defined above. Wiggins & Robinson [1965] devised a recursive procedure for inverting a block Toeplitz matrix, extending Levinson's recursion to the multiple-channel situation. The method is detailed in [Robinson,1978] along with Fortran programs for its implementation.

In practical applications wide-sense stationarity is assumed, and the expectation operator is replaced by an average over time.

It is now possible to consider the design of filters for multiple-channel active control of random sound. As in the single-channel case, the calculation of optimal filter coefficients has to take account of the transfer functions of the secondary sources (*eg* loudspeakers), microphones and interior acoustics of the enclosure. Figure 2.8 shows a block diagram for the multiple-channel case. There are K reference signals $\mathbf{x}_n$, M signals to secondary sources $\mathbf{y}_n$ and L microphones. $\mathbf{z}_n$ represents the microphone signals due to the secondary sources which are superposed with signals $\mathbf{d}_n$ due to the primary noise. The controller is an array of FIR filters with coefficients $\mathbf{h}_i$ (MxK array).

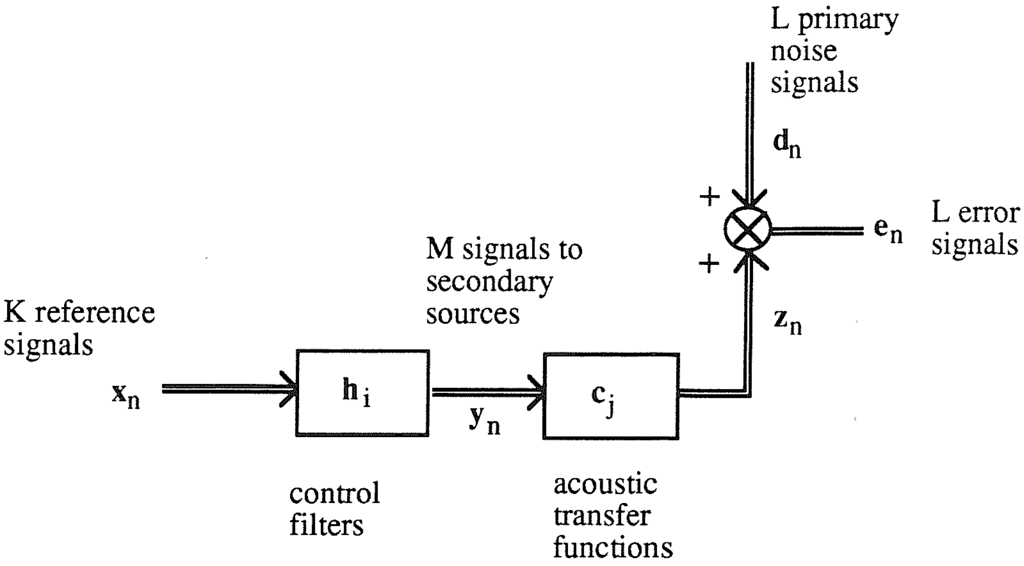

Figure 2.8: Multiple-channel active control

In the single-channel case it was simple to interchange the c-filter and h-filter to define a filtered reference signal r_n and thus restore the problem to a standard form. In the multichannel case this is less straightforward as the arrays $\mathbf{h}_i$ and $\mathbf{c}_j$ do not commute. As in the earlier frequency-domain analysis this problem can be overcome by rearranging the control filter coefficients as a single vector $\mathbf{w}_i$ of length MK.

Generalising the analysis of Section 2.2.3, we write the lth error signal as

$$e_l(n) = d_l(n) + z_l(n) \tag{2.3.16}$$

where now

$$z_l(n) = \sum_{m=1}^{M} \sum_{j=0}^{J-1} c_{lm}(j) \sum_{k=1}^{K} \sum_{i=1}^{I-1} h_{mk}(i) x_k(n-i-j) \tag{2.3.17}$$

which can be expressed as

$$z_l(n) = \sum_{i=1}^{I-1} \sum_{m=1}^{M} \sum_{k=1}^{K} h_{mk}(i) r_{lmk}(n-i) \tag{2.3.18}$$

where the kth reference signal filtered by the path from the mth secondary source to the lth error sensor is:

$$r_{lmk}(n) = \sum_{j=0}^{J-1} c_{lm}(j) x_k(n-j) \tag{2.3.19}$$

The vector of error signals can thus be expressed as

$$\mathbf{e}_n = \mathbf{d}_n + \sum_{i=1}^{I-1} \mathbf{r}_{n-i}\mathbf{w}_i \tag{2.3.20}$$

where

$$\mathbf{w}_i = \left[\, h_{11}(i) \;\; h_{12}(i) \;\; \ldots \;\; h_{1K}(i) \;\; h_{21}(i) \;\; \ldots \;\; h_{MK}(i) \,\right]^T \qquad \text{MK x 1 array} \tag{2.3.21}$$

$$\mathbf{r}_n = \begin{bmatrix} r_{111}(n) & r_{112}(n) & \ldots & r_{11K}(n) & r_{121}(n) & \ldots & r_{1MK}(n) \\ r_{211}(n) & & & & & & \\ \ldots & & & & & & \\ r_{L11}(n) & & & & & & r_{LMK}(n) \end{bmatrix} \qquad \text{L x MK array} \tag{2.3.22}$$

Equation (2.3.20) is on the face of it of similar form to (2.3.10), the earlier equation for the multiple-channel error signal without the extra transfer function $\mathbf{c}_j$. However in this case the filtered reference signals $\mathbf{r}_n$ premultiply the filter coefficients $\mathbf{w}_i$ (In the earlier case the filter coefficients came first in the expression.) The result of this is that when the expectation $E[\mathbf{e}_n\mathbf{e}_n^T]$ is taken, the correlation matrices cannot be extracted. We therefore alter Robinson's development slightly and minimise $E[\mathbf{e}_n^T\mathbf{e}_n]$, which is in fact equal to the trace of $E[\mathbf{e}_n\mathbf{e}_n^T]$:

$$E[\mathbf{e}_n^T\mathbf{e}_n] = \operatorname{tr} E[\mathbf{e}_n\mathbf{e}_n^T] = E[e_1^2(n) + e_2^2(n) + \ldots e_L^2(n)] \tag{2.3.23}$$

We have

$$\begin{aligned} E[\mathbf{e}_n^T\mathbf{e}_n] &= E[(\mathbf{d}_n + \sum_{i=0}^{I-1} \mathbf{r}_{n-i}\mathbf{w}_i)^T(\mathbf{d}_n + \sum_{j=0}^{I-1} \mathbf{r}_{n-j}\mathbf{w}_j)] \\ &= E[\mathbf{d}_n^T\mathbf{d}_n + \sum_{i=0}^{I-1} \mathbf{w}_i^T\mathbf{r}_{n-i}^T\mathbf{d}_n + \sum_{j=0}^{I-1} \mathbf{d}_n^T\mathbf{r}_{n-j}\mathbf{w}_j + \sum_{i=0}^{I-1}\sum_{j=0}^{I-1} \mathbf{w}_i^T\mathbf{r}_{n-i}^T\mathbf{r}_{n-j}\mathbf{w}_j] \\ &= R_{dd}(0) + \sum_{i=0}^{I-1} \mathbf{w}_i^T\mathbf{R}_{rd}(i) + \sum_{j=0}^{I-1} \mathbf{R}_{dr}(-j)\mathbf{w}_j + \sum_{i=0}^{I-1}\sum_{j=0}^{I-1} \mathbf{w}_i^T\mathbf{R}_{rr}(i-j)\mathbf{w}_j \end{aligned} \tag{2.3.24}$$

where the correlation functions are defined as follows:

$$\begin{aligned} R_{dd}(0) &= E[\mathbf{d}_n{}^T\mathbf{d}_n] && \text{(scalar)} \\ \mathbf{R}_{rd}(i) &= E[\mathbf{r}_{n-i}{}^T\mathbf{d}_n] && \text{(1 x MK vector)} \\ \mathbf{R}_{rr}(i-j) &= E[\mathbf{r}_{n-i}{}^T\mathbf{r}_{n-j}] && \text{(MK x MK vector)} \end{aligned} \qquad (2.3.25)$$

Also:

$$\mathbf{R}_{dr}(-i) = E[\mathbf{d}_n{}^T\mathbf{r}_{n-i}] = \mathbf{R}_{rd}{}^T(i) \qquad (2.3.26)$$

$$\mathbf{w}_i{}^T\mathbf{R}_{rd}(i) = \mathbf{R}_{rd}{}^T(i)\mathbf{w}_i \qquad \text{(scalar quantity)} \qquad (2.3.27)$$

Differentiating with respect to each filter coefficient and setting the result to zero yields the equation for the optimum control filter coefficients:

$$\mathbf{R}_{rd}(p) + \sum_{i=0}^{I-1} \mathbf{R}_{rr}(p-i)\mathbf{w}_i = 0 \qquad p = 0,1,2,\dots I-1 \qquad (2.3.28)$$

Writing out the summation in full reveals the block Toeplitz form of the autocorrelation matrix:

$$\begin{bmatrix} \mathbf{R}_{rr}(0) & \mathbf{R}_{rr}(-1) & \mathbf{R}_{rr}(2) & \dots & \mathbf{R}_{rr}(-I+1) \\ \mathbf{R}_{rr}(1) & \mathbf{R}_{rr}(0) & \mathbf{R}_{rr}(-1) & \dots & \\ \mathbf{R}_{rr}(2) & \mathbf{R}_{rr}(1) & \mathbf{R}_{rr}(0) & \dots & \\ \dots & & & & \\ \mathbf{R}_{rr}(I-1) & \dots & & & \mathbf{R}_{rr}(0) \end{bmatrix} \begin{bmatrix} \mathbf{w}_0 \\ \mathbf{w}_1 \\ . \\ . \\ \mathbf{w}_{I-1} \end{bmatrix} = - \begin{bmatrix} \mathbf{R}_{rd}(0) \\ \mathbf{R}_{rd}(1) \\ . \\ . \\ \mathbf{R}_{rd}(I-1) \end{bmatrix}$$

(2.3.29)

Comparison of this result with the earlier multichannel equations (2.3.15) shows that in this case the individual coefficients $w_{mk}(i)$ are arranged as a single vector, since each array $\mathbf{w}_i$ is itself a column vector of length MK. The total vector length is therefore MKI. In the earlier case with no transfer function on the controller output, the controller coefficients were expressed by elements $\mathbf{h}_i$, each $\mathbf{h}_i$ being an LxK array. The arrangement of controller coefficients as a column vector was carried out to allow an array of filtered reference signals to be defined.

The block Toeplitz matrix to be inverted has sides of dimension MKI. Thus in a situation with for example six reference signals (K = 6), four secondary sources (M = 4) and 128 filter coefficients (I = 128), the optimal filter coefficients are obtained by inverting a matrix of dimension 3072 x 3072. This would appear to be a formidable problem, but by noting that the matrix is block Toeplitz and using Robinson's recursive method a system of equations of this dimension can be solved in around 10-15 minutes using a fast desktop computer (Masscomp).

To complete the analysis, we can note that the minimum value of the cost function J_{p0} is given by:

$$J_{p0} = \mathbf{R}_{dd}(0) + \sum_{i=0}^{I-1} \tilde{\mathbf{w}}_i^T \mathbf{R}_{rd}(i) \tag{2.3.30}$$

where $\tilde{\mathbf{w}}_i$ is the optimum value of the controller coefficients.

2.3.3 Effort coefficient

The control filters calculated in practice by solving Equation (2.3.29) were found in some cases to be oscillatory at around half the sampling frequency. The problem was apparently due to ill-conditioning of the block Toeplitz matrix, since both the reference signals and the primary noise had very small high-frequency components. In order to avoid unnecessary controller action a term was added to the cost function which penalised large control filter coefficients:

$$J_p = E[\mathbf{e}_n^T \mathbf{e}_n] + \beta \sum_{i=0}^{I-1} \mathbf{w}_i^T \mathbf{w}_i \tag{2.3.31}$$

which is similar to the control 'effort' term used by Elliott *et al* [1987]. The second term is proportional to the sum of the squares of the filter coefficients. When J_p is minimised, the resulting optimal filters reduce both the sound field and the control action of the filters. The constant β determines the weighting given to the effort term. When the effort term is included in the above analysis, Equation (2.3.29) is modified in that β is added to each element of the principal diagonal of $\mathbf{R}_{rr}(0)$. It was found that even for very small values of β, which had a negligible effect on the minimum value of the sum of errors squared, the oscillatory nature of the filter coefficients was suppressed allowing clearer interpretation.

2.4 Implementation using adaptive filters

The Widrow-Hoff stochastic gradient algorithm [Widrow *et al*,1985] is widely used in electrical adaptive filtering problems to adapt the filters and minimise a desired cost function. It is robust and requires very few arithmetic operations, making it suitable for real-time applications. The method is to calculate at each time step the instantaneous gradient of a suitable cost function (such as squared error) with respect to each filter coefficient. Each filter coefficient is then adjusted in such a direction as to reduce the cost function. The adjustment is by an amount proportional to the gradient, the constant of proportionality being called the convergence coefficient. Provided the cost function has a unique minimum with respect to the filter coefficients and the convergence coefficient is not too high, the algorithm will find this minimum by optimising the filter coefficients.

Elliott *et al* [1987] have shown how the Widrow-Hoff algorithm can be applied to the situation with one reference signal and multiple speakers and microphones, yielding the Multiple-Error filtered-x algorithm. We present here the corresponding analysis for the case with multiple reference signals as well as speakers and microphones. The nomenclature is the same as in Section 2.3.2 above.

The vector of error signals $\mathbf{e}_n$ is given by:

$$\mathbf{e}_n = \mathbf{d}_n + \sum_{i=0}^{I-1} \mathbf{r}_{n-i}{}^T\mathbf{w}_i \qquad (2.4.1)$$

The cost function is:

$$J_p = E[\mathbf{e}_n{}^T\mathbf{e}_n] + \beta\sum_{i=0}^{I-1} \mathbf{w}_i{}^T\mathbf{w}_i \qquad (2.4.2)$$

The stochastic gradient algorithm is :

$$h'_{mk}(i) = h_{mk}(i) - \mu\frac{\partial J_p}{\partial h_{mk}(i)} \qquad (2.4.3)$$

where the $h_{mk}(i)$ are coefficients of the individual FIR control filters. The prime signifies the updated value. Writing out J_p in full we have

$$J_p = E[\sum_{l=1}^{L} e_l^2(n)] + \beta\sum_{i=0}^{I-1}\sum_{m=1}^{M}\sum_{k=1}^{K} h_{mk}^2(i) \tag{2.4.4}$$

The derivative with respect to $h_{mk}(i)$ can thus be expressed by:

$$\frac{\partial J_p}{\partial h_{mk}(i)} = E[\sum_{l=1}^{L} \frac{\partial J_p}{\partial e_l} \cdot \frac{\partial e_l}{\partial h_{mk}(i)}] + 2\beta h_{mk}(i) \tag{2.4.5}$$

But

$$e_l(n) = d_l(n) + \sum_{i=0}^{I-1}\sum_{m=1}^{M}\sum_{k=1}^{K} r_{lmk}(n-i)h_{mk}(i) \tag{2.4.7}$$

so that

$$\frac{\partial e_l(n)}{\partial h_{mk}(i)} = r_{lmk}(n-i) \tag{2.4.8}$$

and thus

$$\frac{\partial J_p}{\partial h_{mk}(i)} = E[\sum_{l=1}^{L} 2e_l(n)r_{lmk}(n-i)] + 2\beta h_{mk}(i) \tag{2.4.9}$$

The Multiple Error filtered-x LMS algorithm to update the filter coefficients uses the instantaneous value of this derivative and is therefore:

$$h'_{mk}(i) = (1 - 2\mu\beta)h_{mk}(i) - 2\mu e_l(n)r_{lmk}(n-i) \tag{2.4.10}$$

where the filtered reference signal $r_{lmk}(n)$ (defined in Sect. 2.3.2 above) is the signal which results when the kth reference signal x_k is applied to FIR filter $c_{lm}(j)$

2.5 Conclusion

This Chapter has set out the theoretical basis for multichannel feedforward active control of linear random sound fields measured by microphones at a number of discrete points. Analysing the problem in the frequency domain has yielded expressions for the optimum unconstrained control filters and the maximum possible sound reductions. The time-domain analysis has provided practical specifications for multiple-channel finite impulse response causal control filters. In Chapter 3 this form of analysis is adapted to the specific model problem of minimising the sound field in a rectangular box; in Chapter 4 the results developed in this Chapter are applied directly to measured vehicle data to predict the sound reductions which could be achieved by a random noise active control system.

3 STRUCTURAL-ACOUSTIC SIMULATIONS

3.1 Introduction

Provided the windows are shut and any exterior openings are sealed, the road noise inside a car arises from vibration of the roof, floor and other panels surrounding the interior cavity. The design of an active noise control system thus depends on the acoustic and vibration properties of not only the interior cavity but also the body panels, including the interaction between them. When designing an active control system, some of the questions which need to be addressed are:

- how many interior loudspeakers would be required for active control
- where they should ideally be located in relation to the vibrating panels
- whether accelerometers attached to the body panels would provide suitable reference signals
- how many accelerometers would be required
- where they should be placed

Useful progress can be made by trial and error, measuring noise and vibration at speed in a particular car on the road and experimenting with different positions of the sensors. However, what is required is some understanding of the physical principles involved. This can be gained by considering a model problem, a simplified situation which has the essential characteristics of the real problem but is simple enough to reveal underlying principles.

For the case of a vehicle we consider the mathematics of a rectangular hard-walled enclosure bounded on one side by a thin plate. A computer program calculates the effect of applying forces with a random waveform at particular positions on the plate. The program includes a description of the plate vibration, the interior noise field and the reductions available with an active noise control system in various configurations. Using this model it is possible to compare different positions of the secondary sources in relation to the vibrating plate; to use either the applied force signals or notional accelerometers on the plate as reference signals for active control and compare the results; and to investigate the effect of various accelerometer locations on the plate.

Section 3.2 reviews two earlier studies of active sound control in enclosures, while Section 3.3 presents the theory for the model. The remaining Sections present the calculated results.

3.2 Active control of sound in a rectangular enclosure

3.2.1 Control of harmonic sound by secondary forces applied to plate

The problem of active control of harmonic sound in a rectangular cavity bounded on one side by a panel (*ie* a thin plate) has been considered by Pan *et al* [1990]. In this theoretical study, noise from a notional exterior primary acoustic source was incident on the panel and was transmitted through it into the cavity. The control was achieved not by acoustic secondary sources inside the enclosure but by a secondary actuator applied to the panel.

The panel and cavity modes were calculated independently and a degree of crosscoupling was included in both directions. The authors minimised the acoustic potential energy in the enclosure. They found that the control action at different natural frequencies depended on whether a mode of the coupled system was panel-controlled or cavity-controlled. (A panel-controlled mode was defined to be one in which most of the energy was in the panel; similarly for a cavity-controlled mode most of the energy was in the cavity.) In the case of panel-controlled modes the secondary force actuator reduced the panel amplitude and hence the cavity mean squared pressure. However, each cavity-controlled mode typically involved contributions from several panel modes. In this case the single secondary actuator acted to alter the amplitude and phase of each panel mode in such a way that the *radiated power* to the cavity was minimised. In the course of doing this the amplitude of individual panel modes was increased in some cases.

3.2.2 Control of random sound by secondary sources in the enclosure

Some of the basic features of random sound control in an enclosure were established by Joplin *et al* [1989,1990]. This numerical simulation described a single primary source and a single secondary source inside a rectangular enclosure. The primary noise signal formed the reference for a feedforward control system in which a causal control filter was calculated to minimise the energy in the enclosure. Both the enclosure dimensions and the source locations were chosen to be the same as in the simulation of harmonic noise control by Bullmore *et al* [1987], reported above in Sect. 1.3.1. Figure 1.4 shows a schematic diagram of the enclosure. In Joplin's simulation only one of the secondary sources was active at a time. The primary signal was white noise, with a low-pass filter applied to avoid aliasing problems in the time-domain calculation of the optimal causal filter.

Figure 3.1 shows the impulse responses of the optimal controllers driving the secondary source from the waveform of the primary in this study for the secondary source in four separate positions; Figure 3.2 shows the corresponding spectra of the potential energy (see Sect 3.3.2 below for a definition of this for random sound) with and without control.

The main conclusions of the study were:

(1) Good cancellation at all frequencies was achieved with source S1, located next to the primary. This source was able to produce a close approximation to the primary sound field by acting with almost a phase-inverted replica of the primary waveform.

(2) The performance of the other sources depended on which modes they were able to excite. As in Bullmore's simulation, a secondary source located close to a nodal plane for a particular mode was unable to excite that mode, and thus unable to control it.

(3) An important part of each filter impulse response was a delayed, inverted version of the primary source signal. (The propagation time from primary to secondary source is marked on each graph in Figure 3.1) The implication of this is that the secondary source acts to some extent as a power absorber.

(4) A characteristic of the random noise control system was that it tended to redistribute energy away from the peaks of the energy spectrum, giving *increased* levels in the troughs (Figure 3.2). This was in contrast to the results for harmonic sound control (Figure 1.6), where the acoustic potential energy was not increased at any frequency by the action of the control system. The difference arises because of the additional constraint of causality for the random noise control system, as will be seen in Sect. 3.4 below.

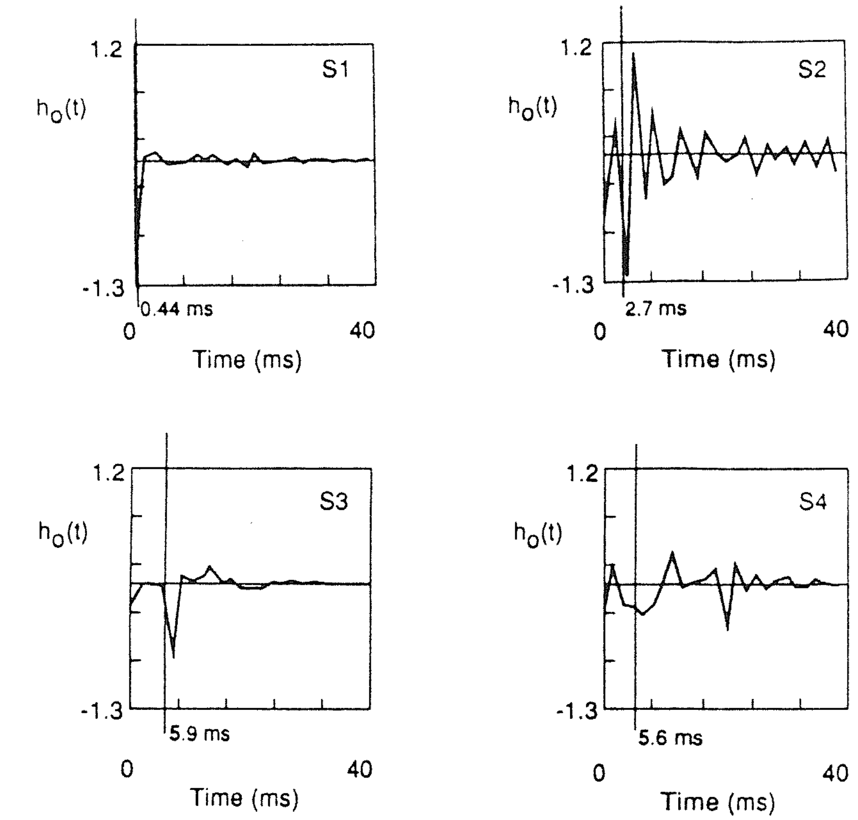

Figure 3.1: The impulse responses of the optimal controllers for source positions S1-S4 (Joplin simulation)

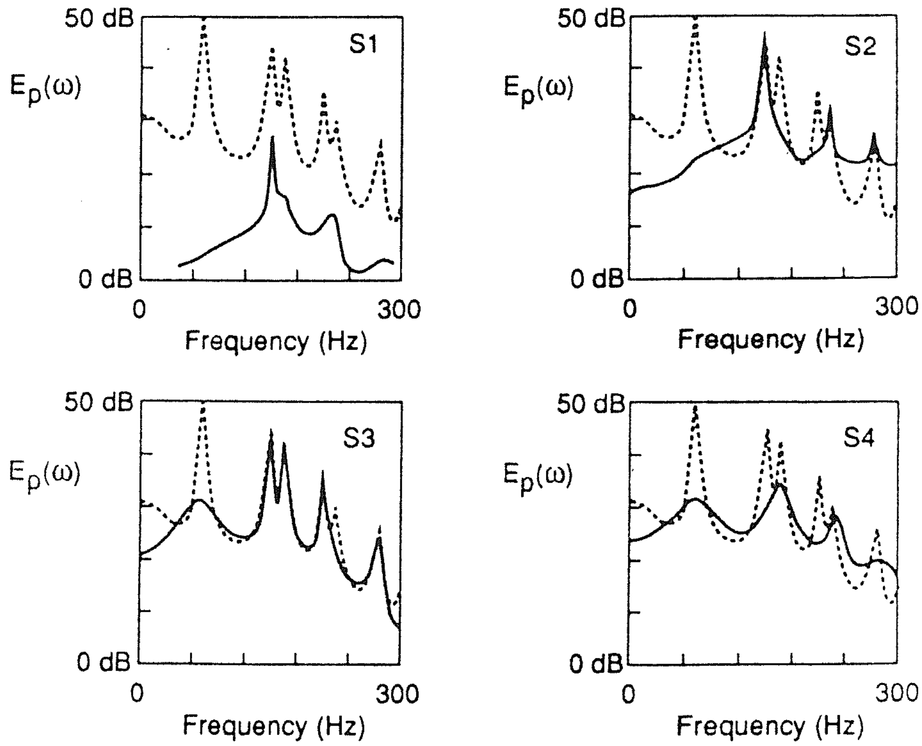

Figure 3.2: The residual energy for source positions S1-S4 (Joplin simulation)

3.3 Active control of random sound in a rectangular enclosure bounded on one side by a thin plate

3.3.1 Equations for plate and enclosure

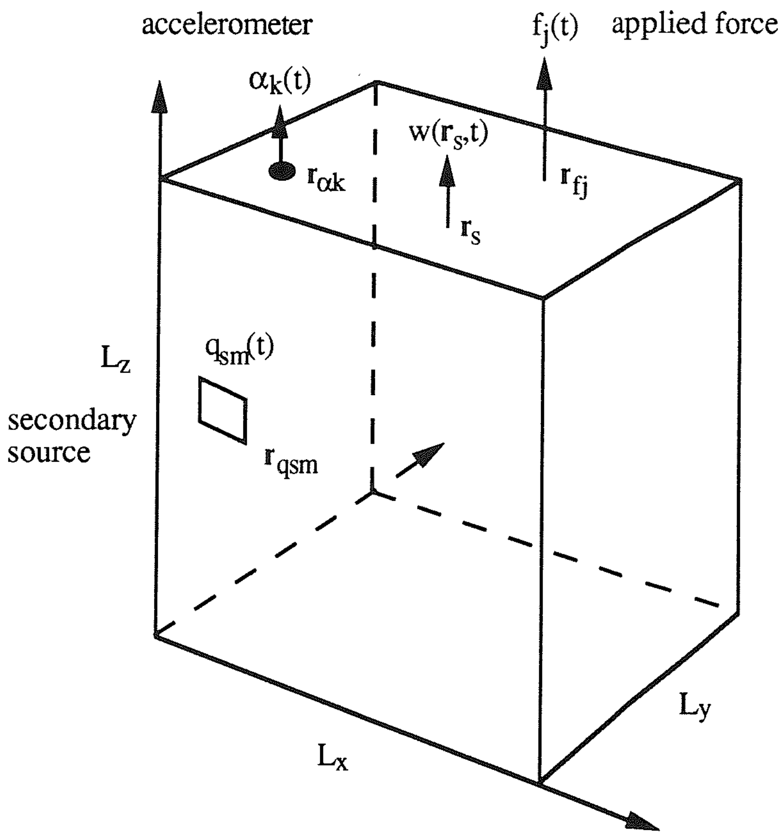

Figure 3.3: Schematic diagram of rectangular cavity bounded by plate

Figure 3.3 shows the hard-walled rectangular enclosure, dimensions L_x, L_y, L_z. A thin, simply-supported plate forms the top surface of the enclosure (*ie* the plane $z = L_z$). $\mathbf{r}$ is the 3D position vector defining an arbitrary point in the volume. $\mathbf{r}_s$, $\mathbf{r}_{fj}$ and $\mathbf{r}_{\alpha k}$ are locations on the plate. J independent point forces $f_j(t)$ are applied normal to the plate at locations $\mathbf{r}_{fj}$ ($j = 1,2 .. J$). Plate vibration is detected by K accelerometers located at $\mathbf{r}_{\alpha k}$ ($k = 1,2 .. K$). The accelerometer outputs are $\alpha_k(t)$. Vertical displacement at a general point $\mathbf{r}_s$ on the plate is given by $w(\mathbf{r}_s,t)$. The forces, accelerations and displacement are taken to be positive away from the enclosure. The M secondary acoustic sources are represented as square pistons set into the walls of the cavity (following Bullmore [1987]). Their locations and volume velocities are respectively $\mathbf{r}_{qsm}$ and $q_{sm}(t)$ ($m = 1,2,..M$).

The dynamics of a simply-supported plate coupled to a cavity are well-established [Fahy,1985] and are set out in Appendix 3.1. To simplify the analysis, it is assumed that there is no coupling from the acoustic cavity to the plate: only coupling from the plate to the cavity is allowed for. The plate motion is thus determined purely by the external forces acting on it and not by the acoustic pressure in the cavity. The acoustic field in the cavity, however, is driven by the motion of the plate. With this simplification the model shows the main characteristics of active sound control in an enclosure and gives useful insights. However it is limited in that it does not include the feedback path from the secondary acoustic sources to the reference accelerometers attached to the plate.

The vibration of the plate and the acoustic pressure in the enclosure are described by the solutions of two coupled sets of modal equations. These equations define

(1) the modal plate displacement for the pth mode, $b_p(t)$ $(p = 1,2,...)$, and
(2) the modal acoustic pressure $a_n(t)$ $(n = 0,1,2,...)$.

Modal hysteretic damping η has been included for the plate and viscous damping ζ for the acoustic modes. The equation for modal plate displacement (written here without damping) is:

$$\ddot{b}_p(t) + \omega_p^2 b_p(t) = \frac{1}{S\sigma} \sum_{j=1}^{J} f_j(t)\, \phi_p(\mathbf{r}_{fj}) \quad p = 1,2,... \qquad (3.3.1)$$

The equation for modal acoustic pressure is:

$$\ddot{a}_n(t) + 2\zeta\omega_n \dot{a}_n(t) + \omega_n^2 a_n(t) = \frac{\rho_0 c_0^2}{V}\left[\sum_{m=1}^{M} \dot{q}_{sm}\, \psi_n(\mathbf{r}_{qsm}) - S \sum_{p=1}^{\infty} \ddot{b}_p(t)\, C_{np}\right]$$
$$n = 0,1,2,... \qquad (3.3.2)$$

Equations (3.3.1) define the modal plate displacement resulting from the J point forces $f_j(t)$ applied to the plate. The $\phi_p(\mathbf{r}_s)$ are the modeshape functions of the plate and the $\psi_n(\mathbf{r})$ are the modeshape functions of the enclosure. S is the surface area of the plate; σ is its mass per unit area. The full nomenclature is given in Appendix 3.1. Equations (3.3.2) define the modal acoustic pressure, which depends on the volume velocity q_{sm} of the M secondary sources and also the primary noise created by the plate motion. The modal coupling factors C_{np} are given by

$$C_{np} = \frac{1}{S} \int_S \phi_p(\mathbf{r}_s)\, \psi_n(\mathbf{r}_s)\, ds \qquad (3.3.3)$$

where the $\psi_n(\mathbf{r}_s)$ are the modeshape functions of the enclosure evaluated at the plate surface. For a simply-supported plate the modeshapes are sine functions while those for a hard-walled rectangular cavity are cosine functions. Thus for some combinations of modes the integral of the product, and thus C_{np}, disappears with this geometry. In fact it turns out that each plate mode couples into only one quarter of the acoustic modes. Nevertheless the essential features of the system are represented because of the generally high density of acoustic and structural modes. In the case of a more complicated geometrical shape such as a car, the modes are all likely to be coupled.

The actual displacement of the plate at any location $\mathbf{r}_s$ on the plate, the accelerometer outputs and also the acoustic pressure at any point $\mathbf{r}$ in the enclosure are all given by the appropriate modal summations:

Plate displacement:

$$w(\mathbf{r}_s,t) = \sum_{p=1}^{\infty} b_p(t)\phi_p(\mathbf{r}_s) \qquad (3.3.4)$$

Accelerometer outputs:

$$\alpha_k(t) = \sum_{p=1}^{\infty} \ddot{b}_p(t)\phi_p(\mathbf{r}_{\alpha k}) \qquad (3.3.5)$$

Acoustic pressure:

$$p(\mathbf{r},t) = \sum_{n=0}^{\infty} a_n(t)\psi_n(\mathbf{r}) \qquad (3.3.6)$$

3.3.2 Cost function: acoustic potential energy

As in the earlier studies by Bullmore *et al* [1987] and Joplin *et al* [1990], the control objective here is to minimise the acoustic potential energy throughout the enclosure. The total time-averaged acoustic potential energy E_p is given by:

$$E_p = \frac{1}{2\rho_0 c_0^2} \int_V E[p^2(\mathbf{r},t)]dV \qquad (3.3.7)$$

where E[...] denotes expected value and V is the volume of the enclosure. Expressing $p(\mathbf{r},t)$ as a sum of modes, and performing the volume integral (Recalling that the modeshapes form an orthogonal set), it follows that:

$$E_p = \frac{V}{2\rho_0 c_0^2} \sum_{n=0}^{\infty} E[a_n^2(t)] \qquad (3.3.8)$$

Thus the minimum acoustic potential energy can be found by minimising the sum of squares of the acoustic mode amplitudes. The method of calculating this minimum value is set out in the next Section. The exact value of acoustic potential energy is given by the infinite sum of modal amplitudes, but in practice a finite sum is carried out over a limited number of modes. In the simulations presented in Sections 3.4 and 3.5 all the acoustic and structural modes up to 750 Hz were included along with some at higher frequencies; the results are plotted on frequency scales up to 300 Hz. For the 3 mm plate discussed below the calculation involved 196 modes of flexural vibration, 53 of which were below 300 Hz; for the enclosure, 287 acoustic modes were included of which 28 were below 300 Hz. Because the acoustic modes were so heavily damped in this case, small differences in the predicted responses were observed if the number of acoustic modes considered in the summation was, for example, doubled. The form of the results was, however, unaltered by these slight changes and the conclusions remain unaffected.

3.3.3 Active control scheme

In this Section the optimal causal filters will be calculated from autocorrelation and crosscorrelation functions using an equation similar to Eqn. (2.3.29) developed in Section 2.3 above. The difference here is that instead of the minimisation being performed with respect to L microphone signals, it is performed with respect to N acoustic mode amplitudes. The form of the resulting equations, however, is identical to (2.3.29). The remainder of this Section (3.3) together with Appendix 3.1 will be concerned with the details of the models used for the structural and acoustic characteristics of the model problem under consideration.

The forces applied to the plate are specified not as time series but as bandlimited white noise sources; hence the correlation functions will have to be found from the corresponding spectral density functions by inverse Fourier transform. Thus it will be necessary to start by writing down frequency-domain expressions for the spectral density functions.

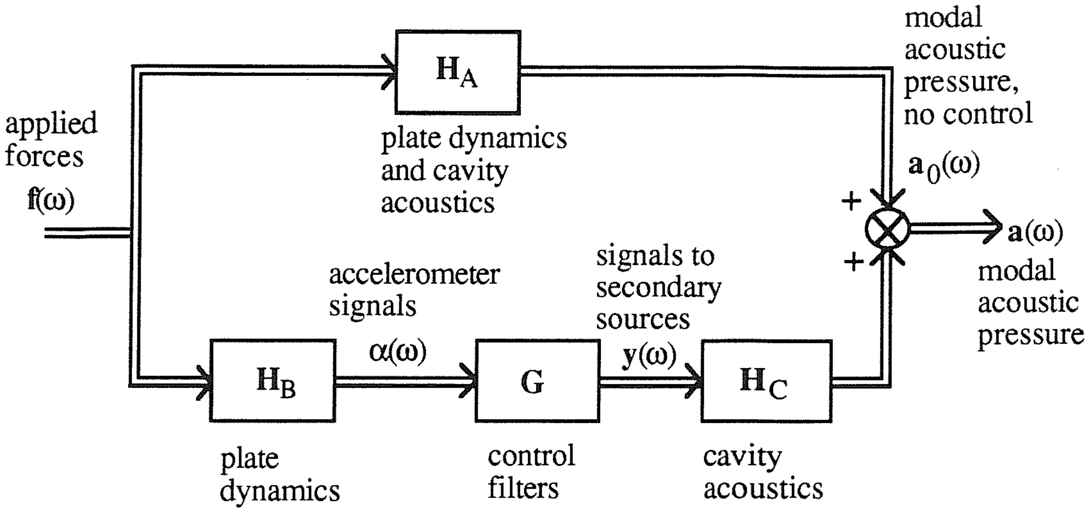

Figure 3.4: Active control of modal acoustic pressure in an enclosure bounded by a plate

Figure 3.4 shows the control scheme for active control of noise in the enclosure of Figure 3.3. The forces, accelerations, secondary source strengths and modal amplitudes are expressed in the frequency domain by taking the Fourier transform of some finite length T of the random time-history. Thus the jth applied force $f_j(t)$ becomes $f_j(\omega)$ where

$$f_j(\omega) = \int_{-T/2}^{T/2} f_j(t) e^{-j\omega t}\, dt$$

and so on. The J applied forces are expressed in vector form by $\mathbf{f}(\omega)$. The nomenclature for Figure 3.4 is thus:

$\mathbf{f}(\omega)$	vector (length J) of forces $f_j(\omega)$ applied to plate
$\underline{\alpha}(\omega)$	vector (length K) of signals from accelerometers $\alpha_k(\omega)$ attached to plate
$\mathbf{q}_s(\omega)$	vector (length M) of secondary source strengths $q_{sm}(\omega)$
$\mathbf{a}_0(\omega)$	vector (length N) of modal acoustic pressure amplitudes due to the primary sources alone (no active control)

$\mathbf{a}(\omega)$	vector (length N) of modal acoustic pressure amplitudes with secondary sources active
$\mathbf{H}_B(\omega)$	KxJ matrix of frequency response functions between the applied forces $\mathbf{f}(\omega)$ and the accelerometer signals $\underline{\alpha}(\omega)$. Individual element: H_{Bkj}
$\mathbf{H}_A(\omega)$	NxJ matrix of frequency response functions between the applied forces $\mathbf{f}(\omega)$ and the N modal pressure amplitudes $\mathbf{a}_0$ (*ie* in the absence of control)
$\mathbf{H}_C(\omega)$	NxM matrix of frequency response functions between the secondary sources $\mathbf{q}_s(\omega)$ and the modal pressure amplitudes of the acoustic pressure due to the secondary sources alone. Individual element: H_{Cnm}
$\mathbf{G}(\omega)$	MxK matrix of frequency response functions for the control filters

The control scheme as drawn shows the reference signals for control taken from accelerometers attached to the plate ($\alpha_k(\omega)$). This configuration is used for some but not all of the simulations. In other cases the applied forces are used directly as reference signals. In these cases $\mathbf{H}_B$ is simply set to the JxJ unit matrix.

The objective of the calculation is to find the appropriate value of $\mathbf{G}$ to minimise the acoustic potential energy in the enclosure. The procedure is similar to the multichannel time-domain calculation given in Section 2.3 above, except that instead of multiple microphones, it is the sum of squares of the acoustic modal amplitudes which is minimised. The applied forces $f_j(\omega)$ are defined to be independent white noise sources, that is their power spectral densities are defined by:

$$\lim_{T\to\infty} E[\tfrac{1}{T} f_i^* f_j] = \begin{cases} A_j & i=j \\ 0 & i\neq j \end{cases} \qquad (3.3.9)$$

where the A_j (j=1,2,..J) are constants. A_j is the power spectral density of the jth applied force. (In practice low-pass filters are applied to these power spectral density values to prevent aliasing in the time-domain calculation of the optimal filters, as explained below.)

The frequency response functions $\mathbf{H}_A$, $\mathbf{H}_B$, $\mathbf{H}_C$ follow directly from the equations for the dynamics of the panel and acoustic enclosure written out above (Equations (3.3.1) - (3.3.5)) by taking the Fourier transforms of a finite record length T. For example the frequency response function relating the jth force $f_j(\omega)$ to the nth acoustic mode without control $a_{0n}(\omega)$ is given by taking the Fourier transform of Equations (3.3.1) and (3.3.2) and combining them to eliminate $b_p(\omega)$. Noting that $q_{sm}(\omega) = 0$ with no active control the result in this case is:

$$\frac{a_{0n}}{f_j}(\omega) = \frac{\rho_0 c_0^2 \omega^2}{\sigma V(\omega_n^2-\omega^2+2j\zeta\omega_n\omega)} \sum_{p=1}^{P} \frac{\phi_p(r_{fj})C_{np}}{(\omega_p^2-\omega^2) + j\eta\omega_p^2} \qquad (3.3.10)$$

where the summation over the plate modes has been taken to P terms. This frequency response forms the (n,j)th element of matrix $\mathbf{H}_A(\omega)$. The elements of $\mathbf{H}_B$ and $\mathbf{H}_C$ follow by similar algebraic manipulation.

The next step is to identify a set of filtered reference signals, as discussed in Chapter 2. In this case each filtered reference signal $F_{nmk}(\omega)$ is obtained when the kth reference signal $\alpha_k(\omega)$ is filtered by the frequency response function $H_{Cnm}(\omega)$ representing the response of the nth mode to the mth secondary source (H_{Cnm} is the (n,m)th element of $\mathbf{H}_C$):

$$\begin{aligned} F_{nmk}(\omega) &= \alpha_k H_{Cnm} \\ &= \sum_{j=1}^{J} f_j H_{Bkj} H_{Cnm} \end{aligned} \qquad (3.3.11)$$

As in Chapter 2 an NxMK array of filtered reference signals is formed:

$$\mathbf{F}(\omega) = \begin{bmatrix} F_{111} & F_{112} & \cdots & F_{1MK} \\ F_{211} & & & \\ \vdots & & & \\ F_{N11} & & \cdots & F_{NMK} \end{bmatrix} \qquad (3.3.12)$$

In this simulation the correlation functions required to calculate the causal control filters using Eqn. (2.3.29) are not available from measured time-histories and will need to be calculated from spectral density functions. The spectral density functions which are needed are the auto-spectral density of the filtered reference signals and the cross-spectral density between the filtered reference signals $\mathbf{F}$ and the modal acoustic pressures without control, $\mathbf{a}_0$.

The auto-spectral density matrix $\mathbf{S}_{FF}(\omega)$ is defined as follows:

$$\mathbf{S}_{FF}(\omega) = \lim_{T\to\infty} E[\tfrac{1}{T}\mathbf{F}^H\mathbf{F}] \qquad (3.3.13)$$

- an MKxMK matrix. This definition gives a form of matrix which is similar in form to the matrix of filtered reference correlation functions, Equation (2.3.25). An individual element (mk,m'k') of S_{FF} is given by:

$$S_{FFmkm'k'} = \sum_{n=0}^{N-1} \sum_{j=1}^{J} A_j H^*_{Cnm} H_{Cnm'} H^*_{Bkj} H_{Bk'j} \qquad (3.3.14)$$

This result is obtained by substituting (3.3.11) into (3.3.13) and noting that the applied forces are specified as independent white noise sources, (3.3.9).

The cross-spectral density matrix between $\mathbf{F}$ and $\mathbf{a}_0$, $\mathbf{S}_{Fa,}$ is similarly defined as follows

$$S_{Fa}(\omega) = \lim_{T\to\infty} E[\frac{1}{T}\mathbf{F}^H\mathbf{a}_0] \qquad (3.3.15)$$

- a column vector, length MK. The mkth element of $\mathbf{S}_{Fa}$ is given by

$$S_{Famk}(\omega) = \sum_{n=0}^{N-1} \sum_{j=1}^{J} A_j H^*_{Cnm} H^*_{Bkj} H_{Anj} \qquad (3.3.16)$$

The frequency response functions $\mathbf{H}_A$, $\mathbf{H}_B$ and $\mathbf{H}_C$ are all calculated from the physics of the coupled plate and enclosure as explained above. The A_j are the power spectral densities of the applied random forces, chosen constants which may vary from problem to problem. The locations of the forces, accelerometers (used as reference signals) and secondary sources are implicit in the frequency response functions $\mathbf{H}_A$, $\mathbf{H}_B$ and $\mathbf{H}_C$ as the locations determine the values of the modeshape functions: see for example Equation (3.3.10). The autocorrelation and crosscorrelation matrices which are required to calculate the optimal causal filters are obtained from $\mathbf{S}_{FF}$ and $\mathbf{S}_{Fa}$ by taking the inverse Fourier transform of each element.

In a practical computer simulation the frequency response functions presented above are calculated over a chosen frequency range and with a chosen frequency resolution. When the discrete Fourier transform is carried out these choices determine the sample-rate and duration of the resulting time-histories of the correlation functions. Special measures are required to avoid aliasing distortion when this process is carried out. For this reason it is not in fact practical to represent the applied forces as pure white noise sources, with constant power spectral density A_j. It is necessary, as noted by Joplin [1989], to apply low-pass filters to the incoming primary excitation signals. In this simulation Butterworth filters are used, so that the power spectral density of the jth applied force $f_j(\omega)$ is given by

$$A_j = \frac{A_j'}{1 + (\omega/\omega_f)^{2p}} \tag{3.3.17}$$

where here p is the order of the filter and A_j' is a constant.

The autocorrelation and crosscorrelation matrices which result from taking the inverse Fourier transform of S_{FF} and S_{Fa} are in exactly the form required to calculate the optimal causal filters using Equation (2.3.29). To apply this equation, the correlation functions are truncated to the length chosen for the optimal FIR filters (I points, say) and time-points before t=0 are discarded. Discarding the points in the cross-correlation function before t=0 makes the filters causal. Inversion of the Toeplitz matrix of autocorrelation functions thus results in a set of MK I-point causal FIR filters which will minimise the sum of squares of the modal pressures in the enclosure.

3.3.4 Acoustic potential energy spectrum

It is useful to display the frequency distribution of the acoustic potential energy. As in the earlier work [Joplin *et al*,1990] an acoustic potential energy spectral density function is defined by:

$$E_p(\omega) = \frac{1}{2\rho_0 c_0^2} \int_V S_{pp}(\mathbf{r},\omega)dV \tag{3.3.18}$$

where $S_{pp}(\mathbf{r},\omega)$ is the acoustic pressure spectral density at a point $\mathbf{r}$ in the enclosure. Expressing acoustic pressure as a sum of modes enables the potential energy spectral density to be written as (see Appendix 3.2):

$$E_p(\omega) = \frac{V}{2\rho_0 c_0^2} \sum_{n=0}^{\infty} S_{aan}(\omega) \tag{3.3.19}$$

where $S_{aan}(\omega)$ is the auto-spectral density of modal acoustic pressure $a_n(\omega)$ (nth mode). With active control $S_{aan}(\omega)$ is given by:

$$S_{aan}(\omega) = \lim_{T\to\infty} E[\frac{1}{T} a_n^* a_n] \qquad n = 0,1,2,... \qquad (3.3.20)$$

Alternatively with no active control:

$$S_{aan}(\omega) = \lim_{T\to\infty} E[\frac{1}{T} a_{0n}^* a_{0n}] \qquad n = 0,1,2,... \qquad (3.3.21)$$

Calculation of $S_{aan}(\omega)$ is straightforward once the optimal causal filters have been found as in the previous Section. It is necessary to calculate the Fourier transform of the optimal causal filters to create MxK matrix **G**, and then the various frequency response functions shown in Figure 3.4 can be combined. In vector notation:

$$\mathbf{a}_0(\omega) = \mathbf{f}\mathbf{H}_A \qquad (3.3.22)$$

$$\mathbf{a}(\omega) = \mathbf{f}[\mathbf{H}_A + \mathbf{H}_B\mathbf{G}\mathbf{H}_C] \qquad (3.3.23)$$

$S_{aan}(\omega)$ follows when the chosen autospectral densities A_j of the applied force signals **f** are substituted into the equation using (3.3.9).

3.4 Number and location of secondary sources

3.4.1 Location with respect to source of noise

The studies by Bullmore and Joplin summarised above in Sections 1.3.1 and 3.2.2 considered a rectangular cavity in which only eight modes had their natural frequencies below 300 Hz. Light damping (1%) was assumed, giving clear peaks in the potential energy spectrum. In this Section we extend these calculations to the control of random sound in a rectangular enclosure of roughly appropriate dimensions for the interior of a car. The dimensions 1.46 x 1.27 x 2.63 m have been taken, giving 28 acoustic modes below 300 Hz. In order to represent the acoustic damping of the interior trim and upholstry, the damping ratio of the modes has been taken to be 10%. This gives a well-damped enclosure. Initially the vibrating plate will be omitted and instead we will assume a small primary source of random sound, a piston as in the earlier work. The primary source is located at the position (0.4,0.3,0), as shown in Figure 3.5.

Both Bullmore and Joplin noted that a secondary source placed in a corner of the enclosure couples into all the acoustic modes. It is therefore natural to use corner locations in this study. Figure 3.5 shows three corner locations for the single secondary source, each at different distances from the primary source. The corresponding reductions in potential energy are shown in Figure 3.6. Each graph shows the potential energy spectrum due to the primary source alone, *ie* with no control. The zeroth mode of the enclosure (uniform pressure) gives rise to a peak at

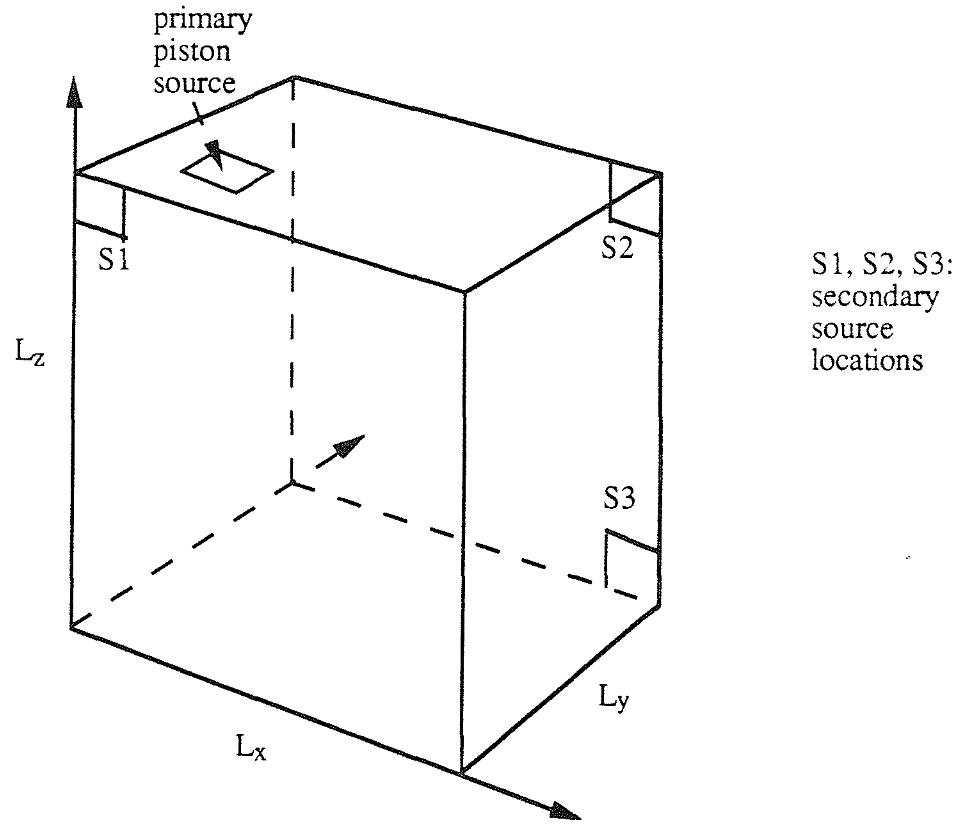

Figure 3.5: Simulation with single primary piston source: locations of secondary sources

low frequencies. There is also a peak at 65 Hz which arises from the first longitudinal mode of the box. The next peak at 134 Hz corresponds to a cluster of five modes between 117 Hz and 150 Hz. The remainder of the curve includes the effect of a further 21 overlapping modes up to 300 Hz. The calculation includes all acoustic modes up to 750 Hz. The graphs in Figure 3.6 also show the calculated reduction with a 128-point causal FIR filter (the optimum filter coefficients having been calculated as shown in Section 3.3.3 above); also the reduction with a filter which is not constrained to be causal. The FIR filter is of adequate length that the results are not affected significantly by filter truncation, so the difference between the two controlled fields in Figure 3.6 is due to the constraint of causality in the controller.

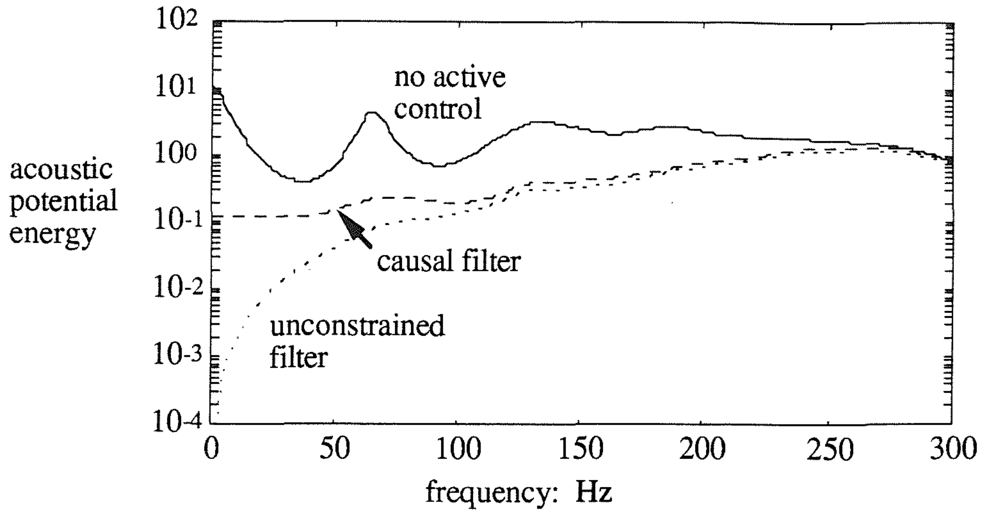

(a) Acoustic potential energy reduction due to source S1 alone

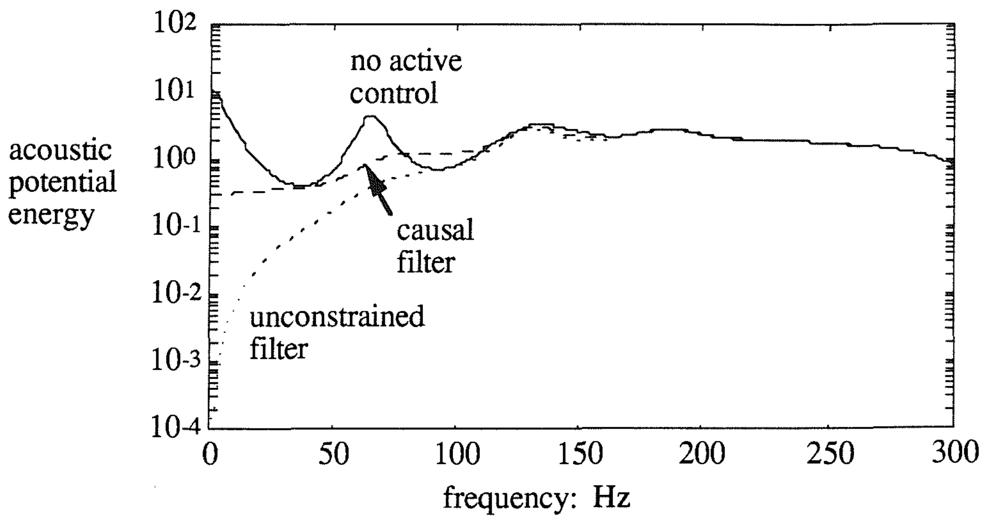

(b) Acoustic potential energy reduction due to source S2 alone

Figure 3.6(a),(b): Active control using one secondary source:
effect on acoustic potential energy
Note: one decade change in energy corresponds to 10 dB

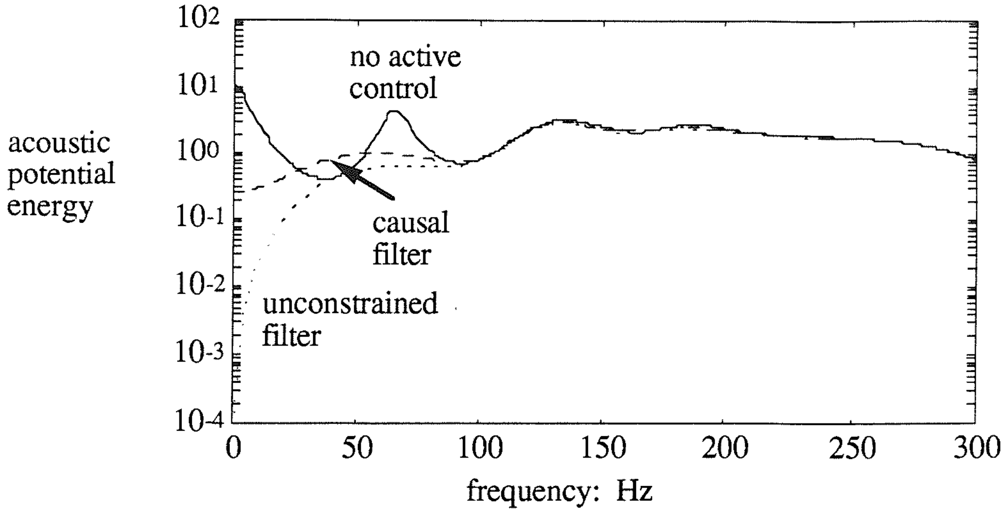

(c) Acoustic potential energy reduction due to source S3 alone

Figure 3.6(c) Active control using one secondary source: effect on acoustic potential energy

Substantial reductions are achieved over a wide frequency range using position S1, which is the closest to the primary source. In the other two cases there is no significant reduction above about 90 Hz, even with an unconstrained filter. These results are less favourable than those found by Joplin and arise because (1) the modal density is higher in the cavity being considered here and also (2) the acoustic damping is higher.

As in the earlier studies, the best reductions are obtained when the secondary source is close to the primary and so is able best to duplicate the primary acoustic field. In modal terms this means that the magnitudes of the various modeshape functions $\psi_n(\mathbf{r})$ at the secondary source are similar to their magnitudes at the primary source. Therefore it is possible to cancel a large number of modes at the same time using a single secondary source.

The situation is different when a secondary source is placed in a corner of the enclosure distant from the primary. All the modeshape functions have maximum magnitude in the corner of the cavity (positive or negative polarity) but a single secondary source can in general cancel only one mode at a time, because the modes form a set of independent single-degree-of-freedom systems. This explains the poor reductions above 90 Hz for secondary source positions S2 and S3. The peak in potential energy at 134 Hz is actually due to a group of five modes which overlap. The high degree of overlap means that little or no global control is possible with a single speaker at these frequencies. However the peak at 65 Hz is due to a single mode (the first longitudinal mode of the enclosure) and is controlled from all the secondary source positions.

3.4.2 Number of sources

Figure 3.7(a) shows the potential energy reduction using 128-point causal filters with four secondary sources located (i) in the bottom corners of the enclosure distant from

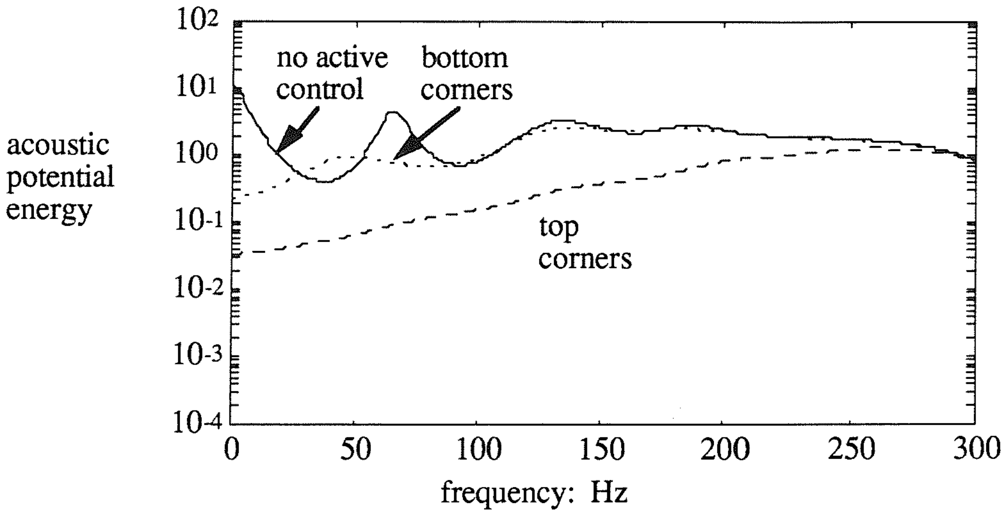

(a) active control using causally-constrained 128-pt filters

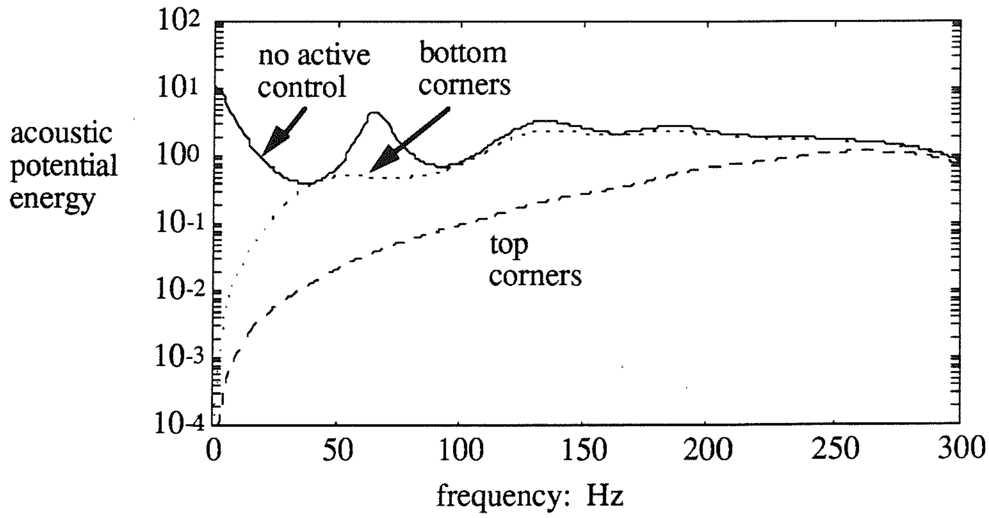

(b) active control using unconstrained filters

Figure 3.7: Acoustic potential energy reductions using four secondary sources (primary is piston source, see Fig 3.5)

the source; and (ii) in the four top corners close to the source. With all the sources positioned away from the primary piston there is some small reduction, but apart from the cancellation of the first longitudinal mode at 65 Hz the reduction is very modest. Even if non-causal filters are allowed (Figure 3.7(b)) the reductions above 90 Hz remain small due to the high modal density and high damping in the cavity. Also shown in Figure 3.7(a) and (b) is the corresponding result when the four secondary sources are placed in the top corners of the cavity, close to the primary source. Here the reduction is substantial, due mainly to the contribution of the source closest to the primary piston. (This source corresponds to S1 in Figure 3.5 above.)

Before introducing panel vibration into the problem we consider the susceptibility of the control system to time delays, still with a small piston as the acoustic primary source.

3.4.3 Susceptibility to delays

The reductions discussed so far for causally constrained filters have assumed that the primary source strength is detected, passed through the control filters and presented to the secondary sources without any delay. (The acoustic delay path from the secondary sources to the various parts of the sound field is however implicitly included in the model.) Practical control systems include anti-aliasing and reconstruction filters, which typically introduce several milliseconds of delay into the secondary path.

Figure 3.8 shows the causally constrained reduction using four secondary sources at the end of the enclosure closer to the primary source (as in Figure 3.7 above). Also shown are the reductions with 1 ms and 5 ms of delay introduced into the control chain. The fall-off in performance is very rapid. With even a short delay of 1 ms the control system is unable to match to primary outgoing sound. The time taken for sound to travel the length of the enclosure and back (2 x 2.63 m) is 15 ms, so the delayed control system is still able to cancel the reflections. However little can be achieved by cancelling the reflections because the cavity is so well-damped. Also shown is the unconstrained result which can be interpreted as that obtained if the secondary source had unlimited time advance and thus represents the best possible performance.

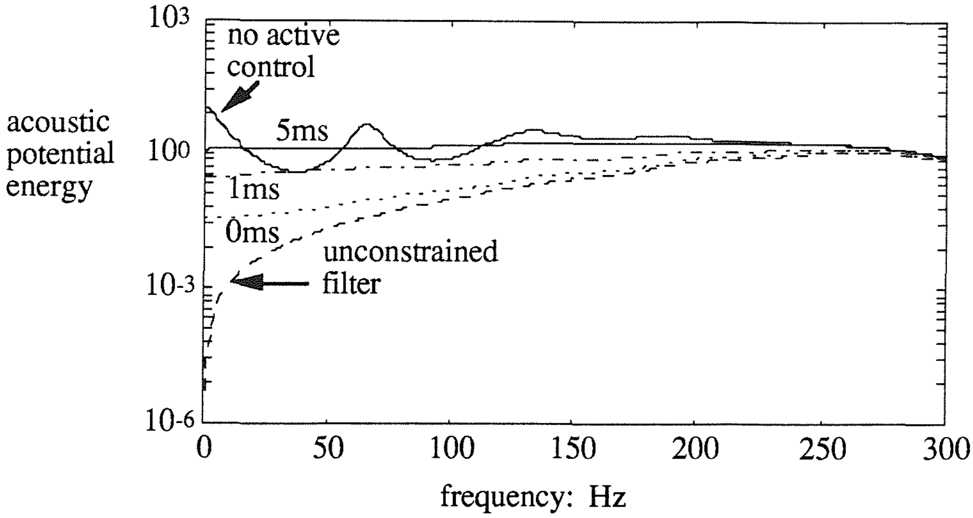

Figure 3.8: Effect of controller delays
(primary piston source, four sec sources in top corners)

Note: factor 10^3 change in energy corresponds to 30 dB

A practical control system would typically include some 6 ms of electronic delay. These results appear to suggest that active control of random sound in a well-damped car-sized enclosure is far from promising. In the next Section we consider the important differences which arise when the source of sound is a vibrating plate.

3.5 Plate vibration as a primary source of sound

3.5.1 Thick plate

It is useful to look first at the effect of having a thick plate as one side of the enclosure. This is physically unrealistic for the practical case of the car, but the behaviour is of interest because a thick plate has only a few modes of vibration in the frequency range being considered. It will thus be possible to see more clearly the mechanisms of sound generation and control. We consider a 20 mm steel plate which has six modes below 300 Hz, the lowest (1,1) mode being at 52 Hz. The plate dynamics are still calculated however by neglecting shear deformation and rotary inertia, so that only flexural waves are considered. The hysteretic damping factor of the plate is assumed to be η=5%. The plate forms the top surface of the enclosure as drawn in Figure 3.5.

The source of vibration is a single point force, located in the same position as the acoustic primary source in Figure 3.5. The reference signal for control is plate acceleration, measured by a notional accelerometer located at the point of application of the force. (The use of input force itself as a reference introduces other complications which will be discussed in the following Section.) The four acoustic secondary sources are located in the top corners of the cavity next to the plate.

Figure 3.10 shows the potential energy spectrum with and without active control using a causally constrained controller. The effect of each of the six plate modes can be clearly seen when this Figure is compared with Figure 3.7. With this geometry each plate mode couples into only one quarter of the acoustic modes, as noted in Section 3.3.1 above. However, the acoustic modes are sufficiently numerous and closely spaced that all the plate modes show up clearly in the acoustic potential energy spectrum.

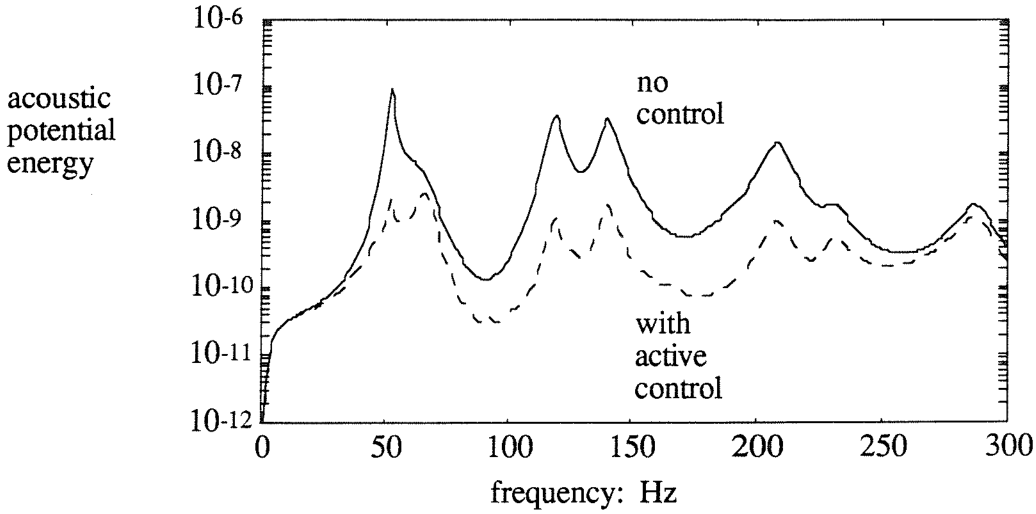

Figure 3.10: potential energy reduction with thick plate
(four secondary sources in top corners)

With four secondary sources located close to the plate, the attenuation is substantial: 15-20 dB reductions are observed at the peaks of the response. The impulse responses of the optimal filters calculated to give this result are shown in Figure 3.11. Each of them has a short impulse response, settling in about 128 ms, the length of the FIR control filter in this case.

As was the case with the primary piston source, the reductions are highly sensitive to the locations of the secondary sources. Figure 3.12 shows the results of using causal filters driving the four secondary sources in the four corners at the opposite (bottom) end of the cavity from the plate. In this case there is hardly any reduction at all. The

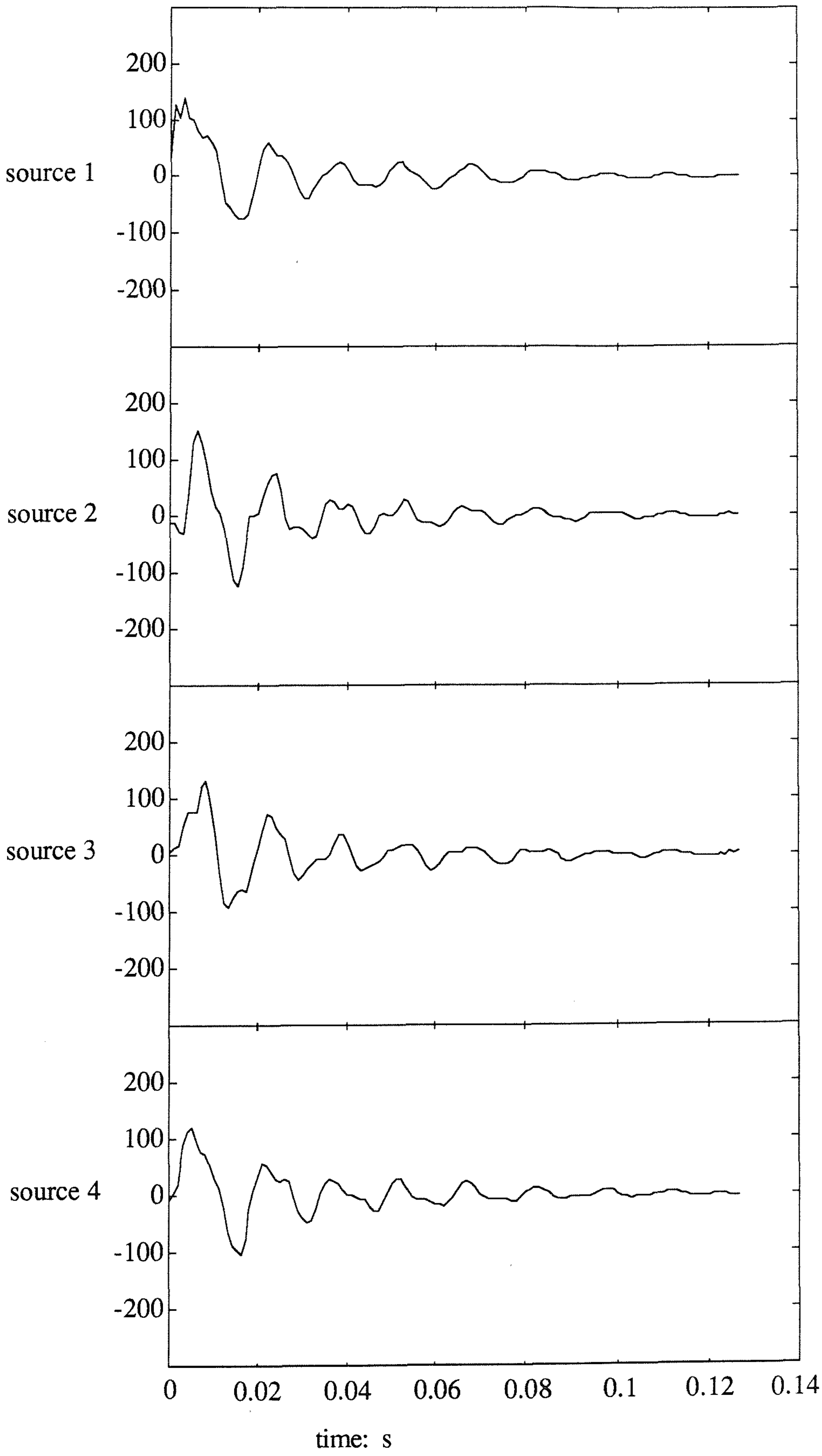

Figure 3.11: Impulse responses of optimal filters for Figure 3.10

result is similar if unconstrained filters are used. The poor reduction can again be attributed to the fact that at any one frequency the potential energy is shared between a number of overlapping acoustic modes which cannot be independently controlled by the four secondary sources. The poor reduction of the first plate mode at 52 Hz appears to be because the secondary sources are all at one end of the enclosure and so are unable to control the zero-order mode and the first longitudinal mode independently. These results suggest that in a well-damped cavity such as a vehicle interior it is important to place the secondary loudspeakers close to the primary source, whether it is a point acoustic source or a vibrating plate.

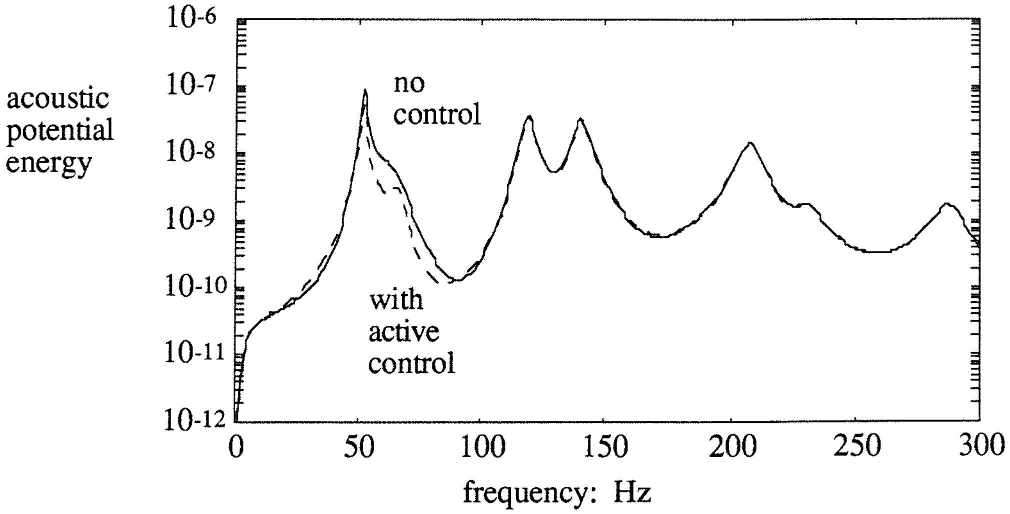

Figure 3.12: Potential energy reduction with thick plate (four secondary sources in bottom corners)

3.5.2 Use of input force as reference signal

It may seem natural to use the applied force to the plate as a reference signal for control, rather than plate acceleration. The force is the primary input driving the plate. Figure 3.13 shows the reduction with the secondary sources close to the plate (as in Figure 3.10), using the input force signal as a reference; the Figure shows the reduction with 128-point and also 512-point causal filters. The longer filter gives around 10 dB better attenuation of the plate (1,1) mode at 52 Hz. The reason for this becomes clear when the filters themselves are examined.

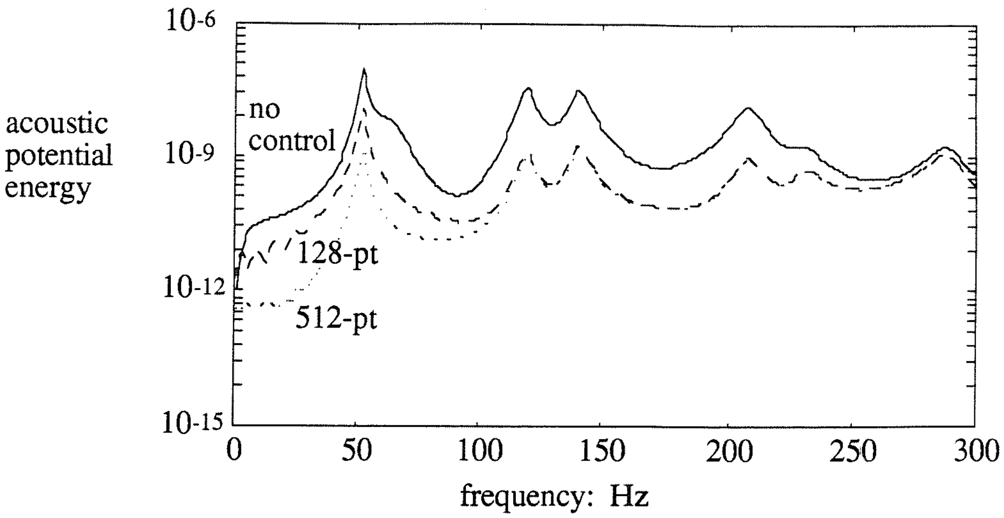

Figure 3.13: Potential energy reduction using input force as a reference: dependence on filter length

Figure 3.14 shows the impulse responses of the filters. Each 512-point filter has a long, ringing response. The 128-point filter response is truncated giving poorer reduction at low frequencies. Thus the result here is significantly affected by the length of the control filters. When the input force is used as a reference signal, the control filters have to model the response of the plate which is lightly damped, thus requiring long filter lengths. This effect becomes very pronounced for thin plates due to lightly damped low-frequency modes. Use of plate acceleration as a reference signal avoids this problem because the cavity acoustic equations (Section 3.3.1) are driven by source terms proportional to plate acceleration rather than input force. If reference signals proportional to input force are used, it may be appropriate to consider using recursive control filters in order to provide the long impulse responses required.

We have seen that plate acceleration provides a good reference signal in that the impulse responses of the optimal filters tend to be short. If however the accelerometers are not located close to the input force but are placed some distance away, problems arise due to the transmission delay through the plate material. This point is further discussed in Section 3.5.5.

3.5.3 Thin plate

Having considered the behaviour of a 20 mm steel plate, we now turn to the more realistic case of a 3 mm steel plate. This has 53 modes below 300 Hz, the lowest plate

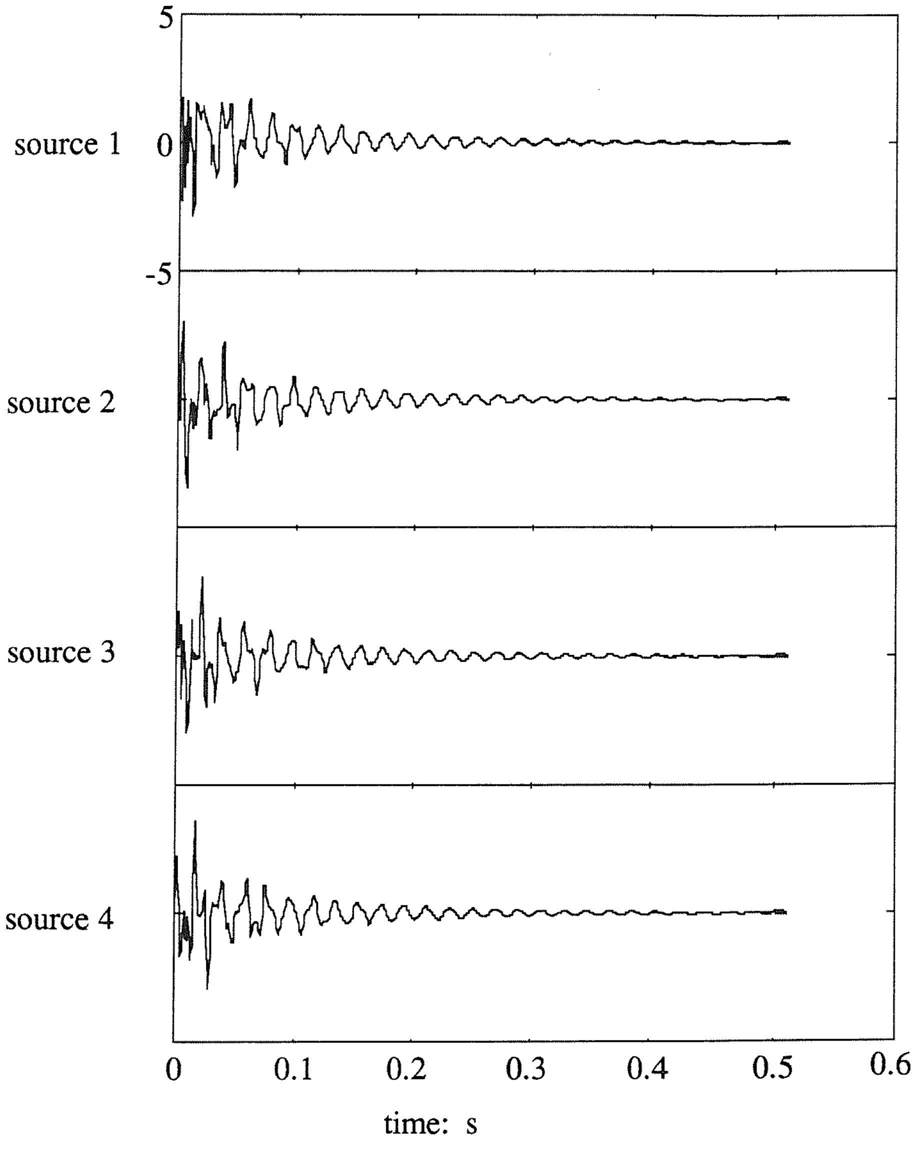

Figure 3.14(a): Impulse responses of 512-pt filters for Figure 3.13

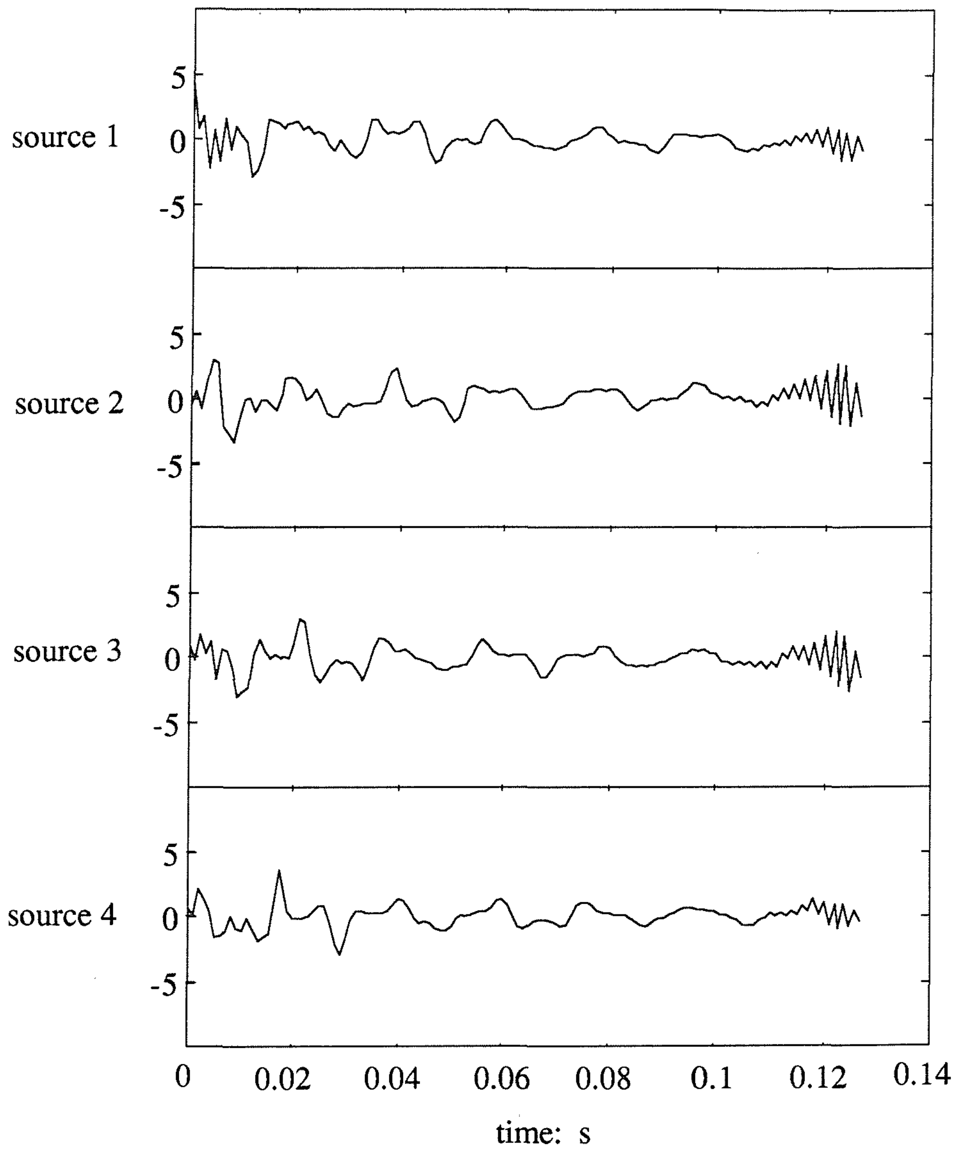

Figure 3.14(b): Impulse responses of 128-pt filters for Figure 3.13

mode (1,1) being at 8 Hz. Exciting the plate with a point force driven by low-pass filtered white noise, and again placing the four secondary sources in the corners adjacent to the plate, the optimal reduction for a causal controller is shown in Figure 3.15. The force is applied at the same position as previously (Figure 3.5) and the reference signal for control is an accelerometer co-located with the force. In this simulation the potential energy spectrum is reduced by more than 10 dB over a frequency range from 60 Hz up to about 200 Hz. There is little or no reduction in the range 20-50 Hz. As in the case with the thick plate (Figure 3.12) the poor reduction in this range arises because the acoustic response is determined mainly by the zeroth and first longitudinal modes: the secondary sources are unable to control these modes independently being placed all at one end of the cavity.

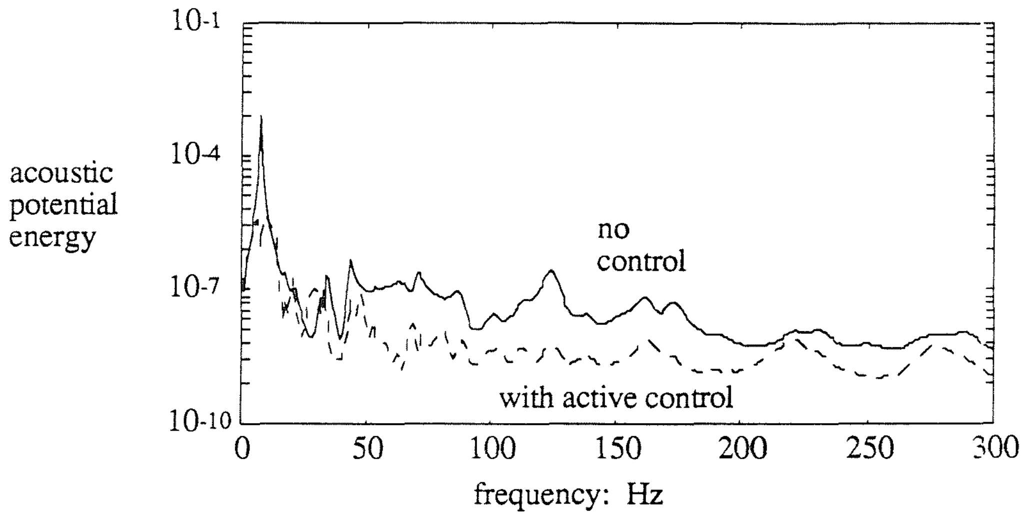

Figure 3.15: Acoustic potential energy reduction with thin plate (four secondary sources in top corners) Note: factor of 10^3 corresponds to 30 dB

3.5.4 Susceptibility to delays

The effect of including a pure delay of 1 ms or 5 ms into the secondary (control) path is shown in Figure 3.16. Comparison with Figure 3.8 shows that with a vibrating plate the system is more tolerant of short (1 ms) delays at all frequencies. However the reduction is largely lost over most of the frequency range if a 5 ms delay is introduced.

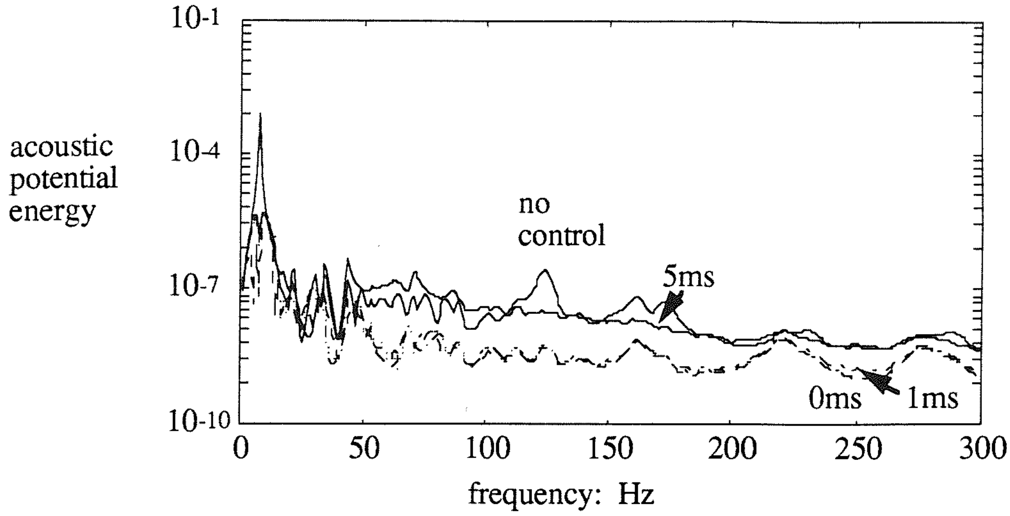

Figure 3.16: Effect of delays: thin (3mm) plate

The total potential energy in the enclosure is dominated by the plate (1,1) mode at 8 Hz whose waveform is almost periodic and so (being predictable) is virtually impervious to delays. (The acoustic field can be thought of as predictable if the cross-correlation function between the filtered reference signals (Section 3.3.3) and the acoustic modes of the cavity diminishes only slowly with lag. Then when the time delay is introduced there is still information with which to calculate the optimal filters.) These results show that control system delays are of crucial importance when controlling broadband sound in a well-damped enclosure. If however the sound is dominated by lightly-damped structural modes, the acoustic field is more predictable and the control system is less susceptible to delays at those frequencies.

Comparison of Figure 3.8 with 3.16 shows that the reductions in the 60 - 200 Hz range drop off rapidly when the vibrating plate is the noise source, but not as quickly as in the case of a piston source.

3.5.5 Accelerometer placement

When plate acceleration has been used as a reference signal in the cases so far, the accelerometer has been located in the same position as the applied force. In this Section we consider the effect of placing the accelerometer elsewhere on the plate. The plate is again assumed to be 3mm steel.

Figure 3.17 compares the reduction when the accelerometer is placed 0.92 m away from the force. Other conditions are as for Figure 3.15. The control system is largely unable to reduce the sound field in this case, except at the narrow peak due to the plate (1,1) mode. The reason is clear when one considers the time taken for disturbances to propagate as flexural waves through the plate material.

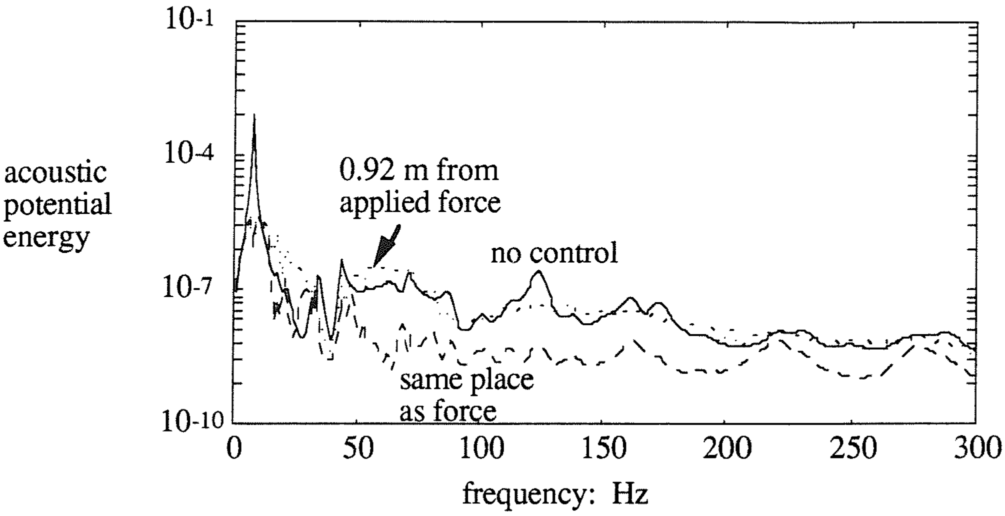

Figure 3.17: Effect of accelerometer location: thin plate
(four secondary sources at top)

The group delay T_d of a flexural wave between two points a distance L apart on a plate is:

$$T_d = L\frac{dk}{d\omega}$$

where k is wavenumber, obtained from the dispersion relation for a thin plate:

$$k = \left(\frac{\omega^2\sigma}{D}\right)^{1/4}$$

where σ is mass/area of the plate (kg/m^2) and the flexural stiffness is given by

$$D = \frac{Eh^3}{12(1-v^2)}$$

where h is plate thickness (m), ν is Poisson's ratio, E is Young's modulus. The group delay is therefore

$$T_d = \frac{L}{2\sqrt{\omega}}(\sigma/D)^{1/4}$$

It follows from this that the group delay T_d is inversely proportional to the square root of frequency. The group delay is plotted in Figure 3.18 for the thin (3 mm) plate. The group delay varies with frequency because of the dispersive nature of flexural waves in plates. For a spacing of 1 m between force source and accelerometer, the delay varies from over 20 ms below 20 Hz down to around 5 ms at 300 Hz. It has already been shown that the active control system does not perform well with control delays of this magnitude, so it is not surprising that there is no potential energy reduction over a wide frequency range.

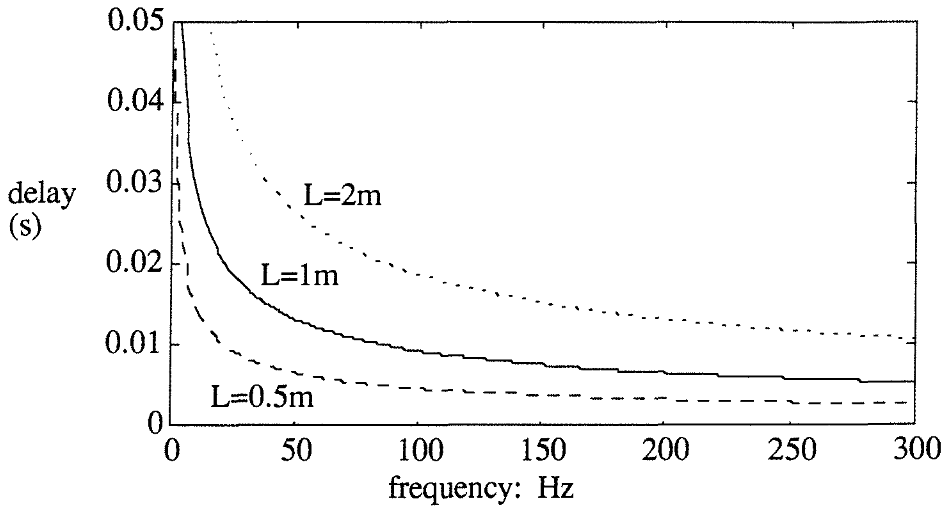

Figure 3.18: Time delay due to flexural wave propagation in plates
(L = distance)

It is clear from these results that in a practical system the accelerometers should be placed as close as possible to the force sources exciting the vibration. Structural propagation delays through floor and other panels can be expected to render ineffective any reference accelerometers placed at an appreciable distance from the primary sources.

3.6 Plate excited by multiple force inputs

3.6.1 Sound cancellation at a point

So far this Chapter has considered the cancellation of noise which arises from a single force applied to a plate bounding a cavity. In the practical case of a car there are a number of partly-correlated forces applied by the wheel/suspension assemblies at different points on the body structure. In this Section we look at the additional problems which arise when there are several force inputs. Instead of considering the reductions in potential energy it is useful in this case to look at the simpler case of sound cancellation at a point.

The earlier Sections have presented graphs showing reductions in the total acoustic potential energy throughout an enclosure, achieved using several secondary sources. Even with causally unconstrained control filters the reductions were limited and highly sensitive to secondary source position. However, it would still have been possible with an unconstrained filter to cancel the sound at a single given point in the enclosure even though this may not reduce the total potential energy. As shown in Chapter 2 the maximum available reduction (using an unconstrained filter) depends on the coherence between the reference signal and the primary sound pressure at the point where attenuation is required. In all the cases considered so far, in which there has been a single primary force input, this coherence has been unity. Therefore the sound reduction at a point has been limited only by causal considerations.

If several forces are applied to the plate, and these forces are detected in some way to form a group of reference signals, then the maximum sound reduction is limited by the multiple coherence $\eta^2_{d:\mathbf{x}}$ between the vector of reference signals $\mathbf{x}(\omega)$ and the primary sound pressure $d(\omega)$ to be cancelled, as shown in Section 2.2.2:

$$\Delta(\omega) \quad = \quad -10\log(1 - \eta^2_{d:\mathbf{x}})$$

where $\Delta(\omega)$ is the available reduction in dB using unconstrained control filters. The multiple coherence may well be less than unity, so this limits the available sound reduction. This limitation is over and above the limitations discussed earlier in this Chapter and arises because the available reference signals do not provide complete information about the sound to be cancelled.

The next Section considers sound attenuation at a point when there are more forces than reference signals. Before concluding, a final Section considers how many accelerometers are required in practice.

3.6.2 More forces than reference signals

The forces arising from wheel vibration on a car are applied by the suspension assemblies to the car body at around ten different locations. The forces applied at each location are only partially correlated with each other (see Chapter 4). It is therefore useful to look in general terms at the scope for controlling interior sound using only a small set of reference signals.

To examine this case we consider six independent randomly-varying forces applied to a 3 mm steel plate forming one boundary of the rectangular cavity considered previously. Between one and six accelerometers are assumed to be attached to the plate. They measure the vibration and represent a set of reference signals for control. All the forces and accelerometers are distributed randomly about the plate; also none of the accelerometers is co-located with a force. The potential active reduction at a point is predicted by the multiple coherence of the accelerometers (*ie* the reference signals) with respect to acoustic pressure at a point in a corner of the enclosure. (Note that this frequency-domain calculation is not causally constrained and so is not affected by propagation delays through the plate.)

Figure 3.19 shows the multiple coherence of various numbers of accelerometers with respect to acoustic pressure at a point. The lowest trace shows the ordinary coherence of a single accelerometer with respect to the acoustic pressure. This ordinary coherence shows a series of narrow peaks at very low frequencies (below 35 Hz). Each of these five peaks corresponds to one of the lowest five modes of the plate. At the lowest (1,1) mode of the plate (7.8 Hz) the coherence of the single accelerometer touches 99%. Thus although there are six independent applied forces randomly spaced on the plate, a single accelerometer is sufficient to detect virtually all contributions to the sound in the box. This arises because the plate modes act as single degree of freedom systems. At the very lowest frequencies the plate response is dominated by individual well-spaced

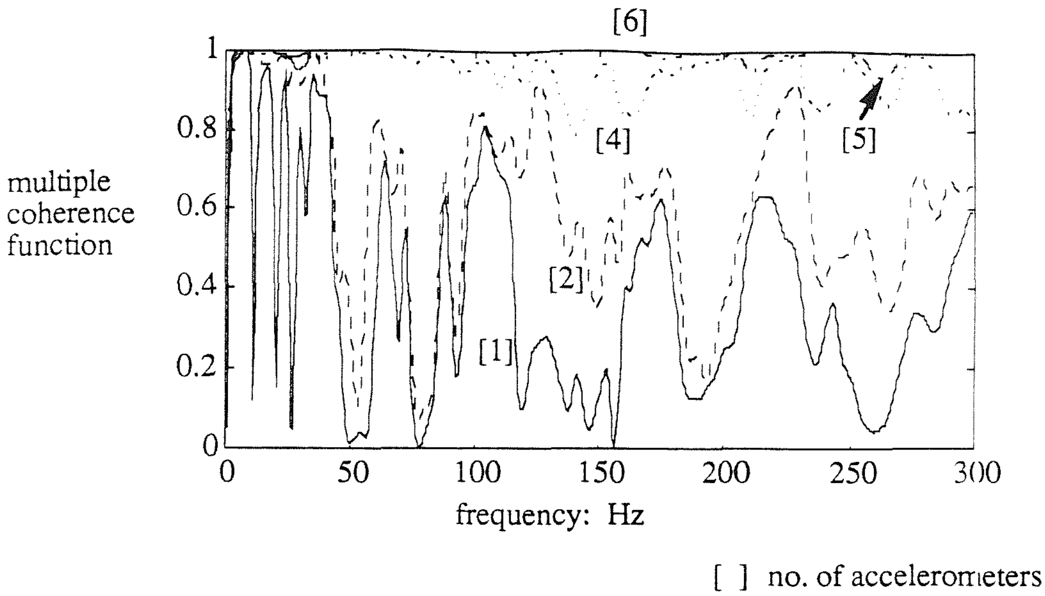

Figure 3.19: Multiple coherence of 1,2,4,5 and 6 accelerometers with respect to acoustic pressure in enclosure (6 independent forces applied to plate)

lightly-damped modes and only one accelerometer is necessary to detect a single mode. At higher frequencies (35 - 300 Hz) the plate response at any frequency is made up of contributions from many structural modes with no single mode dominating; hence the ordinary coherence of sound pressure with respect to a single accelerometer is lower.

The successively higher multiple coherence traces in Figure 3.19 show the effect of using 2,4,5 and 6 accelerometers. When five accelerometers are used to detect the six applied forces their multiple coherence with respect to the sound is better than 94% over the whole range and better than 99% at many points. This would appear to be valuable since it implies that 20 dB reductions (maximum) could be achieved using unconstrained filters. However any significant measurement noise reduces this level sharply. In addition these results depend on the locations of the forces and accelerometers: if two forces are located close to each other then the plate is effectively excited by five independent forces rather than six.

It is only when all six accelerometers are used that the coherence is unity over the whole range. Six independent measurements from different locations on the plate are required to infer the six independent forces and predict the sound field. If less measurements are used, high values of multiple coherence may be achieved over a part of the frequency range (depending on the locations of the forces and sensors) but for high multiple coherence over the whole range the number of measuring points should be equal to the number of independent applied forces.

3.6.3 Number of reference signals required

It is clear from the above that for adequate multiple coherence there should be at least as many reference accelerometers as there are independent input forces. Where the input forces are partially correlated (as they are in practice) it is necessary to establish how many independent contributions there actually are. One technique for doing this is Principal Component analysis, applied to vehicle noise by Otte *et al* [1988]. In this application the signals from a number of measurement points (*eg* accelerometers) are recorded and the auto- and cross-spectral densities between them are calculated. The spectral density results are assembled to form a square array at each frequency. The eigenvalues of these arrays turn out to be the autospectra of a set of *uncorrelated virtual* signals from which the real signals can be considered to have been derived. The number of significant eigenvalues at each frequency is thus the number of significant independent contributors at that frequency. To apply this technique the number of measurement points needs to be greater than the number of forces.

The simpler and more direct approach used in practice is to attach accelerometers to promising locations on the vehicle and measure:

(1) the ordinary coherence between each accelerometer and a microphone inside the vehicle;

(2) the multiple coherence between groups of accelerometers and the microphone.

Thus by trial and error a suitable group of reference accelerometers can be found which give adequate multiple coherence with the sound to be cancelled. (In addition, as noted above, the accelerometers need to be located as close as possible to the applied forces to avoid time delays due to the transmission of flexural waves through the vehicle body-panels.)

The ordinary coherence between a single accelerometer and the microphone gives some indication of usefulness; however it is not possible to obtain the multiple coherence by adding together the individual ordinary coherences unless the accelerometer signals are uncorrelated (which they are not in practice). Furthermore it is not even possible to say that the sum of the ordinary coherences forms an upper bound for the multiple coherence. This can be shown by means of a simple example, which is given in Appendix 3.3.

3.7 Conclusions

This Chapter has examined the active control of random sound in a roughly car-sized rectangular enclosure. The source of sound was taken to be (a) a small vibrating piston; (b) a thin vibrating plate bounding the enclosure on one side, excited by a point force. The calculations have focussed on the scope for reducing the total acoustic potential energy in the enclosure. The main conclusions are:

(1) Where the primary source was a small piston, significant (10 dB) energy reductions could be achieved at frequencies up to around 200 Hz using a single secondary source located close to the primary source. However a single secondary source located elsewhere in the enclosure, even in the corners, achieved virtually no reduction above 90 Hz. It was apparent that a single secondary source could control the acoustic modes where they were well separated (*eg* at low frequencies, the zeroth or first mode) but was ineffective where the modes were bunched together, as they were above 90 Hz with this geometry. This result is in contrast to Joplin's [1990] results, in which the enclosure under consideration had well-separated lightly-damped acoustic modes which could be controlled from a single source location.

(2) The use of *four* secondary sources in the corners of the enclosure away from the source improved the situation only slightly, with energy reductions of only a few dB in the range 90-200 Hz. This may be because

(a) the modes are bunched together and so they still could not be controlled independently even by four secondary sources; and

(b) located at the far end of the enclosure, away from the primary source, the secondary sources were able to cancel the reflections but not the primary outgoing sound. Due to the high modal damping factor this cancellation made only a small contribution to reducing the potential energy in the enclosure.

Good reductions were obtained if the secondary sources were located close to the primary sources.

(3) Using four secondary sources close to the small primary piston source, the control was seriously affected by controller delays of as little as 1ms. With a delay the secondary sources were no longer able to match the primary sound field.

(4) When the primary source was a plate driven by a random external force, the structural modes of the plate tended to dominate the spectrum of the acoustic energy in the enclosure. If the plate was relatively thick, these modes were distinct and

substantial reductions in acoustic energy could be obtained with acoustic secondary sources by exploiting the correlation in the pressure signals indroduced by these modes.

(5) If the time-varying input force to the plate was used as a reference for control, the optimum FIR filters used for control had a long-duration ringing response. This was because they modelled the lightly-damped low-frequency modes of the plate. For the case considered, 512-point filters were needed to avoid truncating the response and degrading the control. However, if the output of an accelerometer attached to the plate was used as a reference, this problem was avoided and shorter (128-point) filters could be used. The sound field in the enclosure depends on plate acceleration and if this can be measured directly there is no need for the plate response to be modelled by the control filter.

(6) Where an accelerometer was used for control, its distance from the applied force had a serious effect on the available reduction. A separation of 1m in a 3mm steel plate introduces delays of between 5ms and 20ms over the frequency range of interest, sufficient to wipe out any potential energy reductions over a wide range of frequencies. This indicates that if reference accelerometers are attached to the body panels of a car, they should be located very close to the suspension points where the force is applied; otherwise they should be located on the suspension itself to give the earliest possible signals.

(7) In principle as many reference accelerometers as input forces are required to achieve good control, although the number may be reduced if the input forces are correlated to some extent or input forces excite relatively few modes.

(8) The multiple coherence function can be used to give an estimate of the reduction available from a control system with a given set of reference signals. The multiple coherence function can be greater than the sum of the ordinary coherence functions from each reference alone to the microphone signal.

4 VEHICLE TESTS

4.1 Introduction

Noise and vibration measurements have been carried out on two models of vehicle: the Vauxhall Astra, a 1300cc four-door family hatchback, and the Citroen AX, a smaller (1100cc) 2-door hatchback car already in use for demonstrating the active control of engine noise. The aims of the measurements were to assess

(1) the feasibility of using active control to reduce road noise;
(2) how many reference accelerometers would be needed to detect vehicle vibration; and
(3) where they should be placed for best results.

Using recordings of vehicle noise and vibration it has been possible to predict by computer simulation the performance of an active noise control system. The required auto- and crosscorrelation functions have been calculated from the measured data, leading to evaluation of the set of optimal control filters using the method described in Chapter 2. Using these filters it has then been possible to predict the sound field reduction at a chosen microphone location. The results of these calculations are presented in Section 4.3.

Lotus Engineering have built an experimental road noise control system and have measured actual noise reductions in a number of cars. Some of their results are reproduced in Section 4.4.

4.2 Road noise measurements

4.2.1 Vehicle instrumentation

The first set of measurements, on the Vauxhall Astra, concentrated on vibration of the suspension assemblies. Ten accelerometers were fitted to the car as shown in Figures 4.1 and 4.2. A further two accelerometers were fitted to the underside of the front floor panels (Figure 4.3). Two microphones were attached to the front seat headrests to measure interior noise: one next to the driver's right ear, the other next

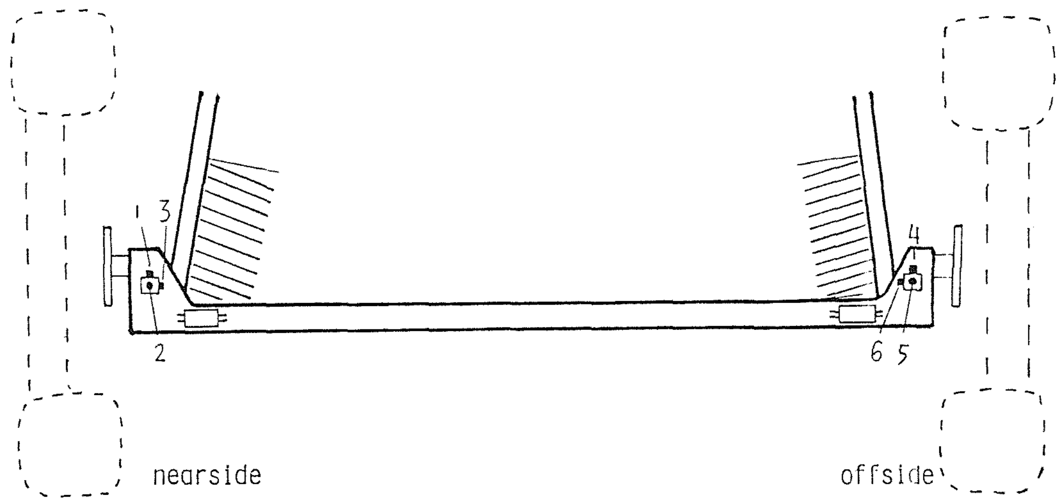

Figure 4.1: Astra rear suspension - view from rear, showing accelerometer locations

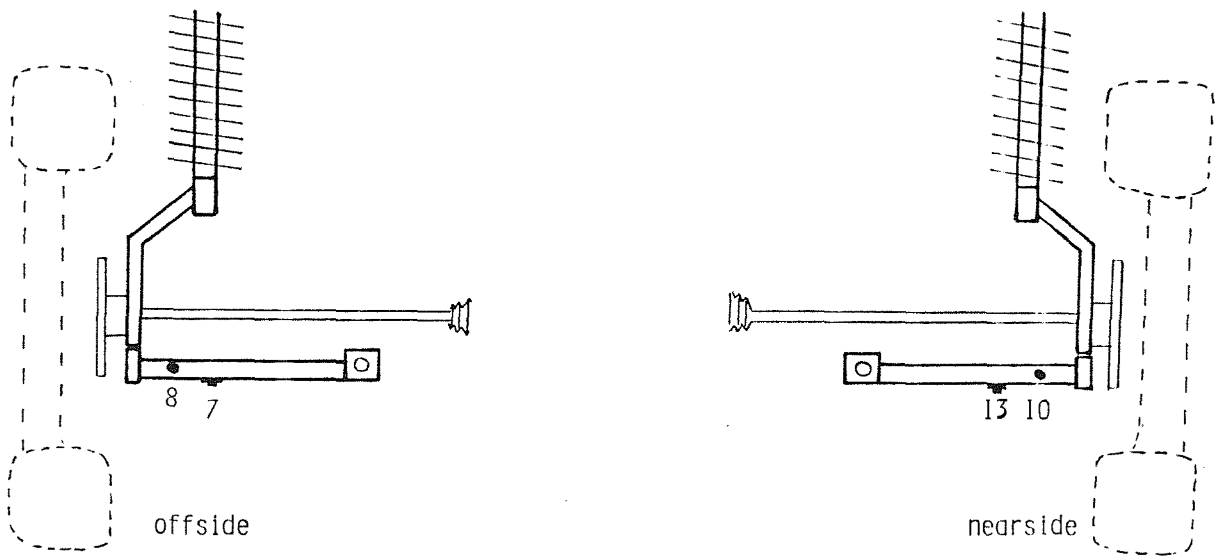

Figure 4.2: Astra front suspension - view from front, showing accelerometer locations

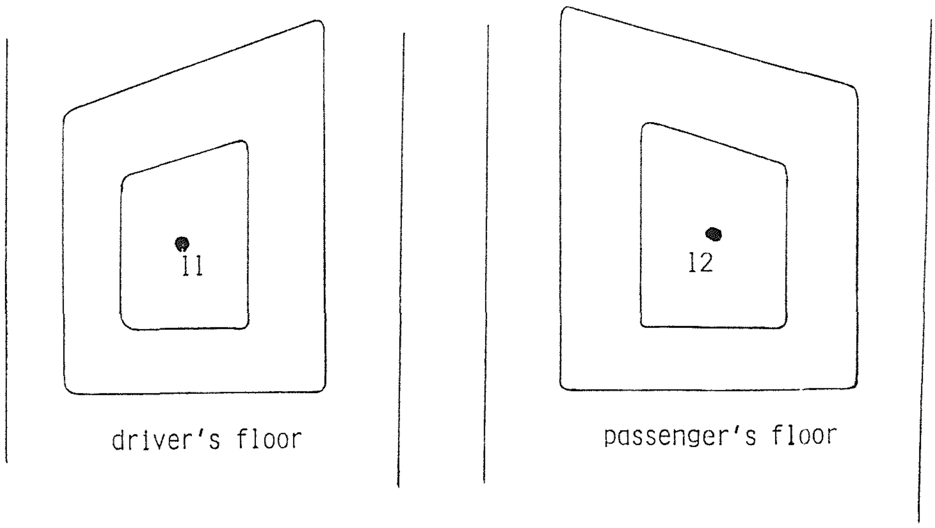

Figure 4.3: Underside of Astra front floor panels, showing accelerometer locations

to the front passenger's left ear. Each microphone was held in position by an adjustable holder attached to the headrest column.

The second set of measurements used a different model of car, the 1100cc Citroen AX hatchback. Six accelerometers were attached underneath the car to the floor panels, some close to suspension mounting points, others further away as shown in Figure 4.4. The two interior microphones were placed one by the driver's left ear, the other in the corresponding position above the back seat.

A number of different tests were carried out with each vehicle configuration. All the road tests were recorded using a 14-channel FM tape recorder (type Racal Store 14DS). They were converted to digital format at ISVR using a Masscomp computer running SPAGS, a suite of data acquisition software by Cranfield Data Systems. The Masscomp was able to sample all 14 channels simultaneously. The sample rate was 1000 Hz for all the tests; anti-alias filters (135 dB/oc roll-off) were set at 330 Hz.

The tests comprised:

(1) Bump test. The Astra was driven over a steel bar raised 25 mm above the road surface. The resulting impulse response was recorded;
(2) Steady speed. The cars were driven over a range of road surfaces.

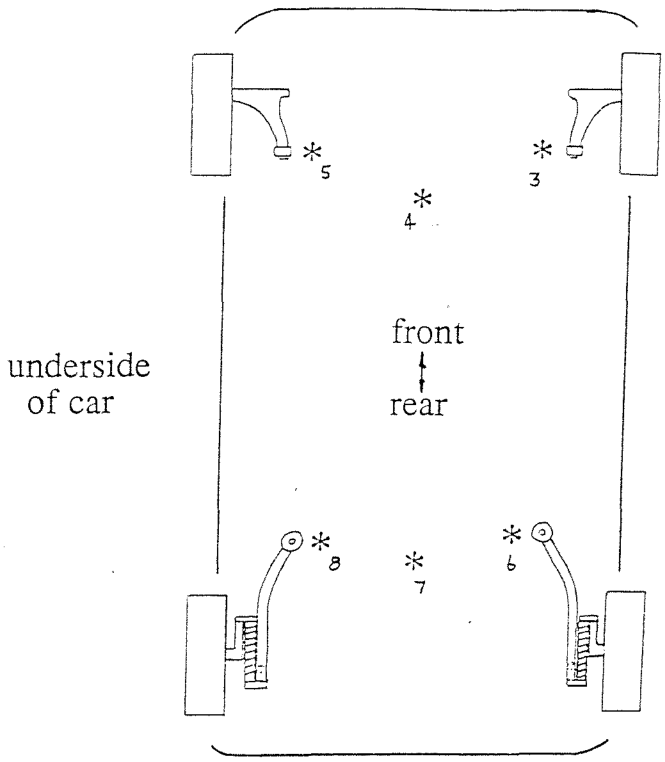

Figure 4.4: Citroen AX - view of underside showing location of accelerometers

The raw measurements and spectra are briefly described in the following two Sections.

4.2.2 Bump test

Figure 4.5 shows the transient vibration of the Astra 1300L suspension as the vehicle crossed a steel bar raised 25 mm above the road surface. It appears from the traces that some of the peaks of these impulse responses have been lost in the recording process, probably due to saturation of the conditioning amplifiers, but the main interest is in the relative time delays between traces and in the different natural frequencies of the responses.

Figure 4.5 shows the expected delay between the response of the front suspension and that of the rear as the two sets of wheels went over the bar. The time difference was 0.21 s, corresponding to a vehicle speed of 26 mph. However a close examination of the traces reveals other delays as each impact propagated around the structure. The transient in vertical suspension acceleration (trace 13) was

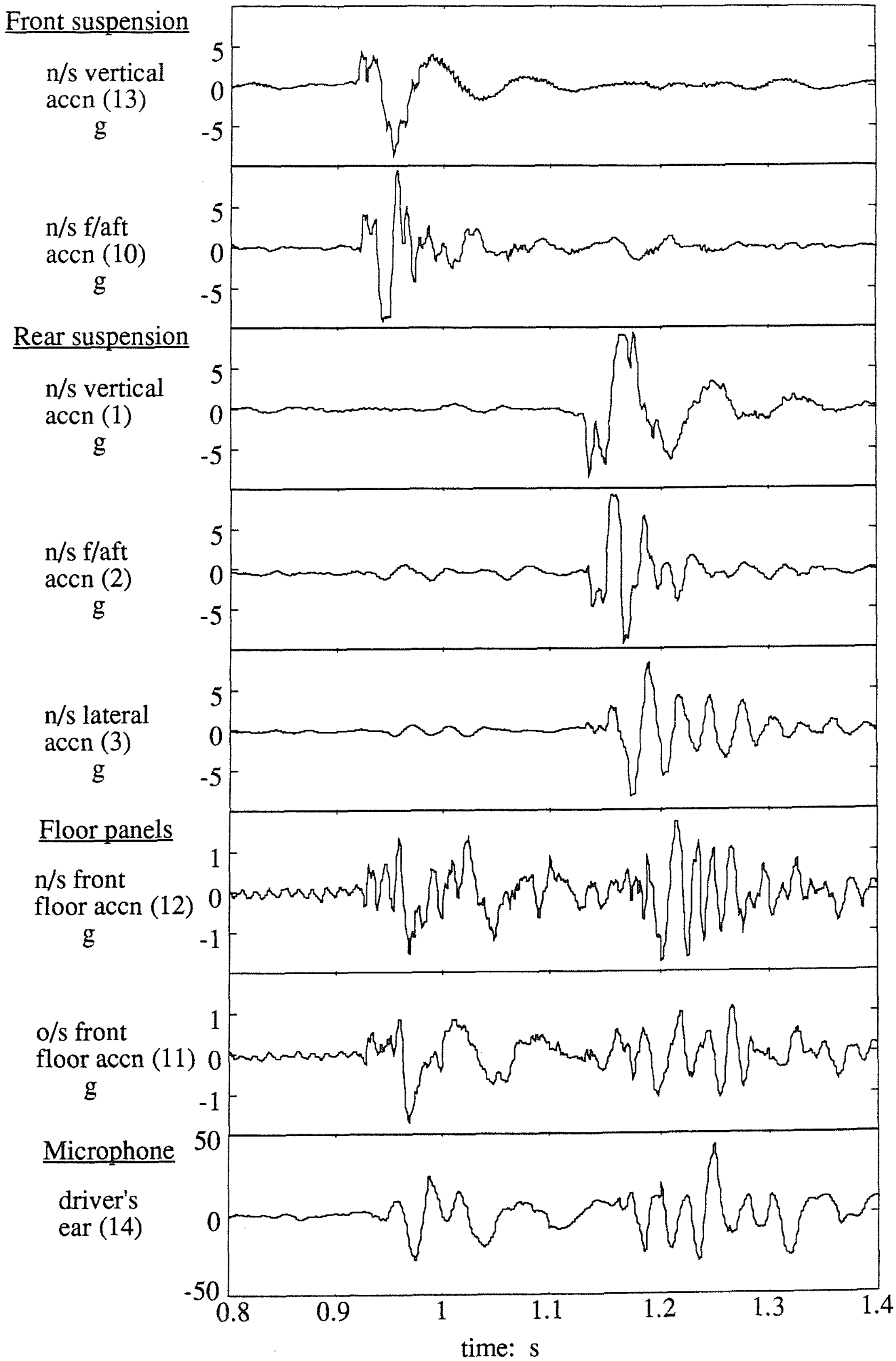

Figure 4.5: Transient response of vehicle driven over a bar
n/s = nearside; o/s = offside; f/aft = fore/aft

reproduced in the floor panels (11 and 12) delayed by 16 ms. The driver's side microphone showed no response at all until 14 ms after the first response of the front suspension. Delays of this order are consistent with the propagation delays for flexural waves in plates, discussed in Chapter 3. For the measurements reported here, the floor panel accelerometers in Figure 4.5 were placed in the centre of the panel, some 0.5 m from the points of application of the forces.

The transients also show the natural frequency and damping of different parts of the structure. The amplitude of response to the rear wheels was generally greater than to the front wheels, reflecting the high degree of vibration isolation designed into the front suspension of this front-wheel drive car. The rear suspension responses showed different natural frequency and damping characteristics in the vertical, lateral and fore-aft directions (traces 1-3), reflecting the different suspension characteristics in each of the three directions.

4.2.3 Spectra of vibration and interior noise at a steady speed

Figure 4.6 shows the spectrum of fore-aft acceleration for the nearside rear suspension of the Astra, with the vehicle travelling at 70 mph. Also shown is the unweighted spectrum of interior noise, measured at the passenger microphone. The wheel rotation frequency (W = 16.2 rev/s) is visible along with its harmonics, as is crankshaft rotation rate (E = 48.2 rev/s).

The main features are:

(1) The wheel rotation frequency and its harmonics form an important part of both spectra. Wheel rotation harmonics up to about the seventh (114 Hz) are visible. There are also other components which appear to be speed dependent (by comparison with other test results at 60 mph): these are at 28.8 Hz (plus first harmonic, 57.6 Hz) and 40.4 Hz.
(2) Engine rigid-body modes and other structural resonances show up in the acoustic spectrum at low frequencies (22.7 Hz, 24.5 Hz, 34.5 Hz); these are also apparently coupled to rear fore-aft suspension acceleration. The engine firing frequency (96.4 Hz) does not show through on rear suspension acceleration.

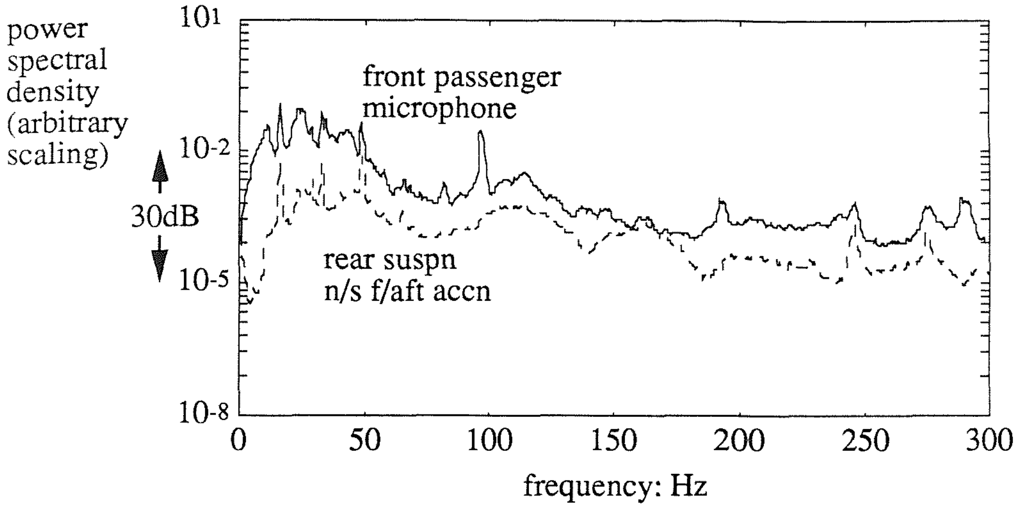

Figure 4.6: Autospectra of rear suspension vibration and interior noise (Astra)

Rear suspension acceleration measurements were also taken in the vertical and lateral directions. Their spectra are broadly similar in form to Figure 4.6; however, coherence analysis indicates that the vibration signals in the three directions are to some degree independent.

Measurements on the Citroen concentrated on vibration of the underside of the body rather than the suspension. Figure 4.8 compares the spectra of accelerometers at the nearside front and nearside rear (positions (3) and (6) in Figure 4.4). The measurement was taken at a steady speed of 50 mph driving over a coarse-grained tarmac road surface. The acceleration spectrum for the front has a strong peak at 76 Hz, the engine firing frequency, due to transmission of engine vibration to the structure. Above about 125 Hz the acceleration at the rear of the structure falls to some 10 dB below the acceleration at the front. The spectrum at 70 mph on a concrete surface had the same form. It appears that in this front-wheel drive car the front wheels are the main contributors to broadband structural vibration above about 125 Hz.

4.2.4 Crosscorrelation of front and rear suspension acceleration

When a car is driven in a straight line, the rear wheels travel over the same section of road as the front wheels but after a time delay. The crosscorrelation function between the front and rear suspension signals can be expected to show this effect.

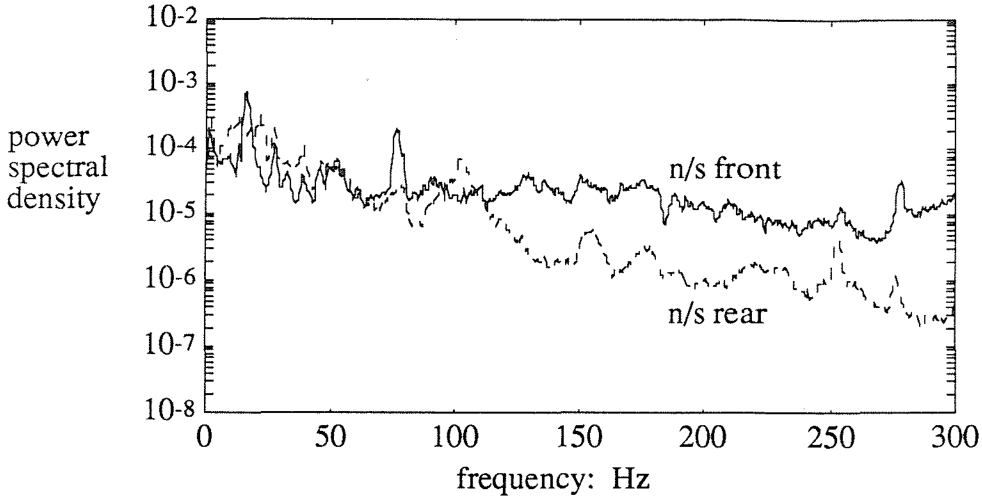

Figure 4.8: Vertical acceleration of Citroen floor, front and rear (50 mph)

Figure 4.9 shows the crosscorrelation function for front to rear vertical suspension acceleration (nearside). The peak is negative because the front accelerometer faced upwards while the rear one faced downwards. The Astra was used for this test and had a mean speed of 65.2 mph, corresponding to a delay of 86 ms between wheels crossing a given point. The input from the road was filtered by the wheel-hop resonance in each case giving the crosscorrelation function a 14 Hz oscillation. The coherence between the two signals is shown in Figure 4.10. It is over 0.75 in the range up to 90 Hz, but falls off sharply above this frequency. The coherence only exceeds 0.9 at very low frequencies, below about 30 Hz. This indicates the somewhat surprising fact that the front suspension vertical vibration is not a good predictor for rear wheel vibration except at very low frequencies. This result shows that both rear-wheel vibration and front-wheel vibration will need to be measured when predicting interior noise.

4.2.5 Coherence: suspension

Ordinary and multiple coherence were discussed in Chapter 2 where it was shown that the maximum reduction which could be obtained with an active sound control system was limited by the multiple coherence between the chosen reference signals and the measured primary noise. It was shown that the unconstrained reduction $\Delta(\omega)$ is given by

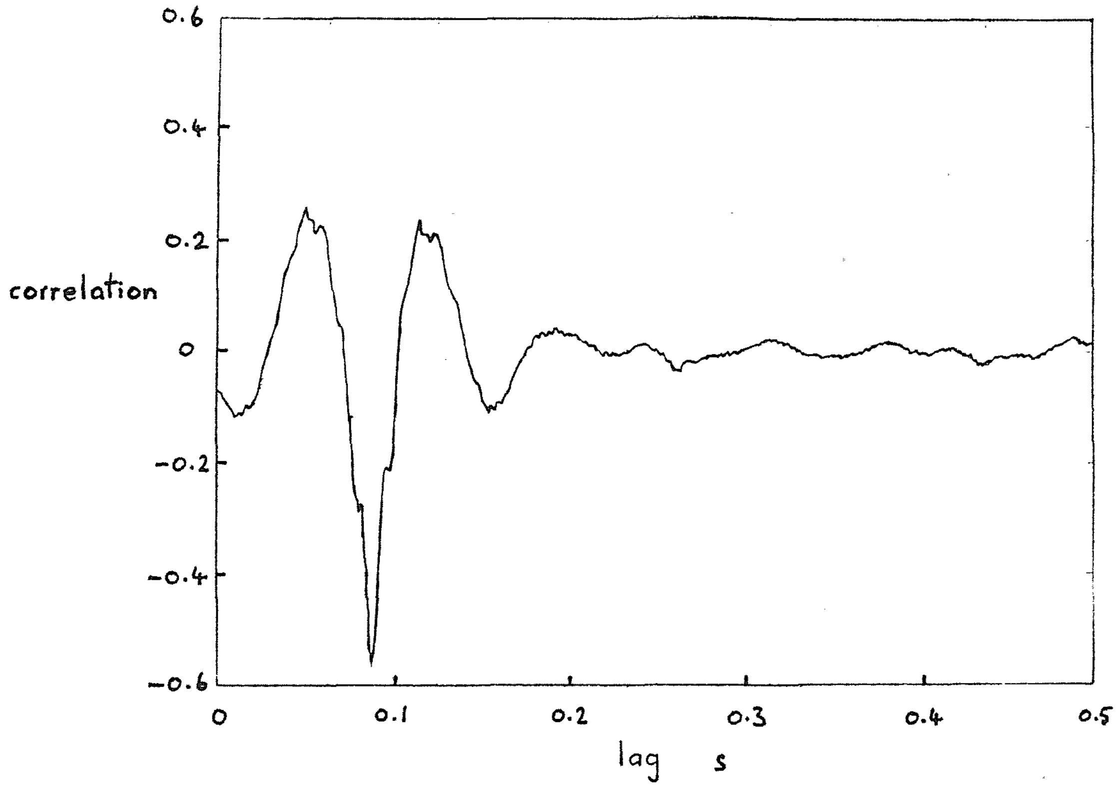

Figure 4.9: Crosscorrelation function, front to rear vertical suspension acceleration (n/s), 65 mph

$$\Delta(\omega) = -10 \log(1 - \eta_{d:\mathbf{x}}{}^2(\omega))$$

where $\eta_{d:\mathbf{x}}{}^2(\omega)$ is the multiple coherence between the reference signals $\mathbf{x}(\omega)$ and the detected primary sound $d(\omega)$. It is therefore important to establish the coherence between accelerometers on the vehicle structure (which could be used as reference signals for control) and the noise detected by microphones inside.

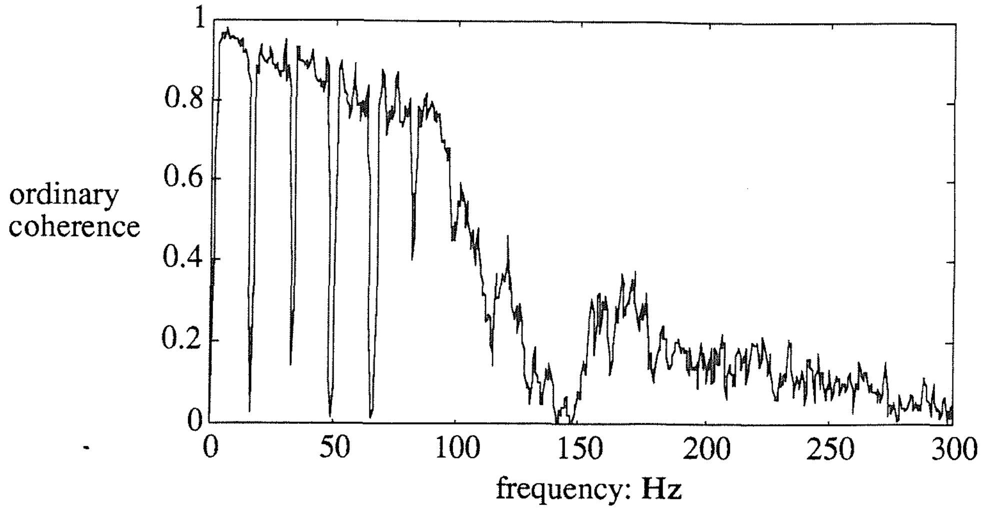

Figure 4.10: Coherence of front and rear n/s suspension vertical acceleration signals (Astra)

Figure 4.11 shows the multiple coherence between the two vertical suspension acceleration signals and the vehicle interior noise (driver's microphone). The measurement was taken on the Astra at 56 mph on a concrete road surface. There is a strong peak at 25 Hz, but otherwise the coherence level is low. The peak may

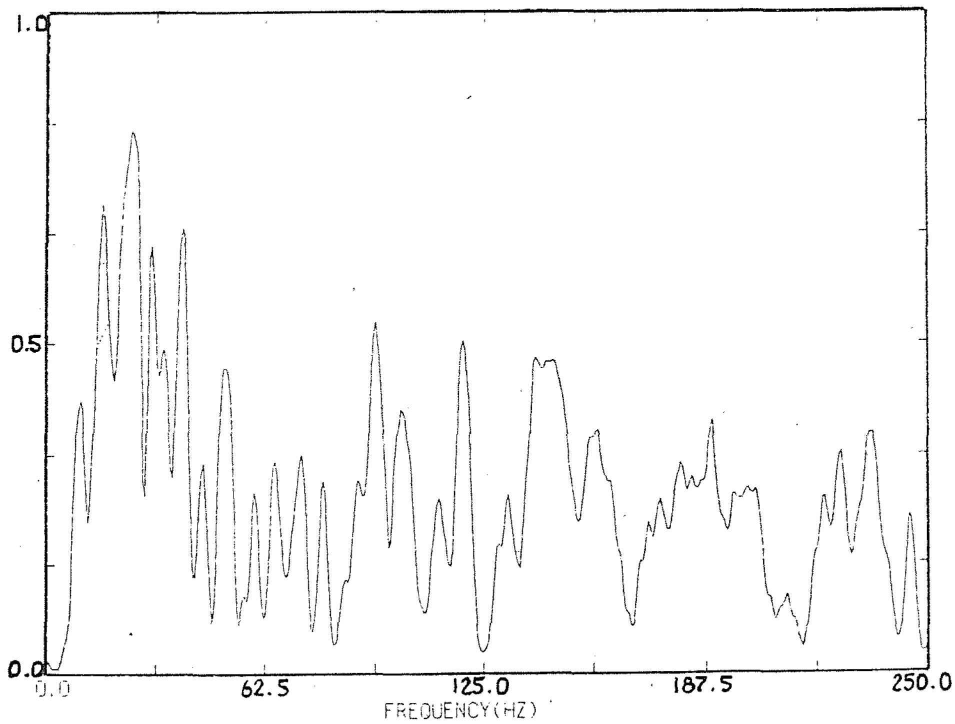

Figure 4.11: Multiple coherence (Astra): driver's microphone w.r.t. rear suspension vertical accleration (n/s and o/s)

indicate a structural resonance excited by the rear suspension which transmits sound into the car. At other frequencies there is no close relation between rear suspension vertical acceleration and noise inside the car.

The results for rear fore-aft acceleration and lateral acceleration are similar in form and all show a peak at 25 Hz. Figure 4.12 shows the multiple coherence between all six rear suspension acceleration measurements and the vehicle interior noise. This represents the fraction of power at the interior microphone which is linearly dependent on the six signals, the remainder being due to other unrelated sources. The main contribution of the rear suspension is at the lowest frequencies (up to around 55 Hz); the coherence is approximately 30% over the rest of the range up to 250 Hz.

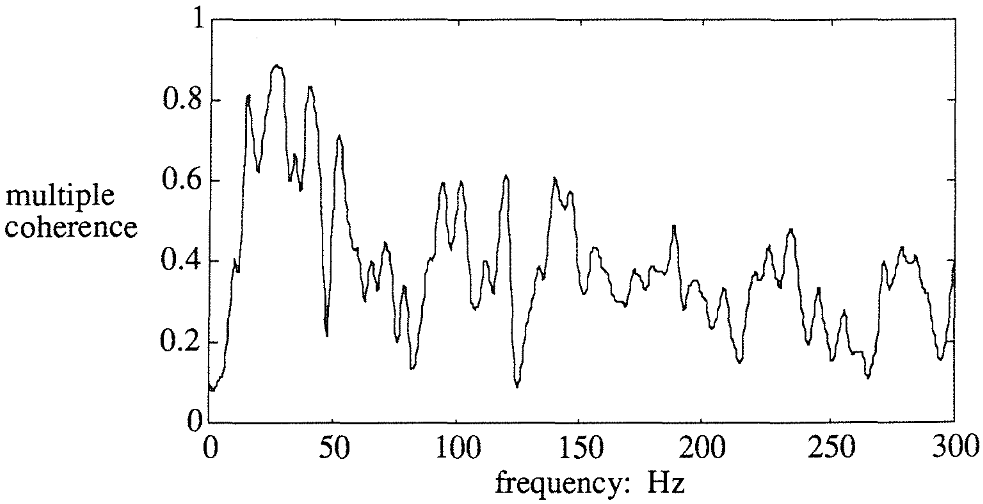

Figure 4.12: Multiple coherence of driver's microphone w.r.t. all six rear suspension accelerometers (Astra)

Combining all the available suspension accelerometers for the Astra yields Figure 4.13, which shows the multiple coherence between the six rear suspension accelerometers, the two front vertical accelerometers and the one front fore-aft accelerometer (n/s fore-aft acceleration not recorded). The area between the two traces represents the change from Figure 4.12 due to the addition of front suspension accelerometers. The mean coherence level is about 0.6. It is clear that a substantial amount of the low-frequency interior noise is not linearly related to suspension vibration. This may be because the coupling between the suspension and vehicle interior is not linear (due to the nonlinear behaviour of the rubber bushes, shock absorbers, *etc*); or it may be that at the speed of this test (56 mph) wind noise was a significant contributor.

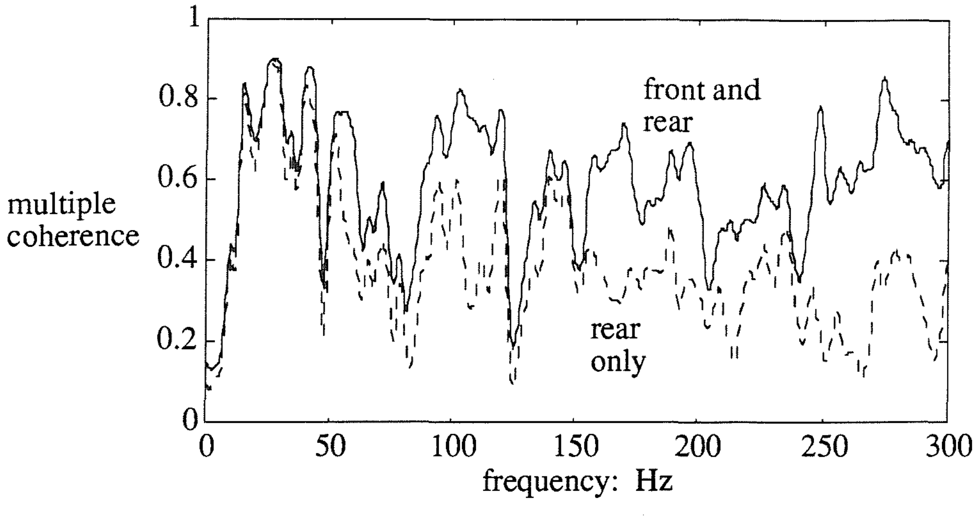

Figure 4.13: Multiple coherence of driver's microphone w.r.t. 6 rear and 3 front suspension accelerometers (Astra)

The main conclusion to be drawn from this analysis is that all three directions of each of the four suspension systems appear to contribute independently to the interior noise, and that none can be ignored if significant reductions in interior noise are to be achieved.

4.2.6 Coherence: body panels

Tests on the Citroen AX included measurements of floor vibration at the six locations shown in Figure 4.4. Figure 4.14 shows the multiple coherence using 4 and 6 accelerometers with respect to the microphone at the back of the car. Good (>90%) coherence was obtained using 4 accelerometers, one close to the suspension mounting point for each wheel (sensors 3,5,6,8) but only at very low frequencies. When all six accelerometers were taken together, there was a substantial improvement in the 100-125 Hz range. This implies that the two centre accelerometers make independent contributions in this frequency range, and are not simply a combination of the signals at the wheels. (The two centre accelerometers gave disappointing results on their own, however.) Chapter 3 discusses the question of detecting multiple forces applied to a plate and shows that there need to be as many accelerometers as independent forces acting on the plate. The number of accelerometers turned out to be more important than their location. Accelerometers placed away from the force sources are of course subject to propagation delays through the body panels, but this does not affect the coherence calculation.

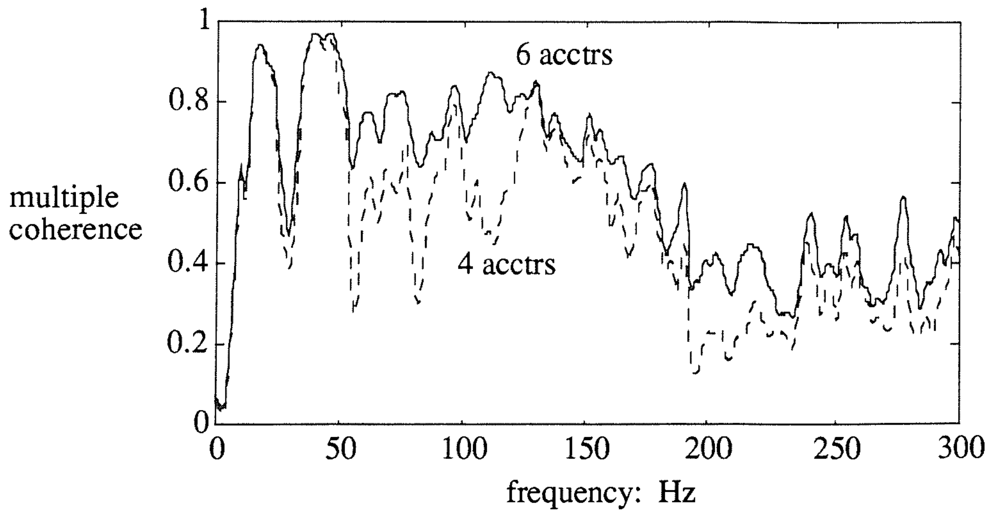

Figure 4.14: Multiple coherence of o/s rear microphone w.r.t. 4 and 6 accelerometers (Citroen)

With six accelerometers the multiple coherence exceeded 0.8 for about half the range 65-130 Hz. This corresponded to a possible reduction of about 7 dB.

4.3 Active control predictions

4.3.1 Calculation method

The measurements reported so far have shown that no single accelerometer signal was sufficiently coherent with the noise inside the car to provide a good reference signal by itself. Each measurement point showed some low level of coherence as the wheels tended to contribute independently to vehicle interior noise. The multiple coherence calculations showed however that useful cancellation could be achieved (at one microphone location) by taking several accelerometers together as reference signals. In this section the recordings of vehicle noise and vibration at steady speed are used to calculate firstly the optimal causal filters for active control and secondly the predicted sound reductions at a microphone inside the car.

The method of calculating the optimal causal filters is described in Chapter 2. The stationary noise and vibration data are used to estimate auto- and crosscorrelation functions which yield the coefficients of the optimal causal filters by means of the multichannel Wiener equation (2.3.29). The measured time series are then passed through the optimal filters, the error time series calculated and hence the error spectrum obtained by FFT. The signals required for correlation analysis are actually the *filtered reference signals*, *ie* the signals which result when the chosen reference signals are passed through filters representing the vehicle interior acoustics. These filters model the response of each error microphone to each secondary source. For the Citroen these filters were obtained by measuring the transfer function of the two interior microphones with respect to a single boxed loudspeaker located on the driver's floor.

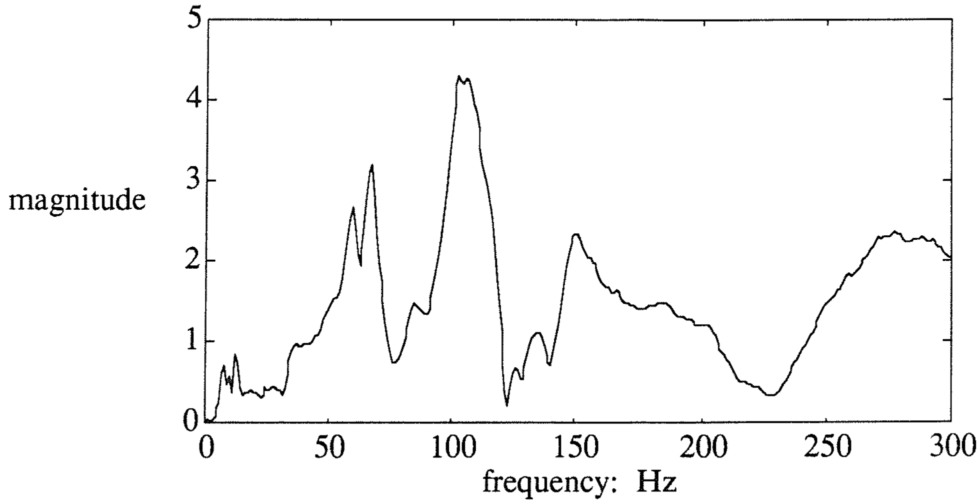

Figure 4.15(a): Interior acoustic transfer function of Citroen (magnitude only)

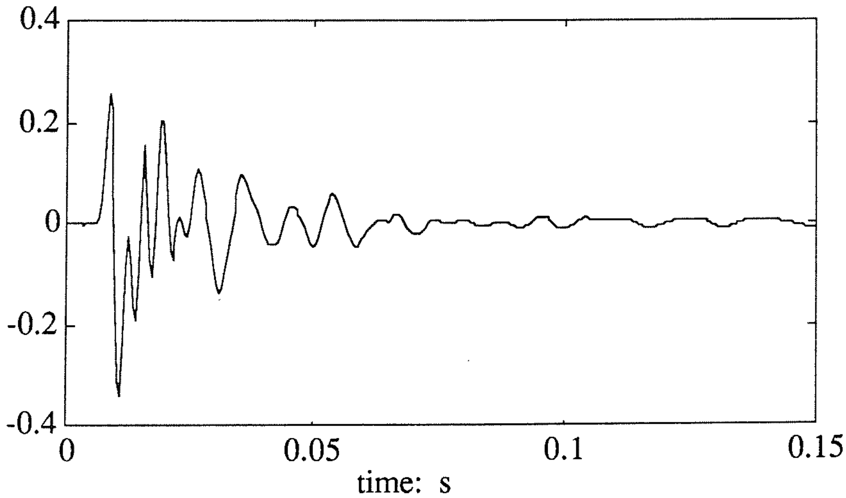

Figure 4.15(b): Acoustic impulse response of Citroen interior

Figure 4.15(a) shows the measured transfer function to the rear microphone including the speaker itself and its power amplifier as well as the acoustics of the car interior with no passengers and all windows and doors shut. The corresponding impulse response (Figure 4.15(b)) includes a pure delay of 5.3 ms. A 64-point FIR filter was used to represent the vehicle acoustics in the predictions of control system response in the following Section (sample rate 1 kHz). The filter consisted of the impulse response of the vehicle interior with an exponential weighting to ensure that the response died away within 64 ms, the length of the filter.

4.3.2 Predicted reductions

The middle trace in Figure 4.16 shows the residual spectrum at the error microphone (rear of car) predicted using an active control system with reference signals taken from all six accelerometers located on the underside of the body of the Citroen. Six 128-point FIR filters were assumed in the calculation. The measured interior acoustic transfer function was included in the calculation, introducing a pure delay of 5.3 ms as noted above. The top trace is the rear microphone spectrum as measured (*ie* with no control); the lowest trace is the calculated spectrum using six reference signals but with unconstrained control filters (non-causal and not limited in length). The calculation indicates that a reduction of around 5 dB is possible at the microphone in the range from 90 Hz to 140 Hz using causal filters. Up to about 160 Hz the predicted reduction using causal filters is roughly speaking 3 dB short of the reduction with unconstrained filters. Exceptions are the reductions at peaks such as engine firing frequency (76 Hz) where the reduction approaches that in the unconstrained case. The reason for this is that components of the signal which are almost-periodic are more predictable, so that information about the signal is not lost by using causal filters. Specifically, periodicity in the signals gives rise to extended periodic components in the autocorrelation and crosscorrelation functions which are not lost in truncation.

The spectrum with unconstrained filters shows that a small reduction is available above 160 Hz. However this possible reduction is lost when causal filters are used. This is because the reference signals do not provide a sufficiently early warning of the broadband road noise to allow an active control system to function.

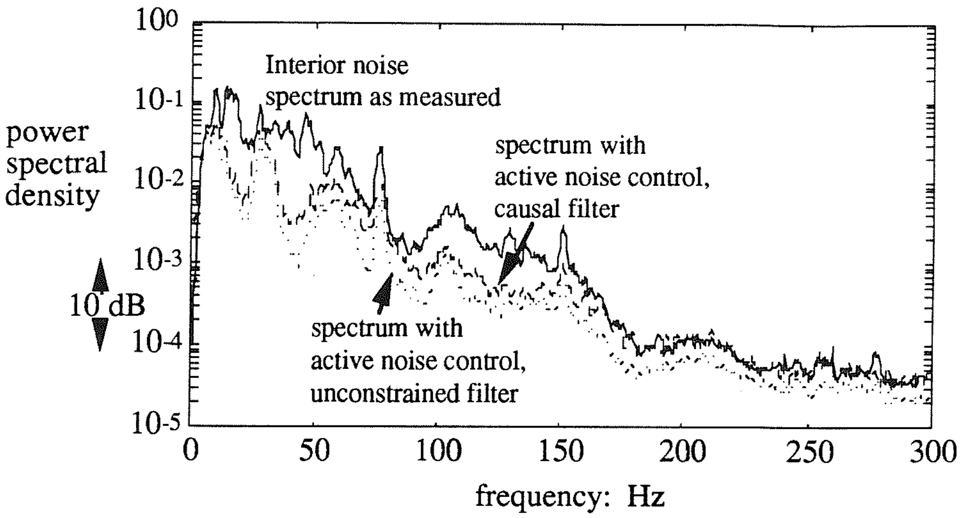

Figure 4.16: Predicted sound reduction using 6 reference signals (Citroen)

It is useful to compare the result predicted for the Citroen (where the accelerometers were located on the underside of the floor panels) with the Astra tests, where the accelerometers were located on the vehicle suspension. Figure 4.17 shows the predicted reduction using nine accelerometer signals as references. The simulation included a 5 ms pure delay to represent the vehicle interior acoustics. Overall the reduction is poorer than in the earlier case with the accelerometers attached to the floor; but it is interesting to note that the reduction using causal filters is only 1-2 dB worse than the maximum available reduction with unconstrained filters. This reduction applies over the whole frequency range to 300

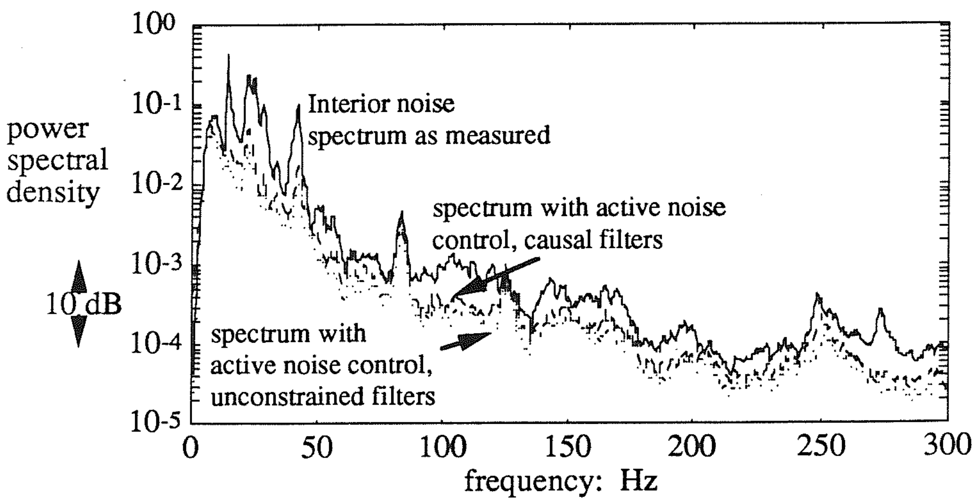

Figure 4.17: Predicted sound reduction in Astra, 9 suspension accelerometers as references

Hz. This result reflects the fact that the reference accelerometers were located close to the wheel-hubs, giving the greatest possible time-advance with respect to the sound in the car. The next Section discusses the susceptibility to delays of the two test configurations.

4.3.3 Effect of delays

Any practical active noise control system will include delays in the control chain. The acoustic delays between the secondary loudspeaker(s) and the error microphone(s) have already been mentioned, and in practice would have a value of up to about 6 ms. Each reference signal will pass through an anti-aliasing filter with typically 3 ms delay; a further low-pass filter will also be required to reconstruct the digital output of the system. If this is omitted, the system output will contain disturbing harmonics caused by step discontinuities at the control system output. This reconstruction filter would typically add another 3 ms to the control delay. The total delay which the system should be able to withstand is thus of the order of 12 ms.

The active control predictions discussed in the previous Section have been carried out with a range of values of pure delay included in the control chain in place of the filter representing the vehicle interior acoustics. The influence of a delay depends on frequency and also on whether any periodic components are present in the

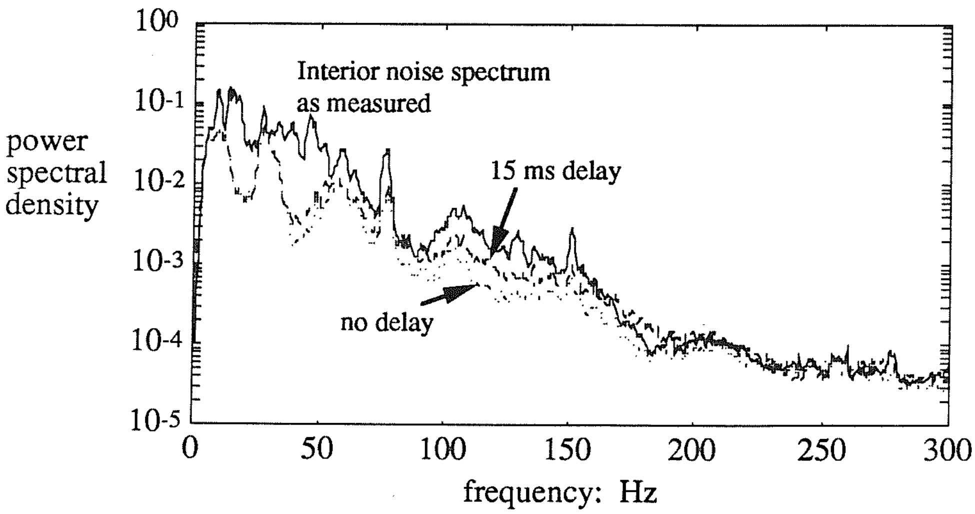

Figure 4.18: Predicted sound reduction in Citroen, no delay and 15 ms delay in control chain

reference signals. Figure 4.18 shows for the Citroen the effect of a 15 ms delay compared with no delay at all (*ie* not even an interior acoustic transfer function is included). Causal 128-point filters were used for both simulations. The deterioration in control at around 125 Hz is clear. There was little reduction above 180 Hz even with no delay, as noted above, although there was some coherence between the reference signals and the microphone.

Figure 4.19 compares the predicted broadband sound reductions at three frequencies and for both configurations of accelerometers (*ie* on the suspension (Astra) or on the underside of the floor (Citroen)). In choosing the frequencies, care has been taken to avoid peaks where the periodicity of the sound makes the control less susceptible to delays. The two configurations of accelerometers are of course not really comparable as they were made on different models of vehicle; nevertheless it is of interest to place the two sets of results side by side.

At all three frequencies the vehicle with accelerometers attached to the floor panels proved more sensitive to time delays. At 111 Hz (Figure 4.19(a)) the reduction available at 0 ms was greater using the floor-mounted accelerometers (due to greater coherence) but it declined more steeply until the system was ineffective with 25 ms delay. The trend was similar at 157 Hz. At 285 Hz the system with floor-mounted accelerometers was ineffective with any causal filter, irrespective of delay. On the other hand, the suspension-mounted accelerometers provided useful reference signals at this frequency.

For the practical situation in which the control system delay (including acoustic delay) is around 12 ms, the simulations show that some reductions can be expected whether the accelerometers are placed on the underside of the floor or on the suspension. However, it is clear that an active control system will tolerate more delay if the reference sensors are placed on the suspension, giving the greatest time advance. For the case where the accelerometers are fitted to the vehicle floor, Chapter 3 has shown that there is a significant time-penalty incurred as flexural waves are transmitted relatively slowly through the thin panels making up the vehicle body. This time-penalty could be minimised by placing the accelerometers as close as possible to the suspension mounting points where the forces are applied.

The disadvantage of placing the reference accelerometers on the vehicle suspension is that more of them appear to be required for adequate coherence with the sound

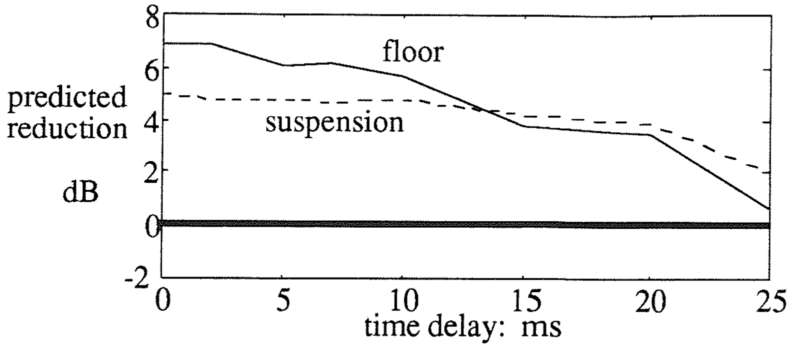

Figure 4.19(a) Effect of time delays: 111 Hz

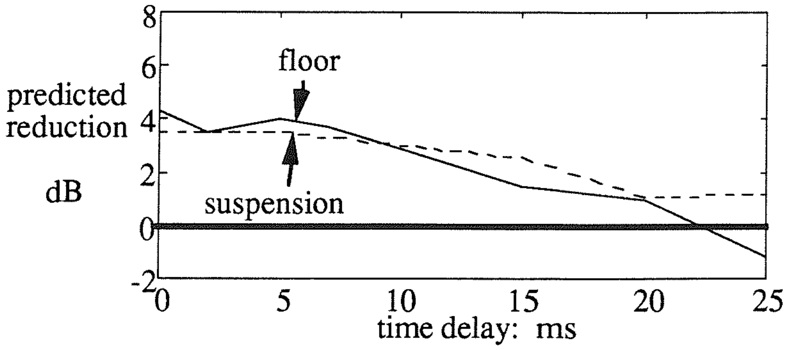

Figure 4.19(b): Effect of time delays: 157 Hz

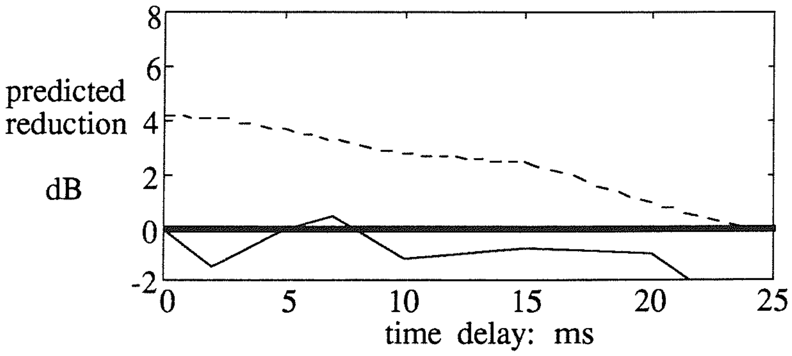

Figure 4.19(c): Effect of time delays: 285 Hz

field. In this case nine accelerometers were placed on the suspension and yielded less reduction than six attached to the floor panels. However it is not possible to draw a firm conclusion on this since different models of car were used for the two test configurations.

4.3.4 Filter length

For simplicity only FIR control filters have been considered in this study. Filters of this type are unconditionally stable and are readily implemented using special-purpose, fast DSP microprocessors. However, they have the disadvantage of requiring many coefficients to define them. The impulse response of an FIR filter consists of the sequence of its coefficients so the filter needed to model a lightly damped, resonant system will require many coefficients to represent the ringing of its impulse response. If an array of filters is to be implemented, as for multichannel active control, the calculation time can easily become excessive. Recursive filters (in which the calculation uses past values of the output) often require less coefficients to define their impulse responses but may become unstable (divergent) during optimisation. Single channel recursive filters have been applied to active sound control by Eriksson and Allie [1987].

The problems which arise when using short-length FIR filters for control have been touched on above in Chapter 3. The simulation study presented in Section 3.5.2 considered a force applied to a vibrating plate. The force was used as a reference signal for control of interior noise, and so the controller needed to model the response of the plate, including its lightly-damped low-frequency modes. As a result, the controller impulse response was of long duration, ringing for around 0.4 s in the case considered. When a short (0.128 s) control filter was used, the truncation degraded the sound reduction at low frequencies below about 100 Hz.

In this Section the measured vehicle noise and vibration are used to calculate the sound reductions which would be available with various filter lengths. For an active control system working in real time, a short filter length would allow more reference channels to be handled by a microprocessor of given capacity. This provides an incentive for keeping the filters as short as possible.

Figure 4.20 shows a comparison of the predicted reduction in the Citroen (floor-mounted accelerometers) using 128-point optimal filters with the reduction using 16-point filters. The impulse response of the 16-point filters lasts just 15 ms. At low frequencies virtually all the reduction is lost with the short filters but in the range 100-150 Hz there is still a significant reduction.

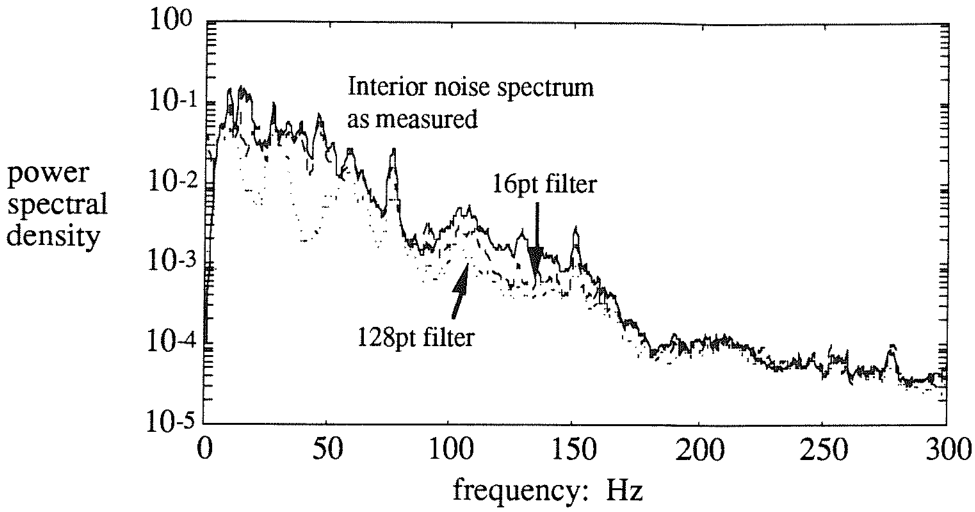

Figure 4.20: Predicted sound reduction in Citroen, 128pt and 16pt control filters (no delay in control chain)

In contrast with the earlier graph showing the effect of time delays (Figure 4.18), narrow peaks in the noise spectrum are not efficiently attenuated by the short filters. The reduction at 151 Hz is poor, for example. As noted above, short FIR filters are unable to model lightly-damped systems with long impulse responses.

The fall-off in performance with reducing filter length is shown at three frequencies in Figure 4.21. At very low frequencies (39 Hz in this example) the predicted reduction falls steadily as the filter length is reduced. The filter impulse response becomes too short to define accurately the magnitude and phase required for cancellation of low-frequency components. At 111 Hz the reduction is not greatly affected by filter lengths down to 64 ms; the performance suffers if the filter length is shorter than this. At 157 Hz only small reductions are available irrespective of filter length, but Figure 4.21 shows much less dependence on filter length and at this frequency the 16 ms filter gives more reduction than at either of the two lower frequencies. The impulse response of one of the six optimal filters is shown in Figure 4.22 for three filter lengths: 32 point, 64-point and 128 point.

These predictions indicate that over the frequency range of interest for active sound contol, a filter length of 64 ms will give adequate results. Short filter lengths can

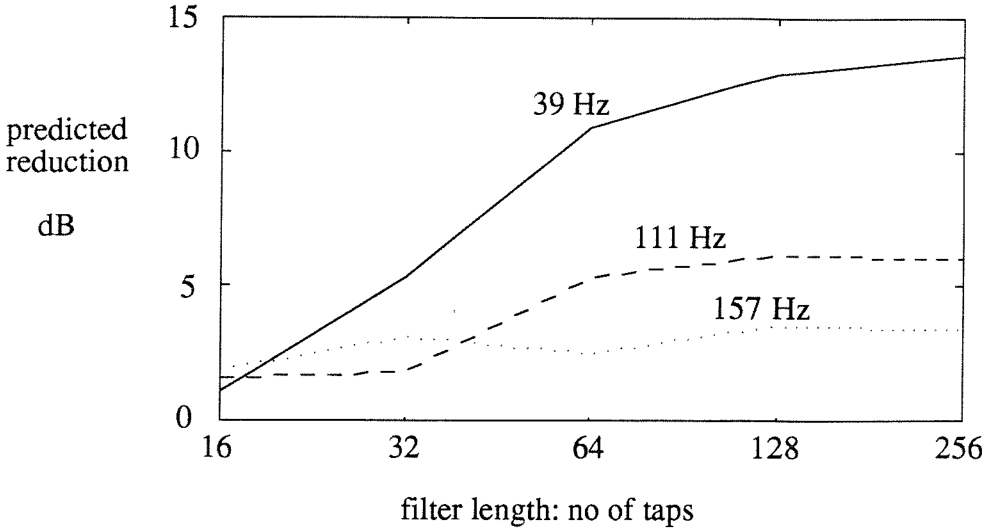

Figure 4.21: Effect of filter length (Citroen)

be expected to improve the control by using the available computing power to handle more reference signals, giving better multiple coherence and correspondingly larger reductions.

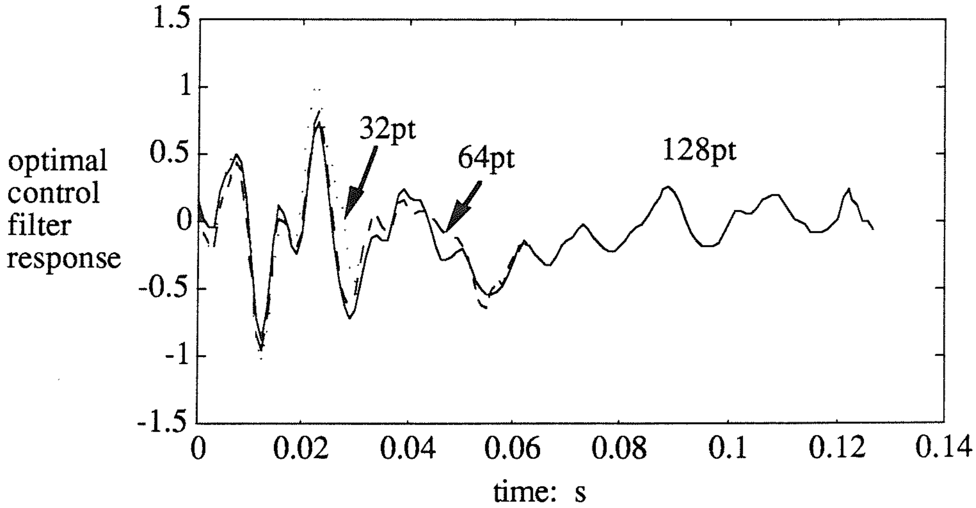

Figure 4.22: Optimal filters of various lengths predicted for sound reduction in Citroen (ref signal 3)

4.4 Active control demonstration

An experimental active control system has been constructed by Lotus Engineering to demonstrate road noise attenuation in cars. It has provision for two reference signals, two interior loudspeakers and two interior microphones. The required fast digital signal processing is carried out by a single microprocessor, the Texas Instruments TMS320C25. The filters representing the vehicle interior acoustics are identified during and initial setting-up phase after the equipment has been switched on. During this initial phase a white noise signal is applied to each loudspeaker in turn. The interior acoustics filters are then held fixed during on-line control. The multiple-error filtered-x LMS algorithm is implemented at each time-step for rapid adaption to changing road conditions (see Section 2.4).

Initial results with this equipment have been reported in [McDonald *et al*,1991] and are reproduced here. The road noise control system was installed in a large saloon car and measurements were made under normal driving conditions. The two reference signals were taken from accelerometers suitably located on the underside of the vehicle. The accelerometer locations were chosen to give the best multiple coherence with respect to the interior noise. Both the two loudspeakers and the two microphones were located at the back of the vehicle, one on each side.

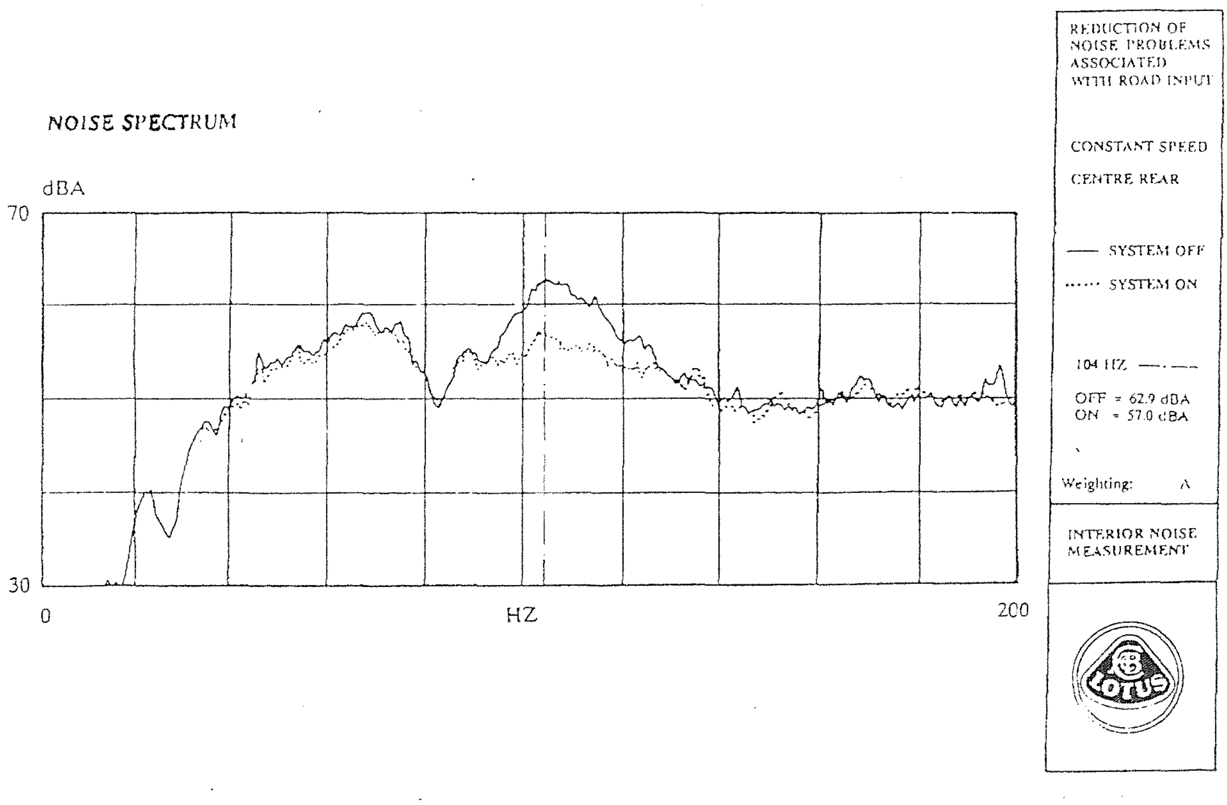

Figure 4.23: Demonstration of active road noise control in large saloon car

The A-weighted noise spectra inside the car with and without road noise control are shown in Figure 4.23. For this test the vehicle was driven for 4 miles at about 70 mph over a range of road surfaces. The solid line shows the interior noise with the system off. The spectrum is dominated by a peak at about 100 Hz which is thought to be due to a structural resonance of the rear suspension which is excited by wheel vibration. There was a reduction of nearly 6 dB at this frequency when the control system was operating.

The results confirmed that there is some scope for control of road noise using linear feedforward controllers. The car used was unusual in that just two reference signals were sufficiently coherent with the interior noise to give a useful attenuation. In the more typical cases examined earlier in this Chapter at least six reference signals have been required for significant road noise attenuation.

4.5 Conclusion

Noise and vibration measurements have been carried out on two popular models of family hatchback car. The measurements were used to calculate the expected performance of an active road noise control system in various configurations. The main conclusions are:

(1) The impulse response of one of the vehicles, obtained by driving over a raised bar, showed delays of 10-20 ms as the transients propagated around the structure. This was consistent with the expected speed of propagation of flexural waves through the body panels.

(2) Vertical suspension acceleration measured at the rear wheels was strongly correlated with the corresponding measurement at the front wheels, as might be expected since both sets of wheels roll over the same road surface; however, the coherence between them was not sufficient to allow the front wheels to be used to predict rear-wheel vibration except at very low frequencies (below 30 Hz).

(3) The multiple coherence was evaluated for various combinations of accelerometers attached to the front and rear suspension (for the Astra) and floor panels (for the Citroen). In all cases the multiple coherence increased progressively with the number of accelerometers used. This suggested that vibration components in different directions on the same wheel-axle were contributing independently to the interior noise. Significant values of multiple coherence were only achieved when all the accelerometers were included.

(4) Even under these conditions the multiple coherence was not high, which may indicate nonlinear transmission paths from these vibration signals to the interior acoustics, a point which will be returned to in Chapter 5.

(5) The six Citroen floor-panel accelerometer measurements were treated as reference signals and the optimal causal 128-pt filters were calculated to minimise mean squared sound level at the rear microphone inside the car. The predicted sound level inside the car using the filters for active control was reduced by 5 dB in the range 90-140 Hz. No reduction was predicted above 160 Hz.

(6) Similar predictions for the Astra, in which suspension accelerometers were used as reference signals, showed small sound level reductions at frequencies up to 300 Hz. It appeared that location on the vehicle suspension gave better time advance allowing the higher frequencies to be attenuated by causally constrained filters. However, more accelerometers were needed on the vehicle suspension than the body to obtain the same coherence level.

(7) The effect of varying the length of the FIR control filters was examined. Naturally, shorter filters gave poorer attenuation as the filter response was truncated. However even very short (16-point) filters were predicted to give some reduction in the range 100-150 Hz, although they were ineffective at low frequencies below 100 Hz.

5 USE OF NEURAL NETWORKS IN ACTIVE SOUND CONTROL

5.1 Introduction to neural networks

5.1.1 Introduction

The test results in Chapter 4 have shown that poor coherence between the reference signals and the sound to be cancelled severely limits the scope for active control of road noise in cars. This poor coherence is due partly to other sources of sound (such as wind noise) which may not be detected by the reference accelerometers. However the test results suggest strongly that the poor coherence arises to some extent from nonlinear transmission of the vibration through the vehicle structure, in particular between the suspension (where the accelerometers may be placed for maximum time-advance) and the body-shell. Such nonlinearities may include rubber bushes whose stiffness varies due to high-amplitude low-frequency vibration; and backlash (hysteresis) in linkages. If it were possible to represent these processes by some nonlinear signal processing operation then better prediction and cancellation of the sound field might be achieved.

This Chapter examines the possibility of using a neural network to model dynamic nonlinear systems. Neural networks are adaptive and offer the possibility of self-adjustment to match changing vehicle conditions. They require substantial computing power but advances in microprocessor technology are rapid and this problem need not limit progress indefinitely. In particular, parallel processors are now coming into widespread use.

Section 5.1 sets out the basic features of neural networks, particularly applied to dynamic nonlinear systems. In Section 5.2 a neural network is used to model two simple nonlinearities. After adaptation the network weighting coefficients are examined, giving insight into the operation of the network. Finally in Section 5.3 some first steps are taken in applying this approach to real vehicle nonlinearities.

5.1.2 Neural networks

The term 'neural network' describes a network of simple computational elements which are densely interconnected. The output of each element normally forms the input to several other elements. In such a network, many computations can be carried out in parallel, rather than serially as in conventional computers. The word 'neural' arises because of similarities with biological nervous systems.

Neural network architectures have been studied since the 1940's [McCulloch and Pitts,1943] but since 1986 they have received wide attention because of the publication of the book 'Parallel Distributed Processing: Explorations in the Microstructure of Cognition' by Rumelhart and McLelland [1986]. Rediscovering earlier work by Werbos [1974], the authors presented the 'backpropagation algorithm' for adapting the coefficients of a neural network. Use of this algorithm has opened up a wide range of applications.

Neural networks have been found to be particularly useful for pattern recognition problems. After an initial setting-up or 'training' phase, they are able correctly to place a set of input data into one of several categories even when the input set is corrupted by noise. They have been found able to 'generalise' the classifications originally obtained from the training set. Thus important areas of neural network research are speech and character recognition. This Chapter will examine the possibility of using a neural network to model nonlinear elements in a car, such as the transmission of structural vibration through rubber suspension isolation bushes.

In his introduction to the subject, Lippmann [1987] identifies six different types of neural network. All involve one or more layers of interconnected computing elements. In some cases the outputs are fed back as inputs, creating a recursive network (*eg* the Hopfield net). However for simplicity the work reported here is confined to the widely-used feedforward architecture. Figure 5.1 shows a fully-connected two-layer feedforward network with three inputs, two outputs and one 'hidden' layer of five elements.

Each computing element has multiple inputs and a single output. The basic element was described by Rosenblatt [1959] and was termed by him the perceptron. It is shown in Figure 5.2. This basic element has been refined more recently as described below but the concept remains the same. Each input x_i is multiplied by a weight w_i and the resulting signals are added together. A constant bias θ is subtracted before applying the sum s(n) to a hard-limiting decision function f_h. The output y(t) is then equal to +1 or -1. The inputs x_i may be binary values (1 or 0) in which case the element performs a Boolean logic function, or alternatively they may take continuous values in which case the element simply makes a decision based on their values relative to one another. In the case of two inputs,

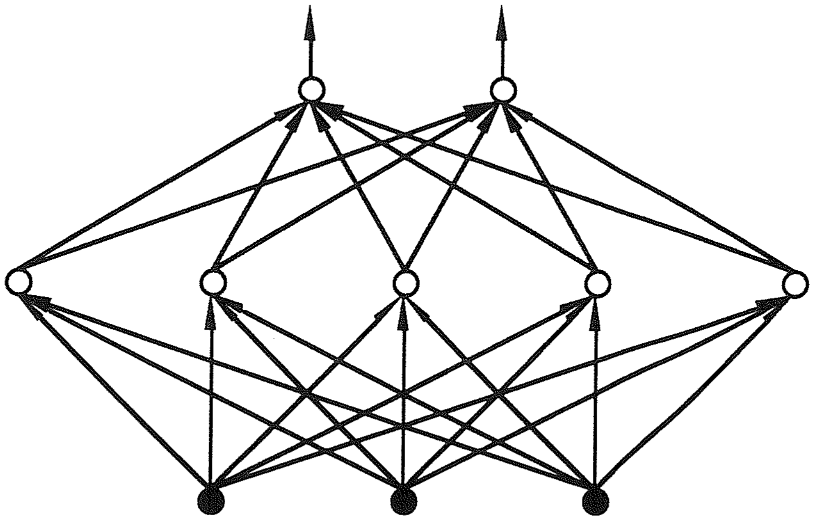

Figure 5.1: Two-layer feedforward neural network

the perceptron decides which side of a line to place the given input pair shown in Figure 5.3. The decision boundary depends on the weights and the bias constant. In the general case of N inputs the decision boundary is a hyperplane in N-dimensional space.

The best location for the boundary is determined during a training process in which trial inputs are presented along with the correctly classified output (+1 or -1 as appropriate). In Rosenblatt's original concept the weights were updated according to the rule:

$$w_i(n+1) = w_i(n) + \eta[d(n) - y(n)]x_i(n) \qquad (5.1.1)$$

where d(n) is the desired output, η is a gain term and the other quantities are as defined in Figure 5.2. If the perceptron decision was wrong, this algorithm moved the weights in a direction to increase the likelihood of a right decision in future. As a result of using this rule the decision boundary moved during training to a point which separated the two input classes.

It is clear that a single perceptron element can only classify inputs into one of two sets which are separable by a hyperplane as described earlier. This is a severe limitation. More subtle classifications can be obtained by combining several elements in parallel to form a

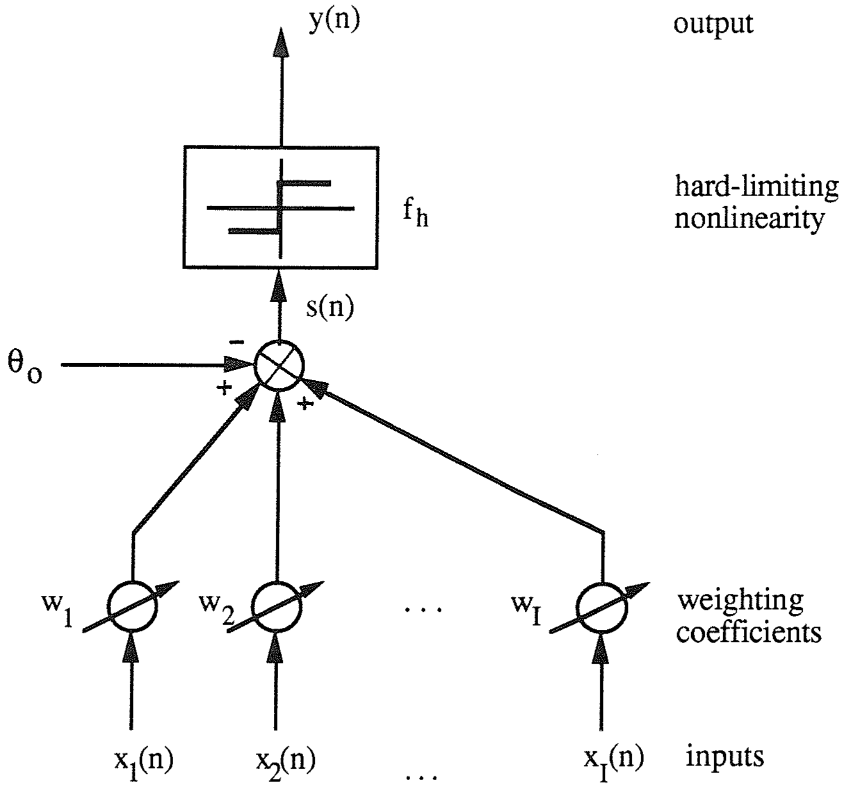

Figure 5.2: Perceptron computing element

so-called hidden layer and then combining their outputs using a further perceptron as an output element. Each element in the hidden layer creates its own hyperplane in the input space and the output element can act as an AND-gate, defining a region formed by all the intersecting half-plane regions formed by the hidden-layer perceptrons. It turns out that a two-layer perceptron with sufficient hidden units can implement any Boolean function [Widrow and Lehr,1990]. The use of multi-layer perceptron (MLP) networks to model nonlinear dynamic systems will be discussed in Section 5.1.4. The next Section briefly reviews how the weighting coefficients are updated in MLP networks.

5.1.3 Backpropagation algorithm

A drawback with Rosenblatt's adaption procedure was that the error [d(n) - y(n)] was either zero or ±2: there was no gradual variation. As a result, if inputs from the two classes were intermingled (so that they could not be separated by a hyperplane) the decision boundary would oscillate. This problem was overcome by Widrow who compared the summed signal before the nonlinearity (s(n) in Figure 5.2) with the desired output to form a linear error: the Widrow-Hoff LMS algorithm was then used to update the weights. This placed the decision boundary so as to minimise mean squared error.

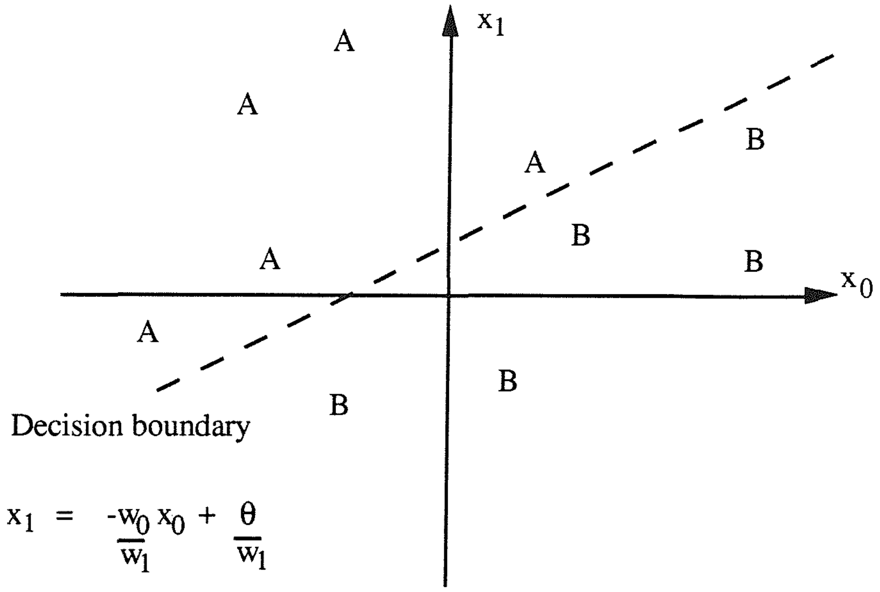

Figure 5.3: Input classification with a single perceptron element (after Lippmann [1987])

Widrow's algorithm could not be used to adapt multi-layer perceptron networks because in a multi-layer network only the outputs of the final layer can be compared with desired values. There are no corresponding desired values to apply to the lower layers. To overcome this limitation the 'backpropagation algorithm' was developed. The first publication of this algorithm was by Werbos [1974] in his doctoral dissertation; the technique was later rediscovered by Parker [1982] and again rediscovered in 1986 by Rumelhart, Hinton and Williams [1986], this time receiving wide attention. The backpropagation algorithm involves two elements: firstly, it is necessary to calculate a sensitivity function which represents the effect each perceptron element has on the final sum of squared output errors; secondly these sensitivities are used to update the weights for each perceptron element using the method of steepest descent. All the weights are updated so as to reduce the final sum of squared errors at the network output, rather than any intermediate quantity.

In order to calculate the sensitivity of the output error to individual perceptrons it is necessary to use a different output nonlinearity in the individual perceptron elements: instead of a hard-limiting function, a smooth, continuously-differentiable nonlinear function is used, forming a soft limiter. Such a function (shown in Figure 5.5) is termed a 'sigmoid' function. Widrow and Lehr [1990] recommends the tanh function, which limits at ±1.

The backpropagation algorithm is developed in [Rumelhart, Hinton and Williams,1986] and explained clearly in Widrow's review paper [1990]. It is stated there for a two-layer network, but can be readily applied where there are more than two layers. Note also that the bias weight is updated as well as the input weights.

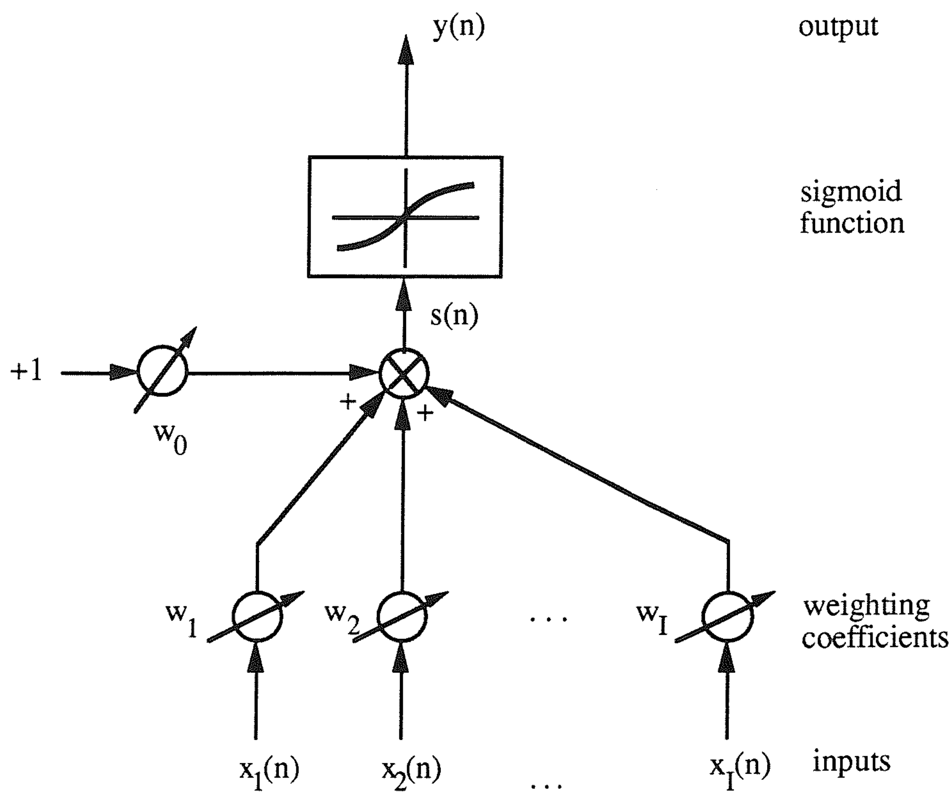

Figure 5.5: Perceptron computing element with sigmoid nonlinearity

5.1.4 Use of neural networks to model nonlinear dynamic systems

In the preceding Sections the multi-layer perceptron network has been presented as a means of classifying input patterns presented on several inputs and placing them into one of several output categories. The output categories were defined by the binary states (±1) of one or more output perceptrons. However the use of soft-limiting sigmoid functions opens up the possibility of a continuously variable output. Thus a neural network can in principle model a static multiple-input multiple-output nonlinear function. It can be shown that a two-layer network can implement any continuous input-output mapping to arbitrary accuracy provided there are sufficient hidden units [Widrow and Lehr,1990].

The possibility of using neural networks to model nonlinear dynamic systems has been discussed by Narendra and Parthasarathy [1990]. They consider a form of feedforward neural network in which the inputs are obtained from a tapped delay line, so that the output y(n) depends on the recent time history of the (single) input x(n) as shown in Figure 5.6. As we are modelling continuous signals there is no requirement for a sigmoid function on the output perceptron: a soft-limiting nonlinearity would only create a need for special scaling of the desired output. Instead the outputs of the hidden-layer sigmoids are simply summed.

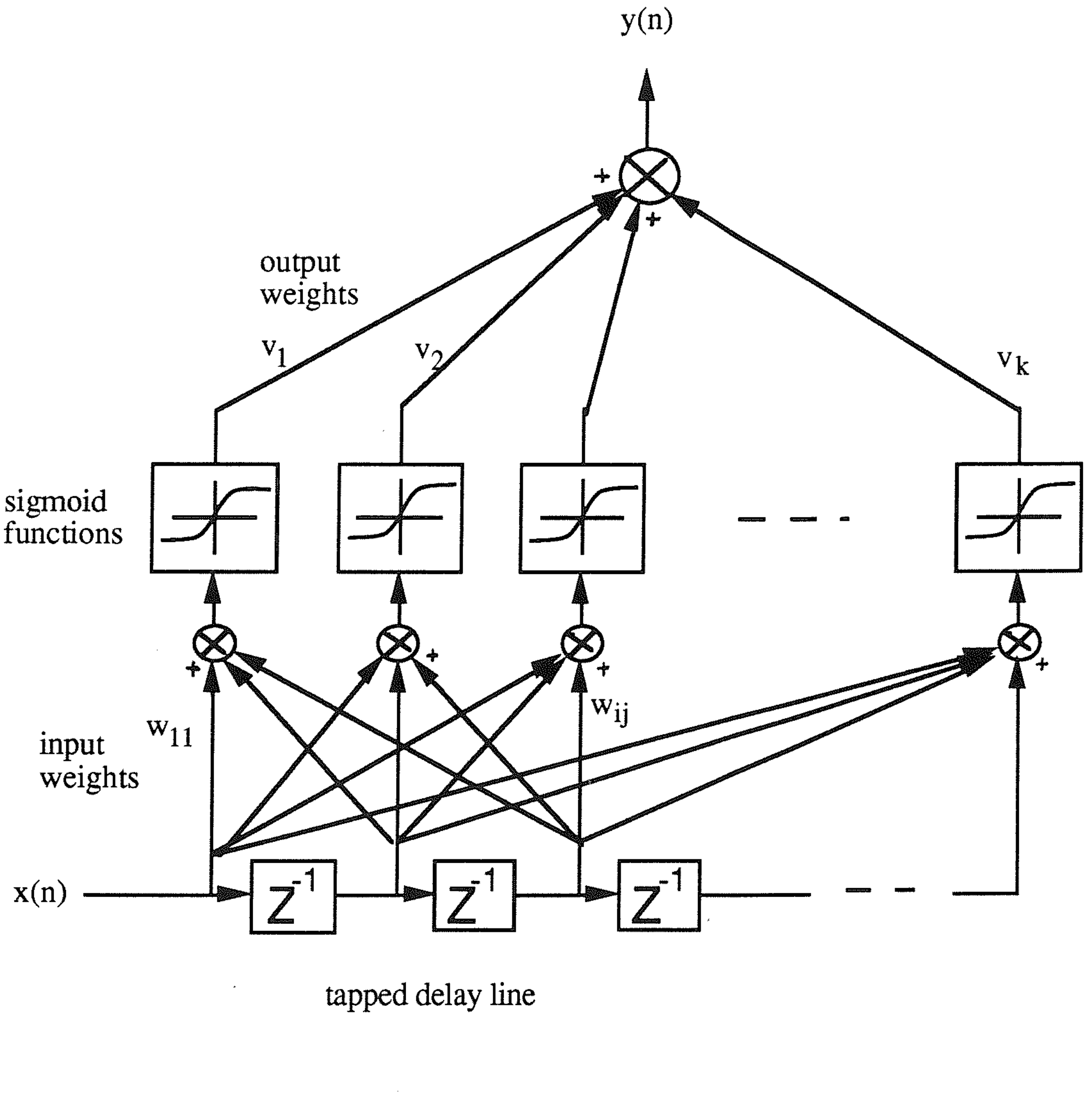

Figure 5.6: Two-layer neural network with tapped delay line on input

In the next Section the use of neural networks will be examined both for modelling static nonlinearities and (with a tapped delay line) for modelling single-input single-output dynamic nonlinear systems.

5.2 Application to model problems

5.2.1 Static nonlinearity

A Fortran program 'neuralnet1' has been written to study the modelling of single-input single-output dynamic systems using neural networks. The scheme is as shown in Figure 5.7. An input x(n) gives rise to a target signal d(n) via the nonlinear system to be modelled. The error between the neural network output y(n) and the target signal is used to update the network. In 'neuralnet1' the network is of the form shown in Figure 5.6 with one hidden layer of sigmoids and a single linear output element. At each time-step the program starts at the input layer, sweeping the calculation forward through the network until the output is found; next the output error is used to update all the weights, starting with the output element and propagating back through the network. Thus all the weights are updated at every time-step.

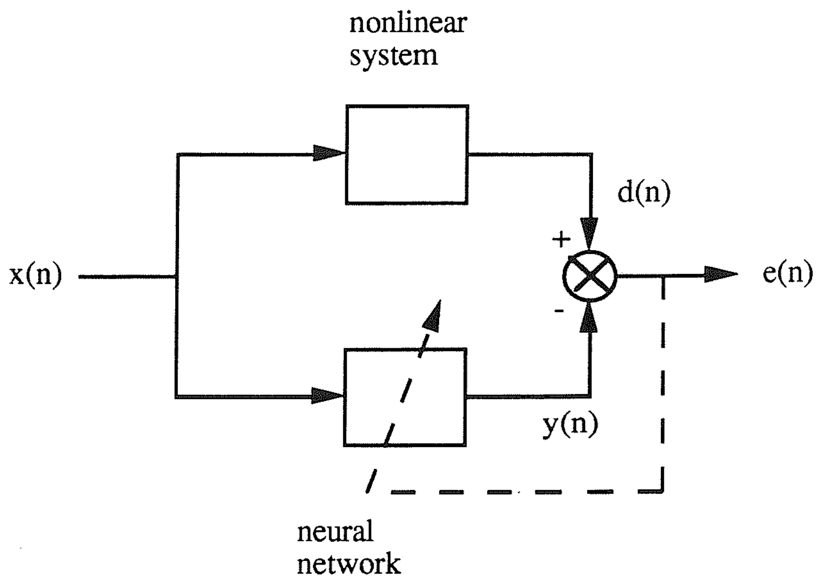

Figure 5.7: Scheme to model a nonlinear system using a neural network

The first model problem was a simple cubic nonlinearity:

$$d(n) = x^3(n) \qquad (5.2.1)$$

For this single-input system with no dynamics, just one input node was used along with five hidden-layer units. The sigmoid functions were chosen to be tanh functions as in [Widrow and Lehr,1990].

The input signal (x(n) in Figure 5.7) was broadband random noise, sampled at 1000 Hz with anti-aliasing filter applied at 330 Hz. The record comprised 180 blocks of 1024 points/block, representing three minutes of sampled data. The target signal d(n) was obtained by simply taking the cube of each input sample. The weighting coefficients on the inputs of the sigmoid functions were initially set to random values in the range ±5; those on the outputs to random values in the range ±1. The entire input record was presented once to the network and the weights adapted at each time-step (input layer convergence coefficient, 0.1; output layer coefficient, 0.01). To assess the resulting network configuration, the weights were then held fixed while a new (unseen) record of input and target data was presented to the network.

The spectra of the time-series with fixed weights and unseen data are shown in Figure 5.8. The Figure shows the spectra of the target data (*ie* with the cubic function applied) together with the error between the network output and the target. After one complete pass of the (training) input record (184 000 weight updates) the error was some 10 dB smaller than the

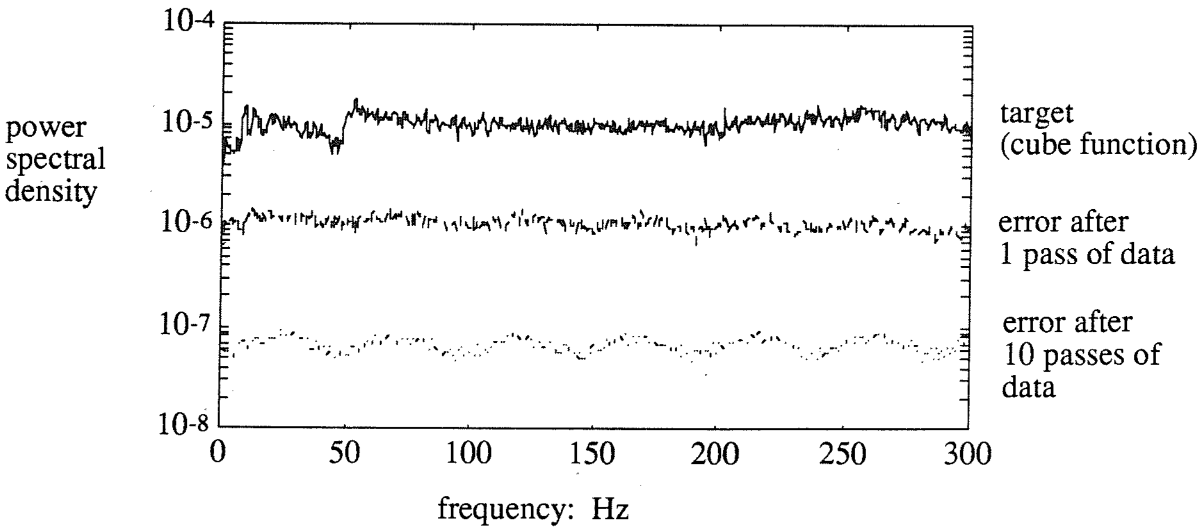

Figure 5.8: 1-5-1 Neural network model of cubic nonlinearity: target and error spectra with random noise input

target. However, when the training record had been presented to the network a total of ten times (1.8 x 10^6 weight updates) the network modelled the cubic function more accurately and the error was reduced by a further 10 dB.

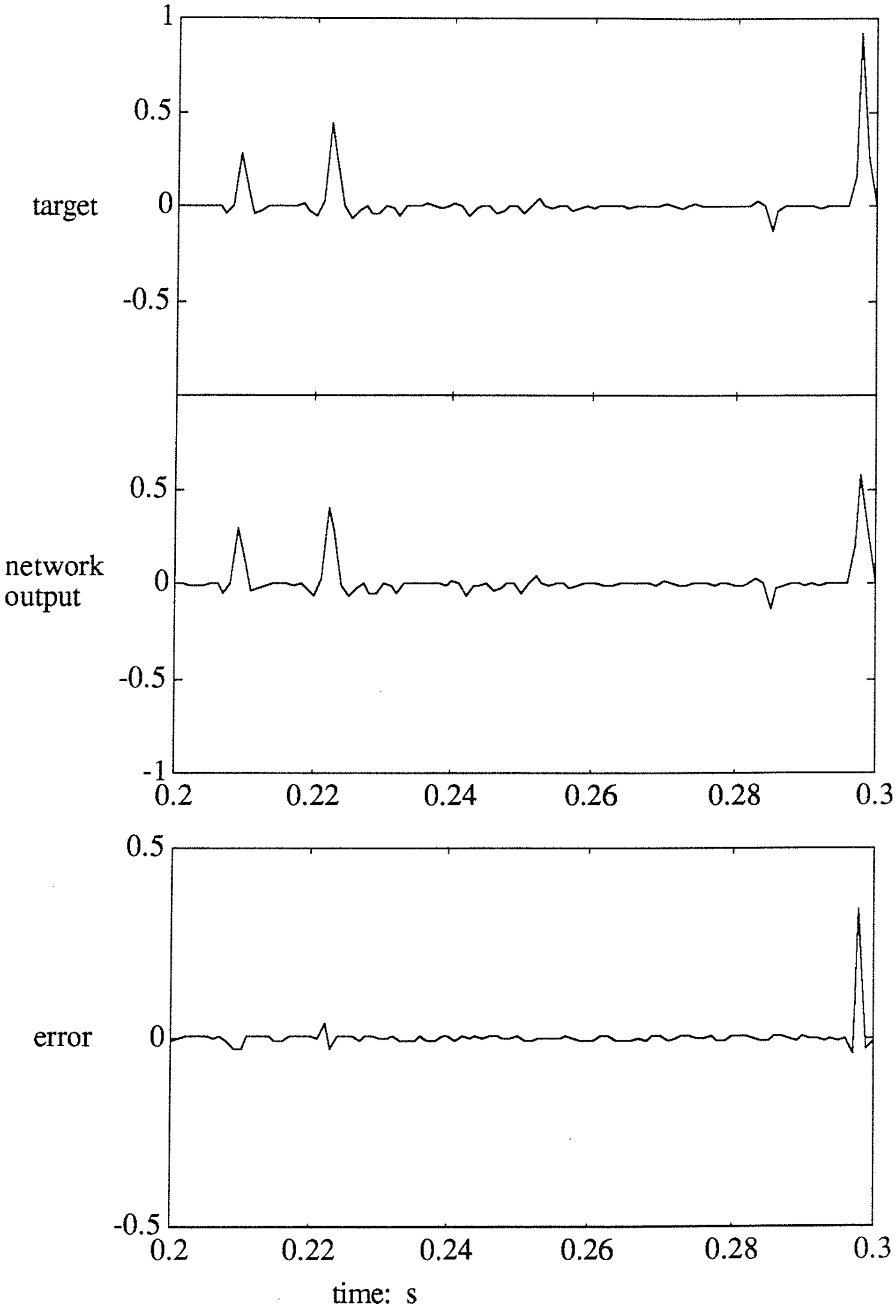

Figure 5.9: Fragment of time-series after one pass of training data

Figure 5.9 shows a fragment of the time-series with fixed weights and unseen input data. After one training pass the error was small except where there were large peaks in the target. It is clear that the network had not yet formed an accurate representation of the cubic function at higher amplitudes. However after ten presentations the high-amplitude excursions were also modelled and the error was reduced to a low level (Figure 5.10).

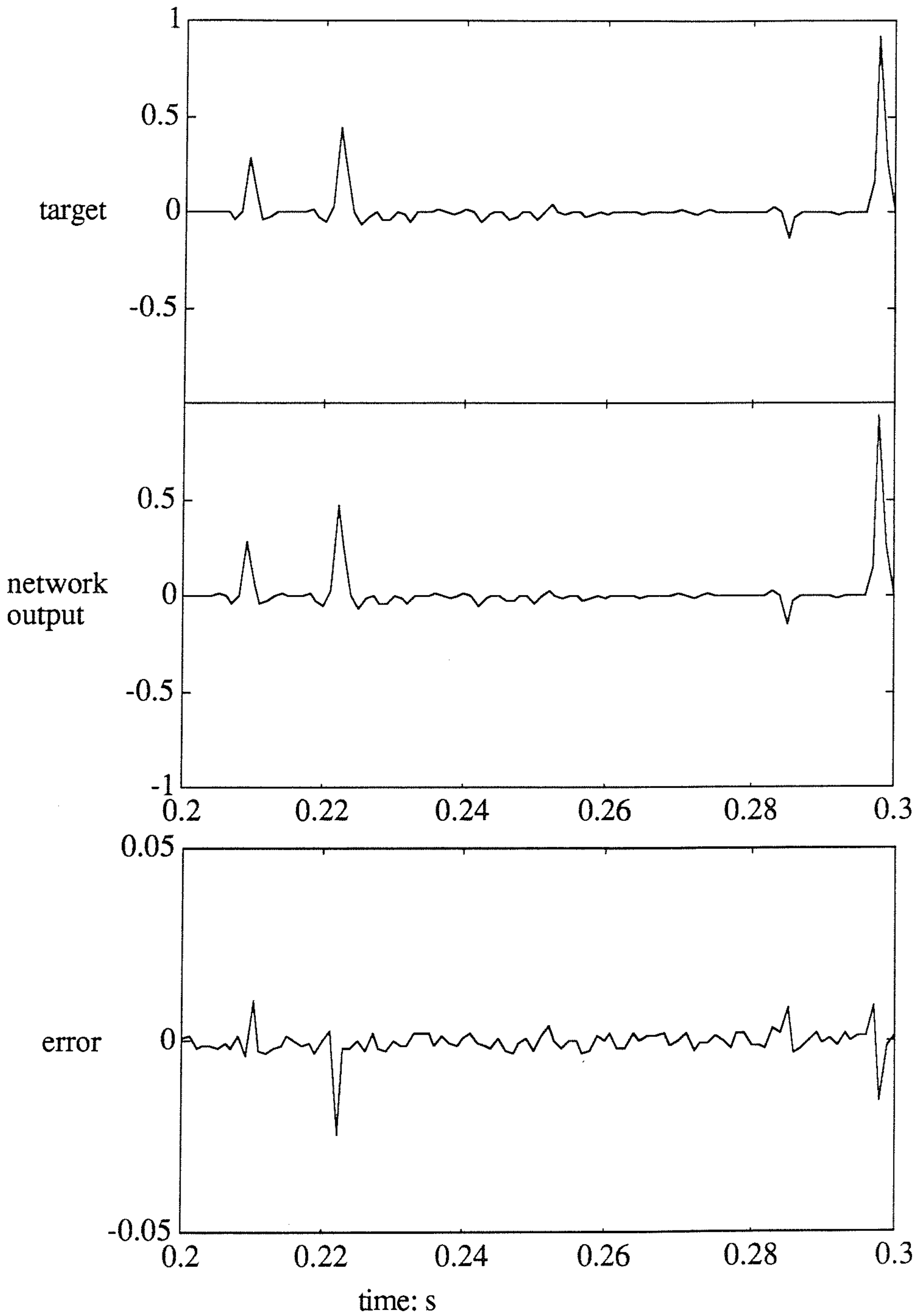

Figure 5.10: Fragment of time-series after ten passes of training data

It is of interest to present a ramp function to the network with the weights fixed after training. The result of doing this is shown in Figures 5.11 and 5.12. The network weights were obtained after ten passes of the training data. Figure 5.11 compares the target d(n) (a ramp passed through a cubic function) with the network output y(n); Also shown is the error. The network has formed a good representation over the restricted input range but elsewhere the representation is poor. It appears that the network is able to interpolate between the data points given during training but in this case does not show any capacity to extrapolate or generalise: it does not infer the nature of the nonlinearity outside of the range seen during training.

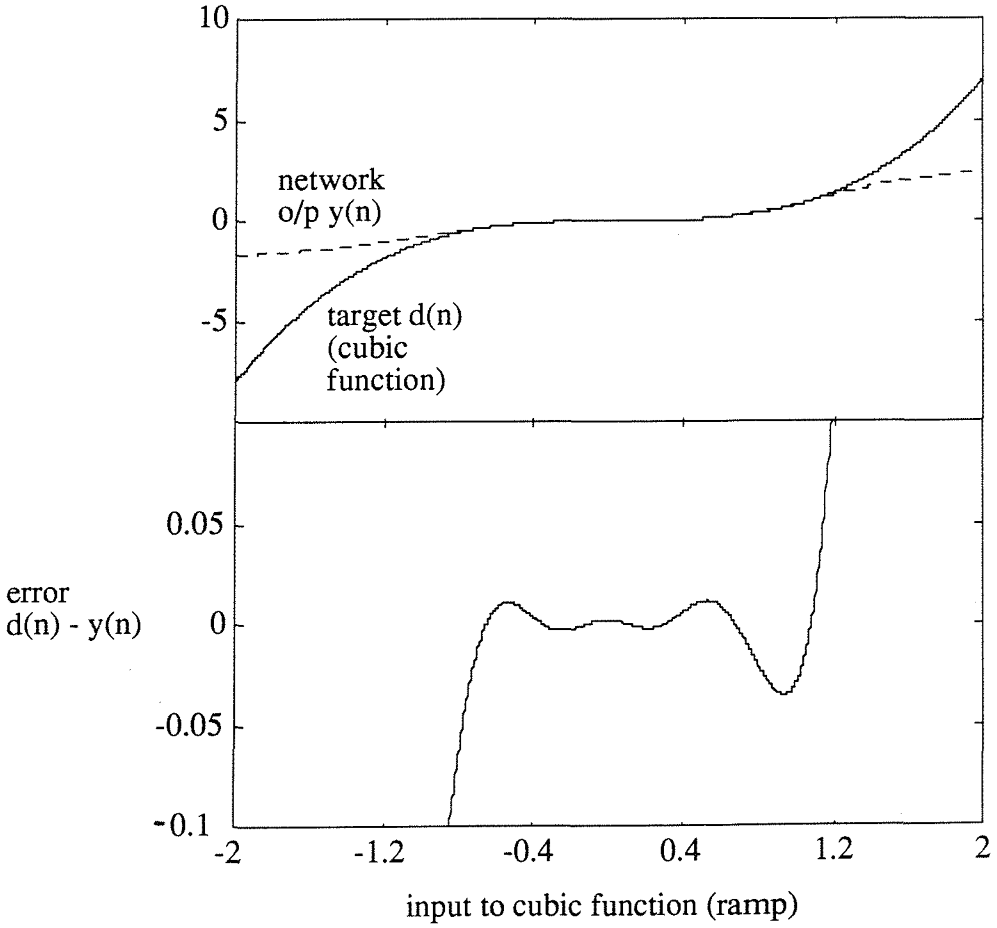

Figure 5.11 Response of trained neural network to ramp input

Figure 5.12 gives some insight into how the network weights have arranged themselves to represent the cubic function. The five traces show the output of each sigmoid, scaled by its corresponding output weight. The network output is the sum of these five contributions plus a fixed bias term. The vertical scaling of each sigmoid function is proportional to the

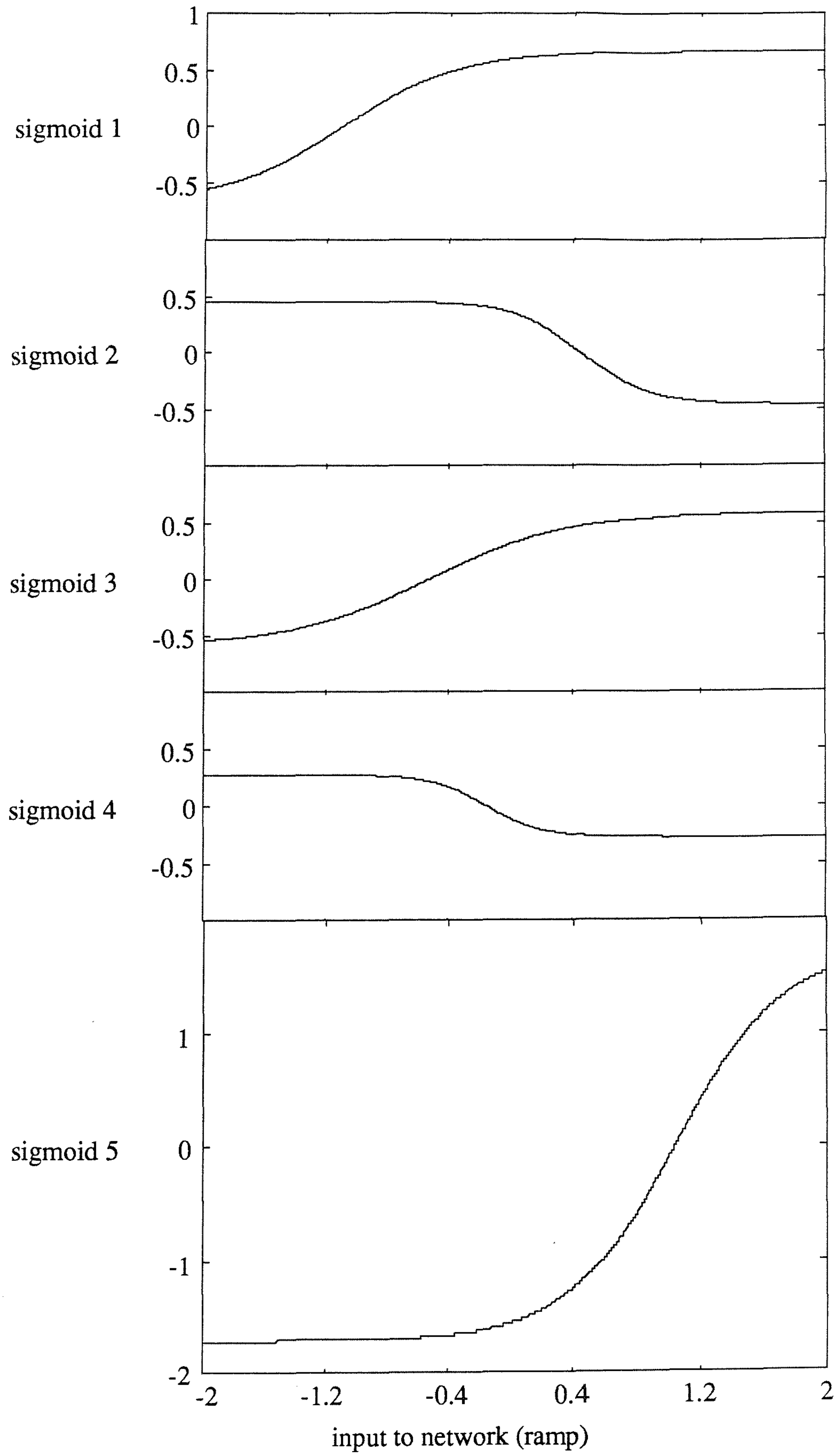

Figure 5.12: Response of trained 1-5-1 network to ramp: scaled sigmoid outputs

output weight; the scaling of the sigmoid along the horizontal axis depends on the input weight, while the input bias shifts the sigmoid to the left or right. (A steep sigmoid, *eg* trace 2, corresponds to a large input weight.) At any given input value the network output is the sum of both positive and negative contributions from the sigmoid functions, which are offset one against another. Comparing Figure 5.11 with Figure 5.12, it is clear that the steeper parts of the cubic function are made up of contributions from sigmoid 1 (negative) and sigmoid 5 (positive). The shallow part of the curve around t = 0 is made up chiefly

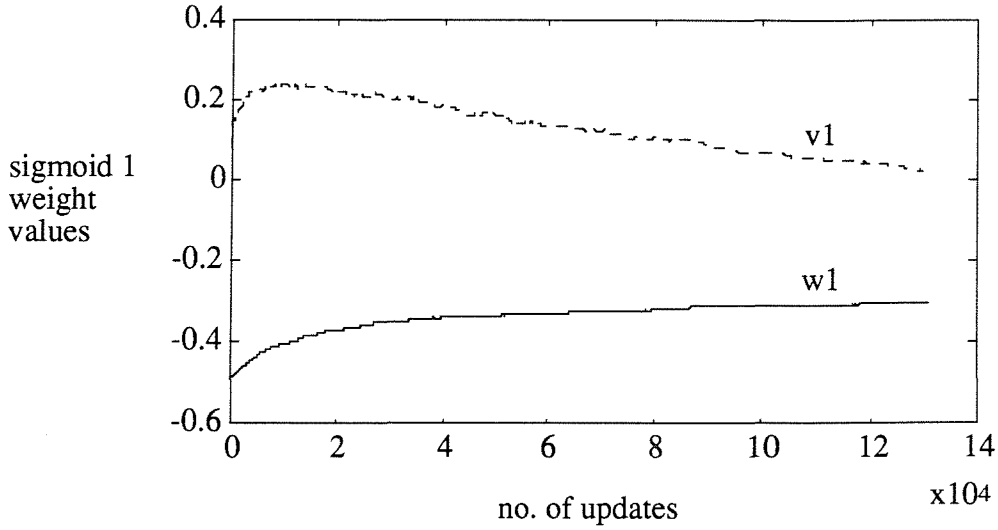

Figure 5.13(a): Weight movements for sigmoid 1 during training: one pass of data

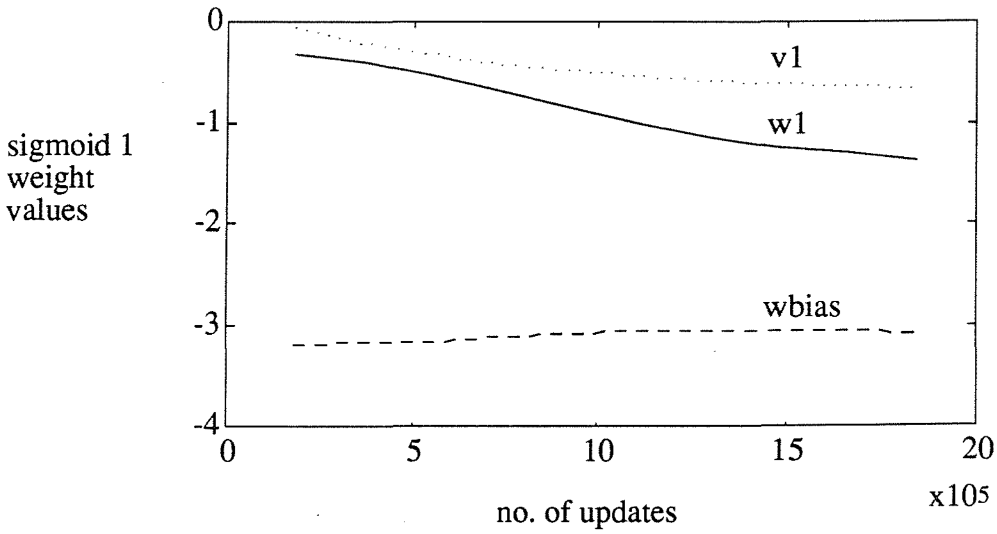

Figure 5.13(b): Weight movements for sigmoid 1 during training: ten passes of data

of sigmoids 2,3 and 4, which have adjusted so that the sum of their gradients is close to zero.

The movements of one input and one output weight are shown in Figure 5.13. Figure 5.13(a) shows the weight changes over the first 140 sec of training data (most of the first pass); Figure 5.13(b) shows the alteration in these weights over the whole ten presentations of the training data. There is a rapid adjustment at the very start, in which the initially large error is reduced. During subsequent slow adjustments the nonlinear features are incorporated as the relative contributions of each sigmoid function are traded one against another.

The neural network is thus able to model a simple static nonlinearity as a combination of sigmoid functions, giving the required mapping from input to output over a restricted range. The situation becomes less straightforward when there is a dynamic relationship between input and output, as the input is presented as a tapped delay line and the number of weights is much greater.

5.2.2 Cubic nonlinearity with delay

A very simple form of time-dependence between input and output is a pure delay. This Section examines how the network modelled the same nonlinearity presented above but delayed by three samples:

$$d(n) = x^3(n-3) \tag{5.2.2}$$

The neural network structure was the same as used above (see Figure 5.6) with five sigmoid units but with four input taps instead of one. The network was therefore presented with x(n), x(n-1), x(n-2) and x(n-3). The network was fully interconnected so there were 25 input weights (including one bias per sigmoid) and six output weights. These were again set initially to random values in the range ±5 (input weights) and ±1 (output weights). It is clear intuitively that the network can be configured to model this function as accurately as the static cubic function: it is only necessary to set all the input tap weights for x(n), x(n-1) and x(n-2) to zero. The weights to each sigmoid for x(n-3) can then be adjusted appropriately. This is not what happened in practice, however.

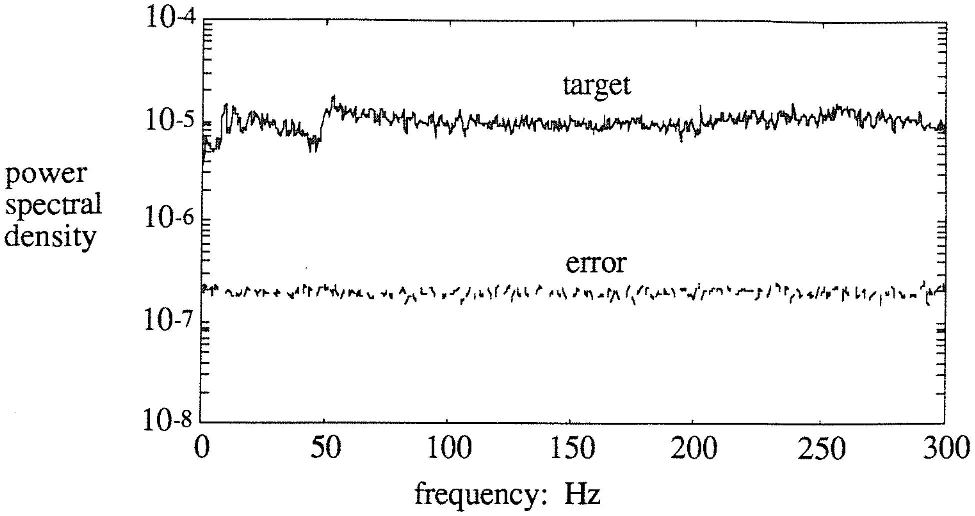

Figure 5.14: cancellation of target by 4-5-1 neural network model of cubic nonlinearity with delay

The complete training set was presented ten times (1.8×10^6 weight updates). The performance of the network was then assessed with the weights fixed and using unseen data. Figure 5.14 shows the spectra of the target data and network error. It is clear that a good model was obtained, though the error was not quite reduced by 20 dB as in Figure 5.8 after the same number of updates. Figure 5.15 shows a fragment of the time-histories. The error has been reduced to very low levels except where there was a high-amplitude peak. However it is most revealing to examine the adjustment of the weights during training and the final structure of the network.

Figure 5.16 shows the initial movement of the five output weights which scale the outputs of the five sigmoid elements. From initially random values in the range ±1 they move relatively rapidly during the first 2000 updates to reduce output error and then much more slowly. During the whole period of 1.8×10^6 updates (Figure 5.17) the output weights v_1 and v_5 take significant values (around 0.9) while the other three (v_2,v_3,v_4) are driven closer and closer to zero. Thus with zero output weights these three sigmoids contribute nothing to the result. Note that since the network is fully connected none of the sigmoid elements has any special significance with regard to time delays: each one is connected to all the input taps and there is no reason why they should not all contribute to the result. Looking at the input weights it is possible to see that these three sigmoids have been effectively locked out of the calculation.

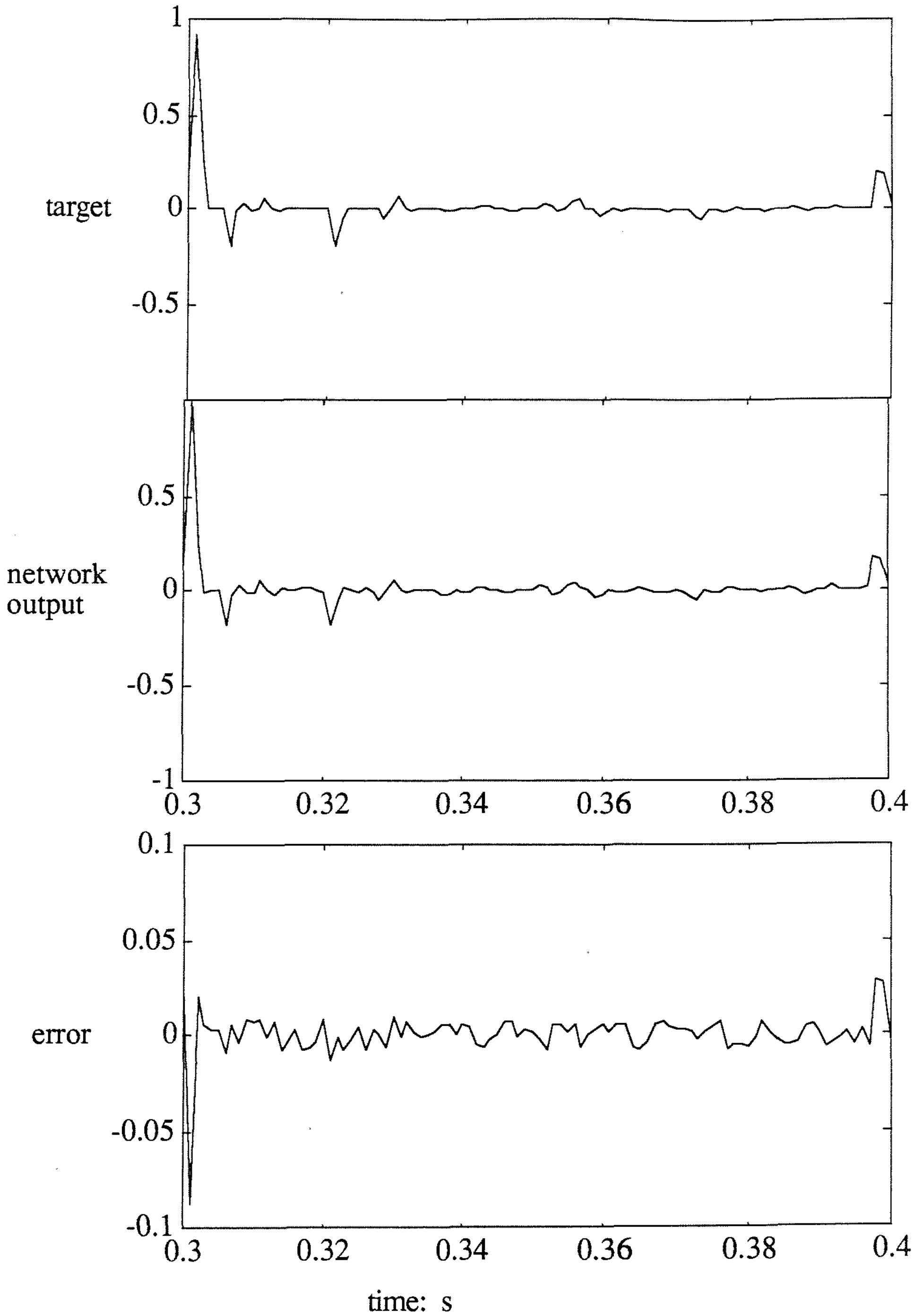

Figure 5.15: Fragment of time series after ten passes of training data

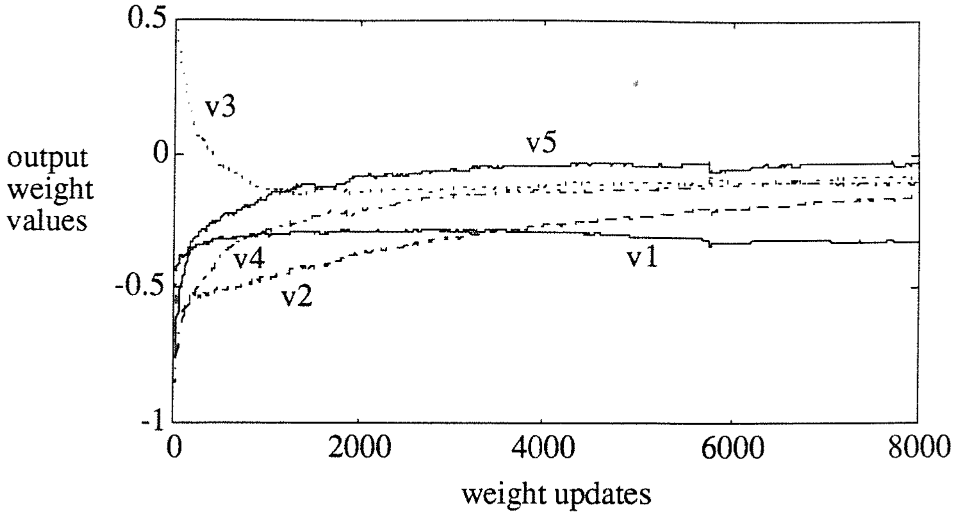

Figure 5.16: Initial movements of output weights

Figure 5.17 shows with each output weight v_j the corresponding five input weights (four tap weights and a bias weight). The input weights for the first and fifth sigmoid units arrange themselves as expected: the first three tap weights reduce to zero while the fourth tap weight which corresponds to a three-sample delay takes up a finite value. The bias weights also take up appropriate values. However all the input weights for sigmoids 2-4 stop moving because their output weights are zero. The reason for this is clear from the backpropagation algorithm. The input weights are adjusted according to the rule:

$$w_{ij}' = w_{ij} + \varepsilon \delta_j x_i$$

with

$$\delta_j = (1 - a_j^2)\, e_n\, v_j$$

Thus the rate δ_j at which the input weights are adjusted depends on the absolute value of the output weight v_j. If v_j is zero the the input weights w_{ij} do not change.

It appears that a situation can easily arise in which the input weights to a sigmoid are so inappropriate that the optimum value of its output weight is zero (The input weights are of course chosen randomly.) In this situation the network converges towards a local minimum error, rather than the lower global minimum value which could be achieved if all the sigmoids were used. With an output weight v_j close to zero the input weights w_{ij} are not altered to rectify the situation. In the simple problem examined here three of the five sigmoids failed to contribute for this reason. Thus in this situation there is a significant reduction in the number of effective neurons in the hidden layer.

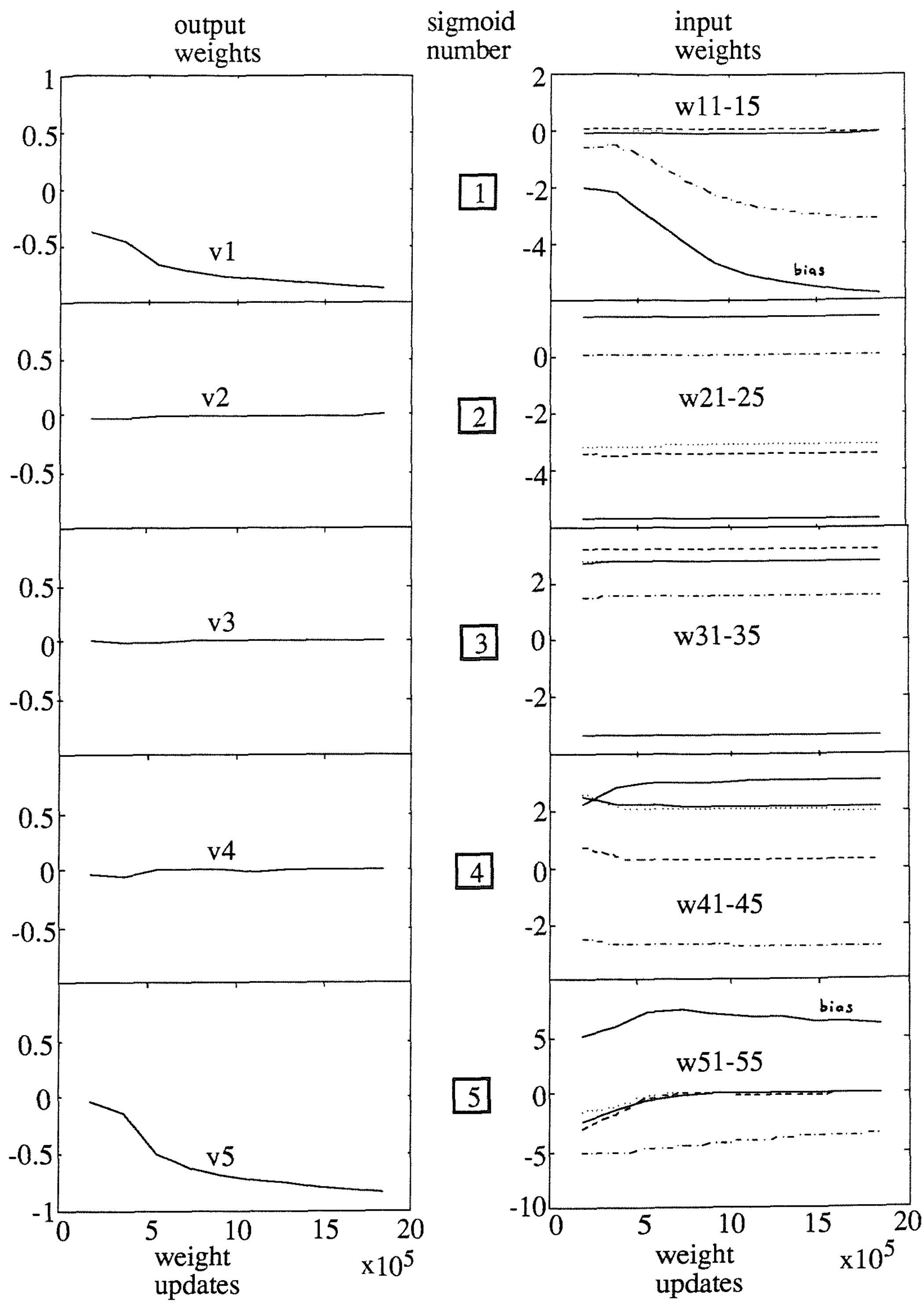

Figure 5.17: Movement of input and output weights, cubic function with delay

Figure 5.18 shows the sigmoid outputs scaled by their output weights in response to a ramp function. The cubic function has been modelled by just the first and fifth sigmoids with the others contributing nothing. Nevertheless the overall network output and error with random input (shown in Figure 5.14) indicate that the network has formed a good model of the given dynamic nonlinear system. The behaviour of the three sigmoids which were 'locked out' of the calculation suggests that in general plenty of sigmoids should be included in the network to allow some redundancy: perhaps twice the number actually needed to model the given nonlinear system.

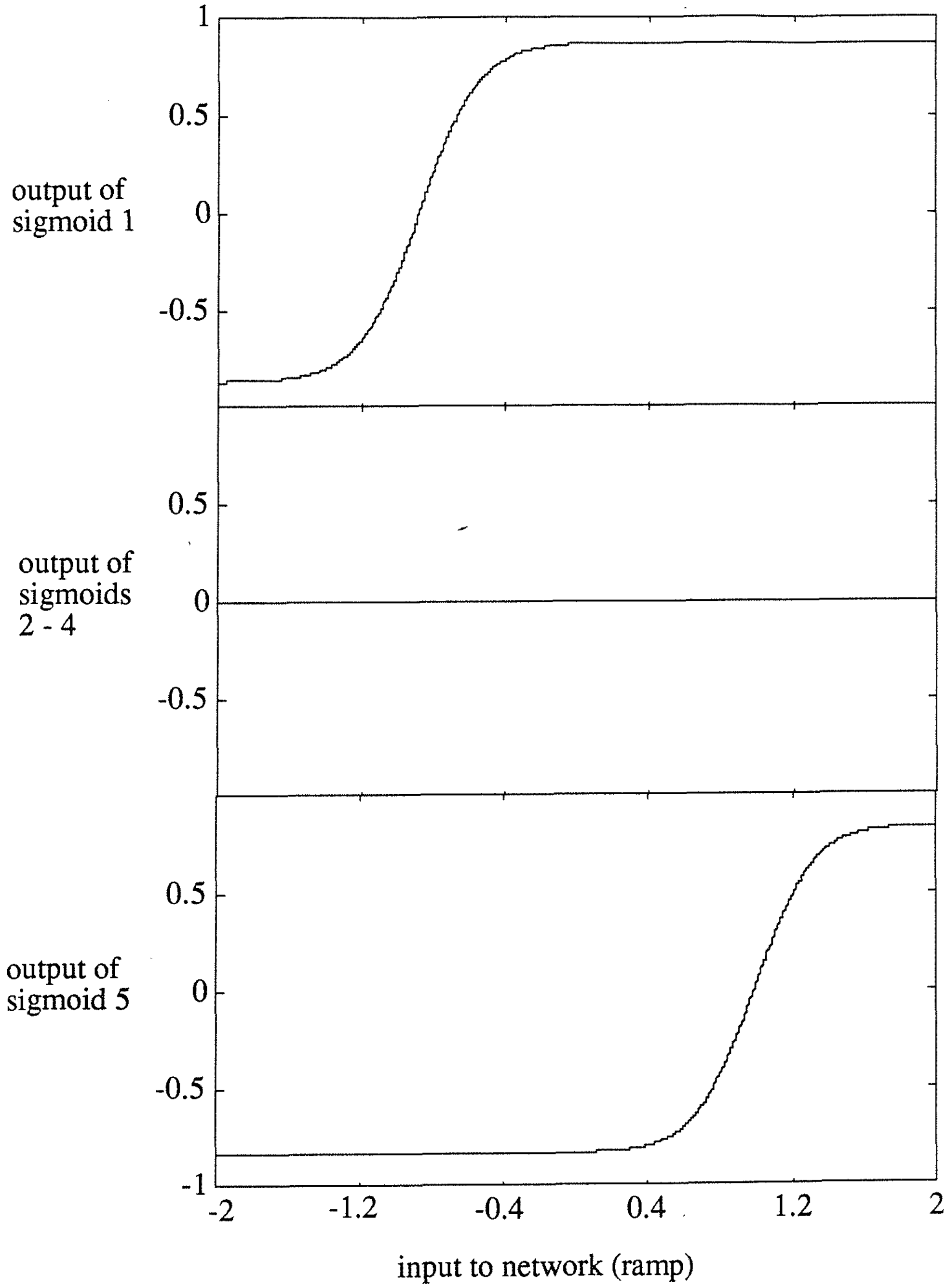

Figure 5.18: Sigmoid outputs in response to ramp, cubic function with delay

5.3 Application to motor vehicles

5.3.1 Shaker test

When a car is driven over a typical road surface, vibration is transmitted to the interior through all four wheels. To simplify this situation and examine nonlinear elements, a medium-sized hatchback car (Vauxhall Astra 1.4L) was set up on stands with just one of the wheels being excited vertically by a large shaker (Figure 5.19). Suspension acceleration, body panel acceleration and interior noise were measured.

Figure 5.19: Photograph of Vauxhall Astra 1.4L showing nearside front wheel excited by shaker (Note: results reported for rear wheel)

Special instrumentation would be required for a detailed measurement and identification of the vehicle nonlinear elements. An assessment of this kind was not felt to be within the scope of the project. Instead, the vehicle response was measured to broadband input noise from a single source, the shaker. Provided background noise levels are low, the vibration at any point on the structure will have been caused by the shaker and will be fully coherent with it, if the structure is linear. In this situation loss of coherence indicates nonlinearity in the structure.

Figure 5.20 shows the coherence of rear vertical suspension acceleration with the primary input signal to the shaker, representing applied force demand. The shaker was applied to the nearside rear wheel in this test. Physically the suspension motion in response to applied force at the tyre can be expected to be influenced by nonlinearities in the rear dampers: rubber bushes at the damper mountings, direction-dependent stiffness characteristics and possible backlash at the linkages.

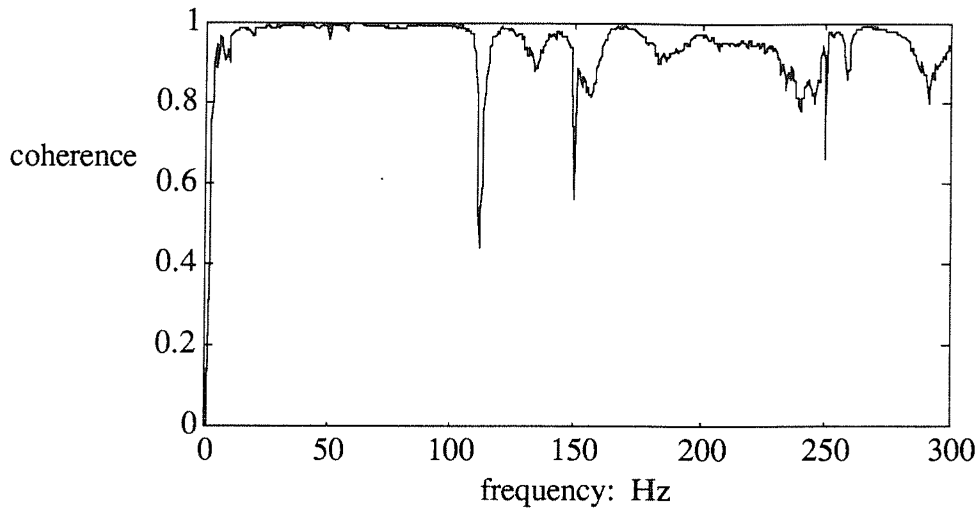

Figure 5.20: Ordinary coherence, primary shaker input signal to rear vertical suspension acceleration

The crosscorrelation between the input signal and measured acceleration indicated a system delay of 5 ms and a system response lasting some 30 ms. On this basis the neural network tapped delay line was chosen to be 32 ms. This was sufficient to include most of the response. In order to avoid an excessive number of network coefficients the data was low-pass filtered and downsampled to 500 Hz, so that a 16-point tapped delay line was sufficient to give 32 ms lag. A number of different sizes of neural network were investigated to map the 16 inputs given by the delayed versions of the reference signal into one output which approximated the measured acceleration. Similar results were obtained to those reported here in which a single hidden layer was used as in the earlier model problems. The number of sigmoids was chosen to be 24, half as many again as in the tapped delay line. The initial values of the input weights were (as previously) set to random values in the range ± 5 and the output weights in the range ± 1. The network was allowed to run for 10^6 updates. As before, the network was assessed by running it with fixed weights and using unseen data from later in the same test record. The results are shown in Figures 5.21, 5.22 and 5.23.

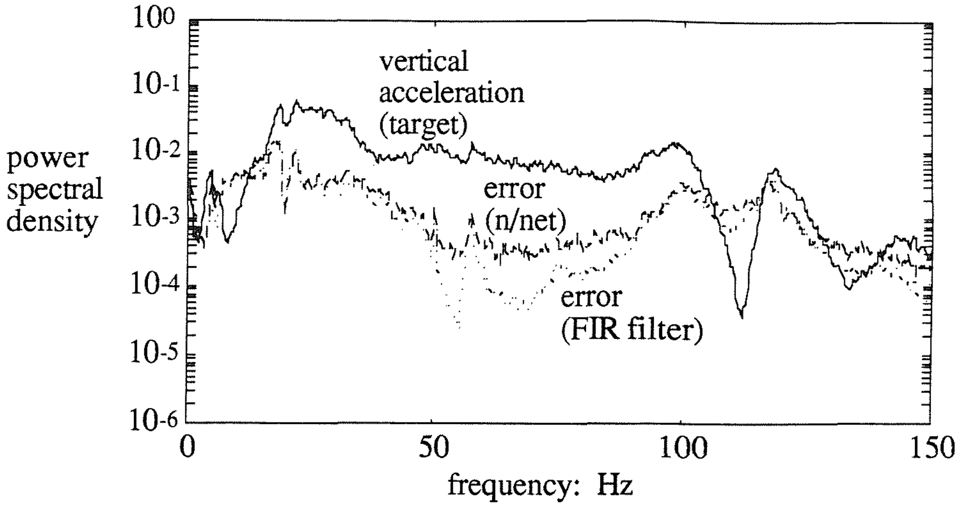

Figure 5.21: Cancellation of vibration data using 16-24-1 neural network

Figure 5.21 shows the spectrum of the vertical acceleration signal (unseen data) along with

(1) the error after subtracting the 16-24-1 neural network output

(2) the error after subtracting the output of a 16-point linear FIR filter. The optimum values of the filter coefficients were found using the same data as was used for training the neural network.

The Figure shows that the neural network did not generally perform as well as the linear system. Only in a narrow frequency band around 14 Hz did the neural network deliver a smaller error than the linear filter. Similar results arose when using a number of different sets of test data and using different network configurations. A fragment of the time-histories is given in Figure 5.22. The movement of some of the weights during training are given in Figure 5.23. Figure 5.23 (a)-(d) shows the movement of some of the output weights: those of the first sixteen of the 24 sigmoids. The behaviour is not dissimilar to that found in the time-delay model problem of Section 5.2.2; many of the output weights drive towards zero while a few settle at non-zero values. Figure 5.23(e), (f) show the input weight transients for two of the sigmoids with output coefficients which settled at non-zero values (16 input weights per sigmoid). In both cases the bias weight continues to move but most of the input weights settle within the 10^6 updates.

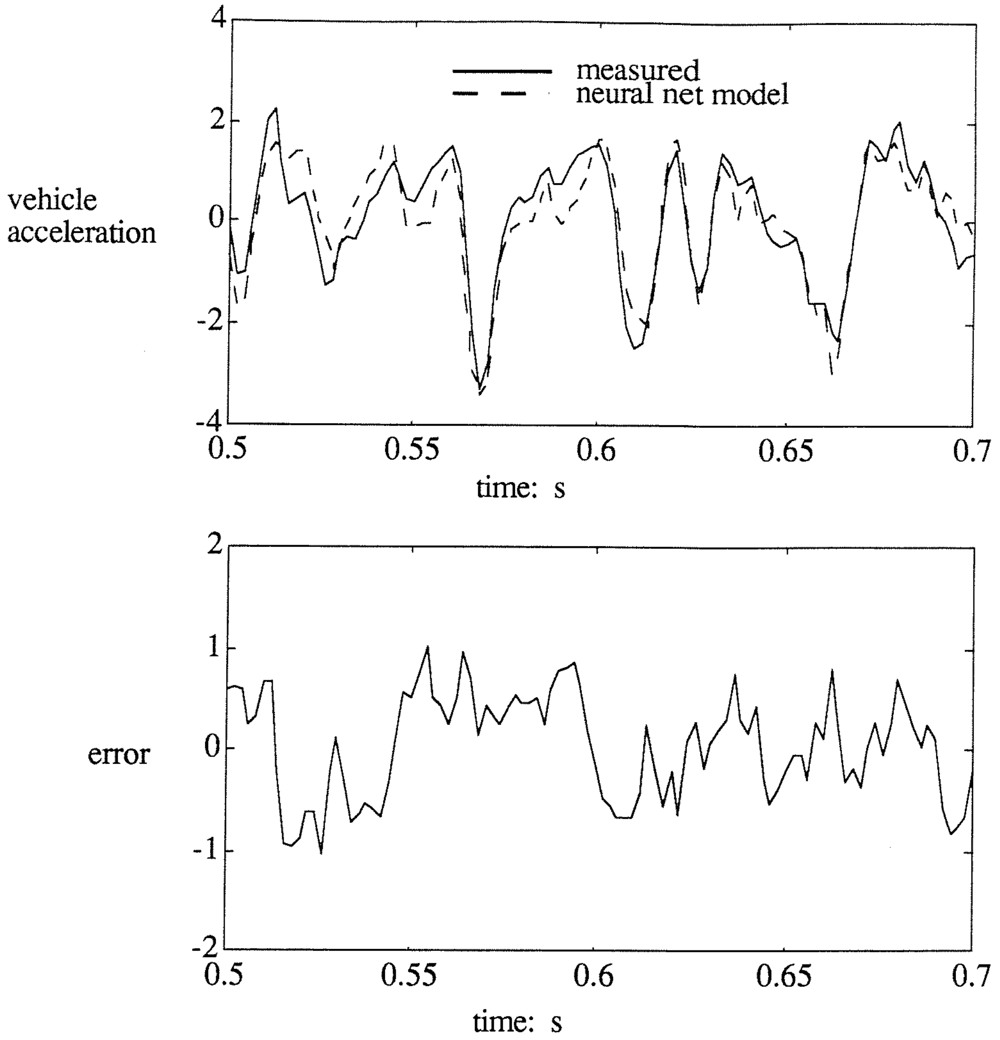

Figure 5.22: Neural network model of vehicle response: fragment of time-series

5.4 Conclusion: scope for use of neural networks in active sound control

It has been seen that the performance of linear feedforward active control of broadband noise in cars is limited to some extent by nonlinearities in the transmission path from the suspension system to the acoustic response. Neural networks have been suggested as suitable models for nonlinear dynamic systems. Unfortunately, when operating on the experimental data recorded in this study, a number of different sized neural networks performed no better than an equivalent linear model. Thus the use of a simple neural network with a single hidden layer has not been successful in this instance in modelling the complex nonlinearities associated with a vehicle suspension. However, application of the

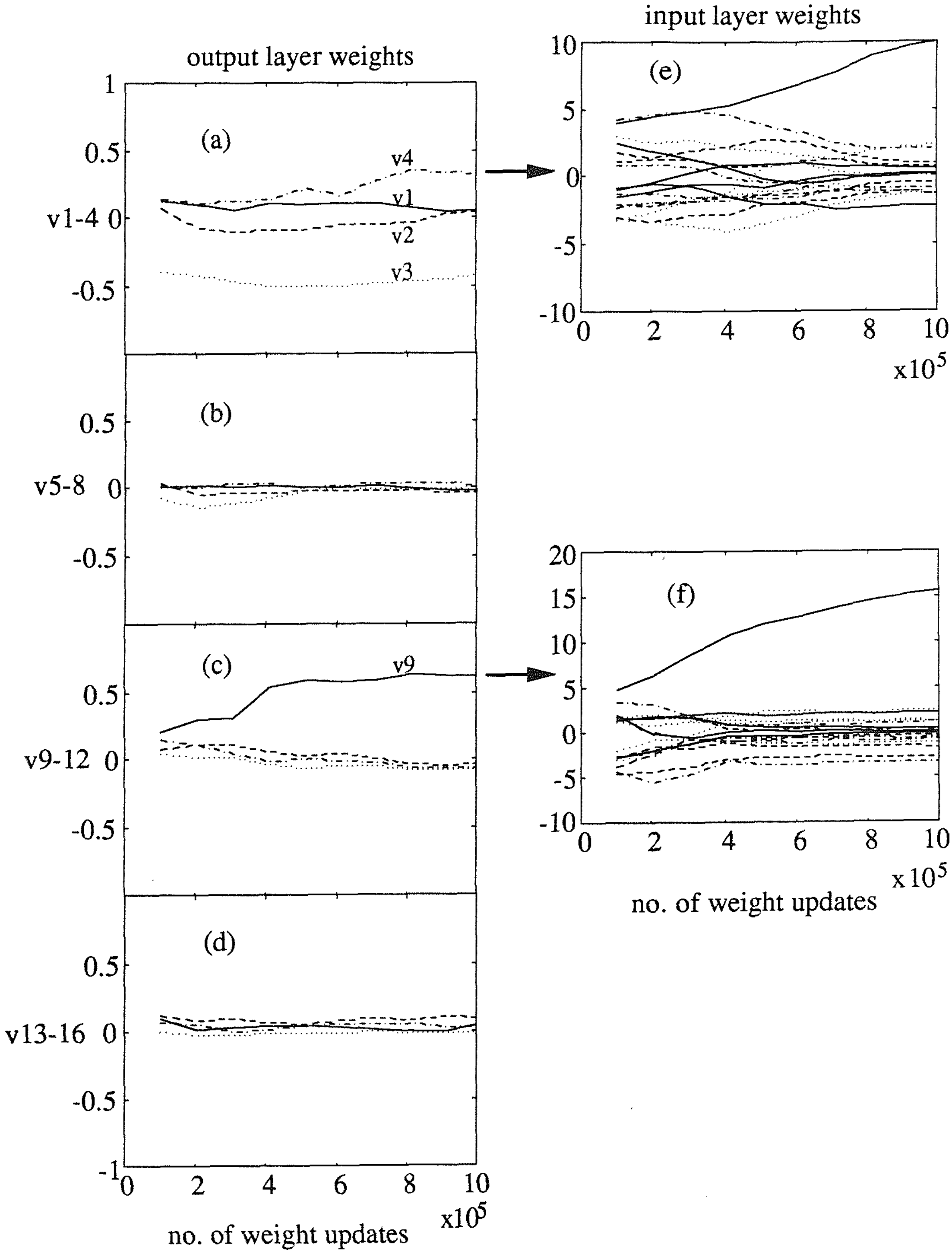

Figure 5.23: Use of 16-24-1 neural network to model vehicle nonlinearity: Movement of input and output weights during training

technique to simple model nonlinearities indicates that the technique may be useful and could be further developed.

The multilayer perceptron architecture with a single hidden layer was investigated here. It appeared to suffer from the problem that some of the weights on the output layer were initially driven to low values because of inappropriate input weights to these hidden units. Because of the nature of the backpropagation algorithm the input weights were subsequently hardly changed for these units, and so the output weights remained low for millions of training iterations. This effect appears to result in a significant reduction if the number of effective units in the hidden layer.

A problem which arises when using tapped delay line neural networks for vehicle noise applications is that the dynamics of the structural vibration require long tapped delay lines. Resonant features in the structure may require lines of 64 points and more, as discussed in Chapter 4. This would call for very large numbers of input weights in a possible neural network controller.

Future work in this direction would involve finding clearly-defined nonlinear features in the vehicle structure and modelling them in isolation; then progressively building up a neural-network based control structure with a minimum of coefficients. The objective would be to use practical sensors such as accelerometers attached to the structure but to obtain better predictions of the sound at interior microphones by means of nonlinear processing of the reference signals.

6 CONCLUSIONS

6.1 Overview

The active control of tonal noise in cars (engine noise) is well-established. The project reported here has been to investigate the extension of this work to the control of random noise in cars: in the first instance, to road noise.

A feedforward approach to control has been considered, in which reference signals related to the primary sources of noise are passed through FIR control filters to loudspeakers inside the car. The control filters are adapted to minimise the interior sound as detected by suitably-placed microphones. A central part of the work was the prediction of the sound reductions which could be obtained in two widely-used family cars based on measurements of vehicle vibration and noise. It was shown that sound reductions of the order of 5 dB could be expected at a point inside the car (*eg* at the driver's head) at frequencies in the range 90 - 140 Hz using six accelerometers attached to the vehicle structure. Different numbers and configurations of accelerometers yielded different results.

The theoretical framework has been developed for calculating the optimal control filters from recordings of vehicle vibration and interior noise. The theory covers single or multiple reference signals, secondary sources and microphones. The analysis was carried out first in the frequency domain, and yielded relatively simple expressions for the available sound reductions along with control filters which are unconstrained by causality. The problem was then framed in the time domain, yielding expressions for multiple-channel, causal, finite-length control filters which could be realised in practice. Care was taken to trace the development of the multichannel optimal filtering problem from the earlier work of Wiggins and Robinson. The prediction method was used to select the best positions for reference accelerometers when active noise control was applied in practice.

In addition to vehicle tests, a theoretical model problem was examined: the active conrol of random sound in a car-sized rectangular box bounded on one side by a thin vibrating plate. A study of this problem gave insight into some of the mechanisms and limitations of active sound control in cars.

The following paragraphs draw together the main conclusions of the work. Numbers in square brackets refer to the relavent Sections in the Thesis.

6.2 Frequency range of active control

6.2.1 Global reductions

The simulation of an idealised rectangular enclosure examined the scope for reducing the total acoustic potential energy in the enclosure. Substantial reductions over a wide range of frequencies were only possible if the secondary sources (loudspeakers) were adjacent to the primary source, that is to the vibrating panel [3.5.1]. As the sound in a car comes from vibration of all the panels which form the passenger compartment this would require many loudspeakers placed around all the interior panels of the vehicle. The simulation showed that if the secondary sources were placed distant from the vibrating panel, significant *global* reductions could only be expected at very low frequencies (up to 90 Hz in the case considered).

6.2.2 Sound reduction at selected points

It was shown in Chapter 2 [2.2.2] that the reduction in the noise spectrum at a single point (*eg* at a microphone) in the enclosure using unconstrained control filters (non-causal and unlimited in length) depended on the multiple coherence between the reference signals and the primary noise signal at the microphone. This reduction at a point would not necessarily bring about a global reduction in acoustic potential energy. However, vehicle measurements showed that the multiple coherence between practical reference signals attached to the body or suspension of a car reach useful levels (*eg* 0.9, corresponding to 10 dB reduction) at up to 140 Hz while smaller reductions were available at frequencies up to 300 Hz [4.3.2].

6.2.3 Practical limit

At frequencies above 200-300 Hz the sound field would typically be diffuse [1.3.2], and the zone of quiet around the error microphone would be limited to around 1/10 wavelength: for example at 1 kHz the zone of quiet would be just 3 cm in diameter. Furthermore the action of the active noise control would increase the sound level elsewhere.

6.3 Reference signals

6.3.1 Detection of primary sources of noise

Road noise at the frequencies of interest arises from road surface features spaced at least 74mm apart and typically much more than this [1.4.1]. Interior noise at frequencies below 300 Hz could thus be expected to depend more on the road surface than on tyre tread details. However, measurements of the vertical vibration at the front and rear wheels rolling over the same road surface were well correlated up to only about 90 Hz, while the linear coherence between the signals was not sufficient to be able to dispense with measurement of rear-wheel vibration when detecting the primary sources of noise [4.2.4].

6.3.2 Choice of reference sensor

The simulation study of active control of random sound in an enclosure bounded by a plate assumed that the source of noise was a time-varying force applied to the plate. A comparison was made between the use of this force signal as a reference signal for control and using instead an accelerometer attached to the plate [3.5.2]. When the force was used, the optimum control filters had a long-duration lightly-damped ringing impulse response corresponding to the low frequency modes of the plate. This arose because the control filters had to represent the dynamics of the plate in order to provide the correct signals to the secondary sources. On the other hand, if plate acceleration was used as a reference signal the filters had a much shorter impulse response. In practical terms this would suggest that it is preferable to measure the acceleration of the vibrating panels creating the interior sound rather than measuring quantities proportional to applied force. However it is more important to obtain the maximum possible time advance.

6.3.3 Number of reference signals required

The simulation of active noise control in a rectangular enclosure bounded by a plate included a case in which multiple forces were applied to the plate [3.6.2]. The simulation showed that when the number of accelerometers attached to the plate (to provide reference signals) was less than the number of independent forces, the multiple coherence between the accelerometers and an interior microphone reached high values over part but not all of the frequency range. It was clear that the number of reference signals for control should not be less than the number of independent forces applied. The number of accelerometers required for a vehicle in practice was assessed by measurement.

Road tests were carried out on two models of vehicle to assess suitable locations for the accelerometers and to see how many would be required. The multiple coherence between groups of accelerometers and an interior microphone was evaluated in road tests at steady speed. It was found that one accelerometer per wheel-hub was not sufficient to detect the vibration input from that wheel [4.2.5]. Further accelerometers were attached to the wheel-hubs to measure vertical, lateral and fore/aft acceleration. The multiple coherence increased as more accelerometers were included in the calculation, indicating that they were making contributions to interior noise which were to some extent independent of each other. Nine suspension accelerometers gave a maximum value of multiple coherence of around 0.8, representing a maximum 7 dB reduction.

Accelerometers attached to the floor panels of a vehicle (rather than to the suspension) generally gave higher values of multiple coherence and less were needed to achieve the same level of coherence; however the accelerometers attached to the suspension gave earlier signals and were less affected by time-delays in the control system [4.3.3]. The measurements showed that a key compromise in selecting reference signals is a choice between:

(a) sensors close to the primary source of noise (*eg* on the suspension) where the signals are obtained at the earliest possible point in time but are subject to distortion as they propagate through nonlinear elements in the structure; and on the other hand,

(b) sensors which measure the vibration of the panels creating the interior sound (*eg* floor panels) where the signals are linearly related to the sound field but arrive later and may be too late to cancel the sound after delays in the controller.

The best locations for accelerometers on a complex structure such as a motor vehicle is to some extent a matter of trial and error, however, and this the specific measured results presented here could almost certainly be improved.

6.4 Control filters

6.4.1 Linear control filter

Finite impulse response (FIR) filters have been assumed throughout because of their unconditional stability. Their principal disadvantage is the large number of coefficients which may be required to define them, particularly in cases where a lightly-damped impulse response is required. The vehicle tests included an examination of the effect on predicted sound reduction of using different lengths of control filter. The performance of the system was not seriously affected with filter lengths down to 64-point (length of impulse response 63 ms for the assumed 1 kHz sample rate).

6.4.2 Nonlinear control techniques

A preliminary study was carried out of the possibility of using a nonlinear controller based on a neural network to model the nonlinear elements in the transmission path from the suspension to the vehicle interior. An attempt was made to model this path using a multilayer perceptron network, but this gave no improvement over a linear filter. Tests with simple idealised dynamic nonlinear elements showed some success, but it appeared that the backpropagation algorithm had the effect of excluding some hidden-layer neurons from the model.

6.5 Suggestions for future work

(1) More detailed measurements of the nonlinear elements in the transmission path from the wheels to the vehicle interior are required to assist in choosing the best locations for accelerometers and to guide the development of nonlinear control techniques. The initial study of neural networks indicated that they are suited to modelling simple, well-defined nonlinear elements.

(2) Sensors other than accelerometers could be examined: these might include infra-red sensors to detect road-surface variations (giving much greater time-advance on the reference signals) and dynamic measurements of tyre pressure.

(3) Wind noise was not examined in detail in the work reported here. A significant component of wind noise at the frequencies of interest arises from vortex-shedding at the front A-pillars of the vehicle [1.4.5] and this could be detected simply using exterior microphones.

7 REFERENCES

BENDAT, J.S., A.G. PIERSOL (1986) Random Data -- Analysis and Meausrement Procedures (John Wiley & Sons 1986)

BERGE, T. (1983) *Proc Internoise 83* pp 457-460 Active noise cancellation of low frequency sound inside vehicle cabs

BOEHM, F. (1966) *Ing.-Arch.* **35** p82 Mechanik des Gürtelreifens

BULLMORE, A.J., P.A.NELSON, A.R.D. CURTIS, S.J. ELLIOTT (1987) *J. Sound Vib* **117**(1) pp15-33 The active minimization of harmonic enclosed sound fields Part II: A computer simulation

CHAPLIN, G.B.B. (1983) *Chart. Mech. Eng.* 1983, pp41-47 Anti-noise -- the Essex breakthrough

CONOVER, W.B. (1956) *Noise Control,* **2,** March 1956 pp78-92 Fighting noise with noise

CAPTAIN, K.M. *et al* (1979) *Vehicle System Dynamics* **8** pp1-32 Analytical tire models for dynamic vehicle simulation

CARME, C. (1987) Absorption acoustique active dans les cavités. PhD thesis, Université d'Aix-Marseille II

CLARKSON, P.M. (1983) Adaptive approaches to signal enhancement and deconvolution. PhD thesis, University of Southampton

DOBRZYNSKI, W. (1986) *Vehicle Aerodynamics,* Von Karman Institute for Fluid Dynamics Lecture Series 1986-05 March 17-21 1986 Wind induced interior and farfield radiated exterior noise from automobiles

DODDS, C.J., J.D. ROBSON (1973) *J. Sound Vib.* **31**(2) pp175-183 The description of road surface roughness

ELLIOTT, S.J., I.M. STOTHERS (1986) *Proceedings of Euromech 213*, Marseille. A multichannel adaptive algorithm for the active control of start-up transients

ELLIOTT, S.J., I.M. STOTHERS, P.A.NELSON (1987) *IEEE Trans ASSP*-**35** (1) pp1423-1434 A multiple-error LMS algorithm and its application to the active control of sound and vibration

ELLIOTT, S.J., I.M. STOTHERS, P.A. NELSON, A.M. McDONALD, D.C. QUINN, T. SAUNDERS (1988) *Proc Internoise 88,* Avignon, France pp987-990 The active control of engine noise inside cars

ELLIOTT, S.J., P.A. NELSON, I.M. STOTHERS, C.C. BOUCHER (1990a) *J. Sound Vib.* **140**(2) pp219-238 In-flight experiments on the active control of propellor-induced cabin noise

ELLIOTT, S.J., P.A. NELSON (1990b) *Electronics and Control Engineering Journal* August 1990 pp127-136 The active control of sound

ERIKSSON, L.J., M.C. ALLIE (1987) *IEEE Trans on Acoustics, Speech and Signal Processing* **ASSP-35**, pp433-437 The selection and application of an IIR adaptive filter for use in active sound attenuation

FAHY, F.J. (1985) Sound and Structural Vibration: Radiation, Transmission and Response (Academic Press, London)

GALBRAITH, J.N. *jnr*, R.A.WIGGINS (1968) *Geophysics* **33**(1) Feb 1968 pp36-48 Characteristics of Optimum Multichannel Stacking Filters

GEORGE, A.R. (1989) *AIAA 12th Aeroacoustics conference* Apr 1989, San Antonio, Texas Automobile Aeroacoustics

GOODMAN, S.D., S.S WISE (1990) *Proc. Internoise 90,* Gothenburg, Sweden 13-15 August 1990 A discussion of commercial experience with active noise control on industrial fans and air handlers used for heating, ventilating and air conditioning

HECKL, M. (1986) *Wear* **113** pp157-170 Tyre noise generation

JHA, S.K., N. CHEILAS (1976) *J Sound Vib.* **47**(4) pp543-558 Characteristics and sources of noise and vibration and their control in motor cars

JOPLIN, P.M. (1989) Feedforward active control for a multimodal acoustic system excited by a random input. MSc dissertation, University of Southampton

JOPLIN, P.M., P.A. NELSON (1990) *J Acoust Soc Am* **87**(6) June 1990 pp2396-2404 Active control of low-frequency random sound in enclosures

JOSEPH, P. (1990) Active control of high frequency enclosed sound fields. PhD thesis, University of Southampton

KROPP, W. (1989) *Applied Acoustics* **20**(?) pp181-192 Structure-borne sound on a smooth tyre

KUNG, L.E., W.SOEDEL, T.Y. YOUNG (1986) *J. Sound Vib.* **107**(2) pp195-213 On the dynamic response at the wheel axle of a pneumatic tyre

LEVINSON, N. (1947) *Jnl Math Physics* **25**(4) pp261-278 The Wiener RMS (root mean square) error criterion in filter design and prediction

LIPPMANN, R.P. (1987) *IEEE ASSP Magazine*, April 1987. An Introduction to Computing with Neural Nets

LUEG, P. (1936) Process of silencing sound oscillations. US patent no. 2 043 416

McCULLOCH, W.S., W. PITTS (1943) *Bulletin of Mathematical Biophysics* **5** pp115-133 A Logical Calculus of the Ideas Immanent in Nervous Activity

McDONALD, A.M., S.J. ELLIOTT, M.A. STOKES (1991) *ASJ International Symposium on Active Control of Sound and Vibration, Apr 9-11 1991, Tokyo, Japan* Active Noise and Vibration Control within the Automobile

NARENDRA, K.S., K. PARTHASARATHY (1990) *IEEE Trans on Neural Networks* **1**(1) March 1990 pp4-27. Identification and Control of Dynamical Systems using Neural Networks

NELSON, P. A., A.R.D. CURTIS, S.J. ELLIOTT, A.J. BULLMORE (1987a) *J. Sound Vib.* **116**(3) pp397-414 The minimum power output of free field point sources and the active control of sound

NELSON, P.A., A.R.D. CURTIS, S.J. ELLIOTT, A.J. BULLMORE (1987b) *J. Sound Vib.* **117**(1) pp1-13 The active minimization of harmonic enclosed sound fields Part I: Theory

NELSON, P.A., T.J. SUTTON, S.J. ELLIOTT (1990) *Proc Institute of Acoustics Spring Conference 1990* Performance limits for the active control of random sound fields

NELSON, P.A., S.J. ELLIOTT (1991) Active Control of Sound (Academic Press, London)

OLSEN, H.F., E.G. MAY (1953) *J. Acoust Soc Amer* Nov 1953, **25**, pp1130-1136 Electronic sound absorber

OTTE, D., F. FYFE *et al* (1988) *IMech E International Conference on Advances in the Control and Refinement of Vehicle Noise, 1988.* Use of Principal Component Analysis for dominant noise source identification

PAN, J., C.H. HANSEN, D.A. BIES (1990) *J Acoust Soc Am* **87**(5) May 1990 pp2098-2108 Active control of noise transmission through a panel into a cavity: I Analytical study

PARKER, D. (1982) Learning-logic. Invention Report S81-64, File 1, Office of Technology Licensing, Stanford University, Stanford, California, Oct 1982

PIERCE, A.D., (1981) Acoustics: An Introduction of its Physical Principles and Applications (McGraw-Hill, 1981)

PRIEDE, T., S.K. JHA (1970) *J. of Automotive Engineering* July 1970 p17 Low-frequency noise in cars -- its origin and elimination

ROBINSON, E.A. (1978) Multichannel Time Series Analysis with Digital Computer Programs (Holden-Day 1967 rev ed 1978)

RUMELHART, D.E., G.E. HINTON, R.J. WILLIAMS (1986) Learning Internal Representations by Error Propagation, in D.E. RUMELHART and J.L. McCLELLAND (Eds) Parallel Distributed Processing: Explorations in the Microstructure of Cognition, Vol I Foundations, MIT Press

ROSENBLATT, R. (1959) Principles of Neurodynamics, Spartan Books, New York

ROSS, C.F., (1982a) *J. Sound Vib.* **80** pp381-388 An adaptive digital filter for broadband active sound control

ROSS, C.F. (1982b) *PhD Thesis, University of Cambridge* Active control of sound

ROURE, A. (1985) *J. Sound Vib* **101** pp429-441 Self-adaptive broadband active sound control system

SCHNEIDER, W.A. *et al* (1964) *Geophysics* **29** (5) (October 1964) pp783-805 A new data-processing technique for the elimination of ghost arrivals on reflection seismograms

SUTTON, T.J., S.J. ELLIOTT, P.A. NELSON, I. MOORE (1990a) *Proc Institute of Acoustics* **12**(1) pp689-695 Active control of multiple-source random sound in enclosures

SUTTON, T.J., S.J.ELLIOTT, P.A. NELSON, I. MOORE (1990b) *Proc Inter-noise 90* pp1247-1250 The active control of road noise inside vehicles

SUTTON, T.J., S.J. ELLIOTT, I.MOORE (1991) *Recent Advances in Active Control of Sound and Vibration*, Virginia Polytechnic Institute and State University, Blacksburg, Virginia 15-17 April 1991. Use of nonlinear controllers in the active attenuation of road noise inside cars

SWINBANKS, M.A. (1973) *J Sound Vib* **27**(3) pp411-436 The active control of sound propagation in long ducts

TAKAHASHI, F., G. WATANABE, M. NAKADA, H. SAKATA, M. IKEDA (1987) *Int. J. of Vehicle Design* **8** nos 4/5/6 pp588-597 Tyre/suspension system modelling for investigation of road noise characteristics

WALKER, J.C., D.I. EVANS (1987) *Proc 16th ISATA* **2** pp577-585 Improvement of road-excited internal vehicle noise by analysis of suspension transmission paths using replica road surfaces

WALKER, J.C., D.I. EVANS (1988a) *Acoustics Bulletin* Jan 1988 p19 Tyre design and noise control

WALKER, J.C., D.I. EVANS (1988b) *Proc IMechE International Conference on Advances in the control and refinement of vehicle noise* 1988-2 The effect of vehicle/tyre/road interaction on external and internal vehicle noise

WERBOS, P. (1974) Beyond Regression: New Tools for Prediction and Analysis in the Behavioural Sciences. PhD thesis, Harvard University, Cambridge, Massachusetts, Aug 1974

WHEELER, P.D., (1986) Voice communications in the cockpit noise environment - the role of active noise reduction. PhD thesis, University of Southampton

WHEELER, P.D., (1987) *Proc Royal Aeronautical Soc Symp on Helmets and helmet mounted devices* The role of noise cancellation techniques in aircrew voice communications systems

WIDROW, B., S.D. STEARNS (1985) Adaptive Signal Processing (Prentice-Hall, 1985 Englewood Cliffs)

WIDROW, B., M.A. LEHR (1990) *Proc IEEE* **78**(9), Sept 1990. 30 Years of Adaptive Neural Networks: Perceptron, Madaline and Backpropagation

WIGGINS, R.A., E.A. ROBINSON (1965) *J. of Geophysical Research* **70**(8) (April 1965) pp1885-1891 Recursive Solution to the Multichannel Filtering Problem

WOOD, L.A., C.A. JOACHIM (1984) *Proceedings IMechE Conference on Vehicle Noise and Vibration,* 5-7 June 1984 Variability of interior noise levels in passenger cars

APPENDIX 3.1 Structural-acoustic equations for an enclosure bounded by a thin plate

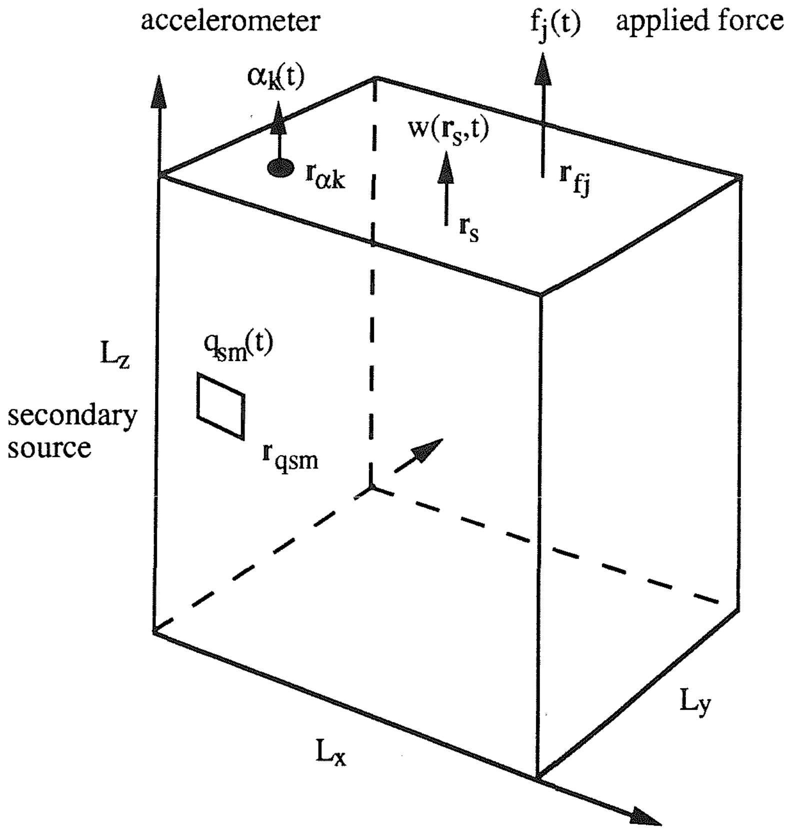

Figure A3.1 Schematic diagram of rectangular cavity bounded by plate

Figure A3.1 shows a hard-walled rectangular cavity bounded on one side by a thin, simply-supported plate. The plate is in the x-y plane at $z=L_z$, forming the top surface of the enclosure as shown. $\mathbf{r}$ is the 3D position vector defining a point in the enclosure. J independent point forces $f_j(t)$ are applied normal to the plate at locations $\mathbf{r}_{fj}$ ($j = 1,2,...J$). Plate vibration is detected by K notional accelerometers located at $\mathbf{r}_{\alpha k}$ ($k=1,2..K$). The accelerometer outputs are $\alpha_k(t)$. Vertical displacement at a general point on the plate $\mathbf{r}_s$ is given by $w(\mathbf{r}_s,t)$. The forces, accelerations and displacement are taken to be positive away from the enclosure.

The general equation governing the undamped vibration of a uniform plate or shell structure is [Fahy,1985]:

$$L[w(\mathbf{r}_s,t)] + \sigma \frac{\partial^2 w}{\partial t^2}(\mathbf{r}_s,t) = p_f(\mathbf{r}_s,t) + p_{ac}(\mathbf{r}_s,t) \tag{A3.1}$$

where

L	is the linear operator governing elastic forces in the structure (see below)
$p_f(\mathbf{r}_s,t)$	is the distribution of mechanically applied forces per unit area (Pa) (in this case $f(\mathbf{r}_s,t)$ consists of the assembly of point forces $f_j(t)$)
$p_{ac}(\mathbf{r}_s,t)$	is the distribution of surface acoustic pressures on the plate (Pa)
σ	is mass/area of the plate (kg/m^2)

The surface pressure $p_{ac}(\mathbf{r}_s,t)$ will be omitted when using this equation, thus neglecting for simplicity the coupling from the fluid to the plate.

For a thin flat plate the elastic forces are given by

$$L[w(\mathbf{r}_s,t)] = \frac{Eh^3}{12(1 - \nu^2)} \left(\frac{\partial^4 w}{\partial x^4} + 2\frac{\partial^4 w}{\partial x^2 \partial y^2} + \frac{\partial^4 w}{\partial y^4} \right) \tag{A3.2}$$

where E, h, and ν are the Young's modulus, thickness and Poisson's ratio respectively for the plate in SI units.

The modeshapes and natural frequencies of the plate are obtained from the homogeneous equation corresponding to (A3.1):

$$L[\tilde{w}(\mathbf{r}_s,t)] + \sigma \frac{\partial^2 \tilde{w}}{\partial t^2}(\mathbf{r}_s,t) = 0 \tag{A3.3}$$

where $\tilde{w}(\mathbf{r}_s,t)$ denotes the free motion of the plate. Solutions are of the form

$$\tilde{w}(\mathbf{r}_s,t) = \phi_p(\mathbf{r}_s)\, e^{j\omega_p t} \qquad p = 1, 2, \ldots \tag{A3.4}$$

where the $\phi_p(\mathbf{r}_s)$ are the modeshapes and the ω_p are the natural frequencies of the plate. ϕ_p and ω_p can be evaluated when the plate boundary conditions are applied to (A3.3). For a simply-supported plate the natural frequencies and modeshapes are:

$$\omega_p = \pi^2 \sqrt{\frac{D}{\sigma}\left(\frac{i^2}{L_x^2} + \frac{j^2}{L_y^2}\right)} \qquad i=1,2,..; \quad j=1,2,..; \quad p=(i,j)$$

with $D = \dfrac{Eh^3}{12(1 - \nu^2)}$;

$$\phi_p(\mathbf{r}_s) = 2 \sin\left(\frac{i\pi x}{L_x}\right) \sin\left(\frac{j\pi y}{L_y}\right)$$

We choose to normalise the modeshapes such that

$$\int_S \phi_p^2(\mathbf{r}_s)\, ds = S \tag{A3.5}$$

(S is the surface area of the plate.) The modeshapes are orthogonal, having the property that

$$\int_S \phi_p(\mathbf{r}_s)\, \phi_q(\mathbf{r}_s)\, ds = 0 \qquad p \neq q \tag{A3.6}$$

They form a complete set, able when combined to describe any surface shape which is consistent with the boundary conditions. By expressing the plate surface displacement $w(\mathbf{r}_s,t)$ and the distribution of applied forces $p_f(\mathbf{r}_s,t)$ as a sum of modeshapes with time-varying amplitudes, it is possible to obtain a set of uncoupled modal equations to describe the motion of the plate. Thus

$$w(\mathbf{r}_s,t) = \sum_{p=1}^{\infty} b_p(t)\, \phi_p(\mathbf{r}_s) \tag{A3.7}$$

$$p_f(\mathbf{r}_s,t) = \sum_{p=1}^{\infty} c_p(t)\, \phi_p(\mathbf{r}_s) \tag{A3.8}$$

where

$b_p(t)$ is the modal amplitude of the plate displacement (pth mode)
$c_p(t)$ is the modal amplitude of the force distribution (pth mode)

The modal amplitude of the force distribution $c_p(t)$ is given by multiplying (A3.8) by $\phi_q(\mathbf{r}_s)$ and integrating over the plate surface:

$$c_p(t) = \frac{1}{S} \int_S p_f(\mathbf{r}_s,t)\, \phi_p(\mathbf{r}_s)\, ds \tag{A3.9}$$

The force distribution $p_f(\mathbf{r}_s,t)$ comprises the applied point forces $f_1(t)$, $f_2(t)$, $..f_J(t)$, that is:

$$p_f(\mathbf{r}_s,t) = \sum_{j=1}^{J} f_j(t)\, \delta(\mathbf{r}_s - \mathbf{r}_{fj}) \tag{A3.10}$$

so that

$$c_p(t) = \frac{1}{S} \sum_{j=1}^{J} f_j(t)\, \phi_p(\mathbf{r}_{fj}) \tag{A3.11}$$

Substituting for $w(\mathbf{r}_s,t)$ and $p_f(\mathbf{r}_s,t)$ in (A3.1) and noting that

$$L[\phi_p(\mathbf{r}_s)] = \sigma\omega_p^2\, \phi_p(\mathbf{r}_s) \tag{A3.12}$$

from (A3.3), we obtain

$$\sum_{p=1}^{\infty} \phi_p(\mathbf{r}_s)\, [\sigma\omega_p^2\, b_p(t) + \sigma\, \ddot{b}_p(t) - c_p(t)] = 0 \tag{A3.13}$$

Using the orthogonality property of the modeshapes, we multiply by $\phi_q(\mathbf{r}_s)$ and integrate each term over the surface area of the plate to obtain the uncoupled modal equations:

$$\ddot{b}_p(t) + \omega_p^2\, b_p(t) = \frac{1}{\sigma} c_p(t) \qquad p=1,2,... \tag{A3.14}$$

The plate displacement and accelerometer outputs are therefore given by the solutions to:

$$\ddot{b}_p(t) + \omega_p^2\, b_p(t) = \frac{1}{S\sigma} \sum_{j=1}^{J} f_j(t)\, \phi_p(\mathbf{r}_{fj}) \tag{A3.15}$$

$$w(\mathbf{r}_s,t) = \sum_{p=1}^{\infty} b_p(t)\, \phi_p(\mathbf{r}_s) \tag{A3.7}$$

$$\alpha_k(t) \quad = \sum_{p=1}^{\infty} \ddot{b}_p(t)\, \phi_p(\mathbf{r}_{\alpha k}) \tag{A3.16}$$

3.3.2 Acoustic pressure in cavity

The acoustic cavity shown in Figure A3.1 is assumed to contain M secondary sources of volume velocity $q_{sm}(t)$. Each source is a square piston of side Δ with centre located at $\mathbf{r}_{qsm}$. Acoustic pressure at a general point $\mathbf{r}$ is $p(\mathbf{r},t)$.

Acoustic pressure is given by the solution to the inhomogeneous wave equation:

$$\nabla^2 p(\mathbf{r},t) - \frac{1}{c_0^2}\frac{\partial^2 p}{\partial t^2}(\mathbf{r},t) \quad = \quad -\rho_0 \frac{\partial q}{\partial t}(\mathbf{r},t) \tag{A3.17}$$

where

$q(\mathbf{r},t)$ is the distribution of source volume velocity per unit volume
ρ_0, c_0 are air density and sound speed respectively

The source volume velocity is made up of two contributions:

(1) the vibration of the plate. This vibration is treated as a volume velocity distribution confined to a thin layer on the surface $z = L_z$. The boundary itself is then represented as a hard wall.
(2) the secondary acoustic sources, taken to be square pistons with uniform surface velocity.

The modeshapes $\psi_n(\mathbf{r})$ and natural frequencies ω_n are the solutions of the homogeneous wave equation with hard-walled boundary conditions :

$$\nabla^2 \tilde{p}(\mathbf{r},t) - \frac{1}{c_0^2}\frac{\partial^2 \tilde{p}}{\partial t^2}(\mathbf{r},t) \quad = \quad 0 \tag{A3.18}$$

for which solutions are of the form

$$\tilde{p}(\mathbf{r},t) \quad = \quad \psi_n(\mathbf{r})\, e^{j\omega_n t} \qquad\qquad n=0,1,2... \tag{A3.19}$$

As in the case of the plate the modeshapes $\psi_n(\mathbf{r})$ are orthogonal:

$$\int_S \psi_m(\mathbf{r})\, \psi_n(\mathbf{r})\, ds \;=\; 0 \qquad\qquad m \neq n$$

and they are normalised such that

$$\frac{1}{V} \int_V \psi_n{}^2(\mathbf{r})\, dv \;=\; 1 \qquad\qquad n=0,1,2... \qquad\qquad (A3.20)$$

For a hard-walled rectangular enclosure the natural frequencies and modeshapes are:

$$\omega_n \;=\; \pi c_0 \sqrt{\frac{i^2}{L_x{}^2} + \frac{j^2}{L_y{}^2} + \frac{k^2}{L_z{}^2}} \qquad\qquad (A3.21)$$

$i=0,1,2,...;$ $j=0,1,2,...$
$k=0,1,2,...;$ $n = (i,j,k)$

$$\psi_n(\mathbf{r}) \;=\; A_n \cos(\frac{i\pi x}{L_x})\cos(\frac{j\pi y}{L_y})\cos(\frac{k\pi z}{L_z}) \qquad\qquad (A3.22)$$

with

$$A_n \;=\; \sqrt{\varepsilon_x \varepsilon_y \varepsilon_z} \qquad\qquad (A3.23)$$

$$\varepsilon_x = \begin{cases} 1 & i=0 \\ 2 & i>0 \end{cases} \qquad \varepsilon_y = \begin{cases} 1 & j=0 \\ 2 & j>0 \end{cases} \qquad \varepsilon_z = \begin{cases} 1 & k=0 \\ 2 & k>0 \end{cases}$$

Expressing the acoustic pressure $p(\mathbf{r},t)$ and volume velocity distribution $q(\mathbf{r},t)$ as sums of modeshapes:

$$p(\mathbf{r},t) \;=\; \sum_{n=0}^{\infty} a_n(t)\, \psi_n(\mathbf{r}) \qquad\qquad (A3.24)$$

$$q(\mathbf{r},t) \;=\; \sum_{n=0}^{\infty} d_n(t)\, \psi_n(\mathbf{r}) \qquad\qquad (A3.25)$$

where

$a_n(t)$ is the modal amplitude of total acoustic pressure (nth mode) due to plate and secondary sources

$d_n(t)$ is the modal amplitude of volume velocity distribution (nth mode)

Substituting for $p(\mathbf{r},t)$ and $q(\mathbf{r},t)$ in (A3.17) and using the orthogonality property of the modeshapes, the set of uncoupled equations is obtained:

$$\ddot{a}(t) + \omega_n^2 a_n(t) = \rho_0 c_0^2 \dot{d}_n(t) \qquad \text{(A3.26)}$$

$d_n(t)$ is derived from (A3.25) and is given by

$$d_n(t) = \frac{1}{V} \int_V q(\mathbf{r},t)\psi_n(\mathbf{r})\, dv \qquad \text{(A3.27)}$$

Substituting in the contributions to acoustic volume velocity source distribution $q(\mathbf{r},t)$ from the plate and the secondary source pistons gives

$$d_n(t) = -\frac{1}{V} \int_S \frac{\partial w}{\partial t}(\mathbf{r}_s,t)\psi_n(\mathbf{r}_s)\, ds + \sum_{m=1}^{M} \frac{q_{sm}(t)}{V} \frac{1}{\Delta^2} \int_{S_{pm}} \psi_n(\mathbf{r})\, ds \qquad \text{(A3.28)}$$

where

S indicates integration over the whole surface of the plate

S_{pm} indicates integration over the area of the mth piston

Δ side dimension of each square piston (m)

The first term gives the contribution due to the vibrating plate. The second term gives the contribution due to M pistons.

It is convenient to define $\bar{\psi}_n(\mathbf{r})$ as the mean value of the modeshape over the area of a piston side Δ centred at $\mathbf{r}$:

$$\bar{\psi}_n(\mathbf{r}) = \frac{1}{\Delta^2} \int_{S_p} \psi_n(\mathbf{r})\, ds \qquad \text{(A3.29)}$$

The modal amplitude of acoustic pressure is thus given from (A3.26):

$$\ddot{a}(t) + \omega_n^2 a_n(t) = \frac{\rho_0 c_0^2}{V}\left[\sum_{m=1}^{M} \dot{q}_{sm} \bar{\psi}_n(\mathbf{r}_{qsm}) - \int_S \frac{\partial^2 w}{\partial t^2}(\mathbf{r}_s,t)\, \psi_n(\mathbf{r}_s)ds\right] \quad \text{(A3.30)}$$

The input forcing functions to these equations are the plate acceleration $\frac{\partial^2 w}{\partial t^2}$ and the volume velocity of the secondary sources $q_{sm}(t)$. The plate acceleration follows from equation (A3.7) above:

$$\frac{\partial^2 w}{\partial t^2} = \sum_{p=1}^{\infty} \ddot{b}_p(t)\, \phi_p(\mathbf{r}_s) \quad \text{(A3.32)}$$

The final term of (A3.30) thus becomes

$$\frac{\rho_0 c_0^2}{V} \ddot{b}_p(t) \sum_{p=1}^{\infty} \int_S \phi_p(\mathbf{r}_s)\, \psi_n(\mathbf{r}_s)\, ds \quad \text{(A3.32)}$$

The surface integral represents the degree of coupling between the pth plate mode and the nth acoustic mode. It turns out that for this geometry there is only coupling between the plate and enclosure when the sum of the plate and acoustic mode numbers is an odd number for both the x and y directions. Defining a coupling coefficient C_{np}:

$$C_{np} = \frac{1}{S} \int_S \phi_p(\mathbf{r}_s)\, \psi_n(\mathbf{r}_s)\, ds \quad \text{(A3.33)}$$

It is now possible to express the modal amplitude of the pressure in the enclosure as a function of plate modal amplitude $b_p(t)$ and secondary source strength:

$$\ddot{a}_n(t) + \omega_n^2 a_n(t) = \frac{\rho_0 c_0^2}{V}\left[\sum_{m=1}^{M} \dot{q}_{sm}(t)\, \bar{\psi}_n(\mathbf{r}_{qsm}) - S \sum_{p=1}^{\infty} C_{np}\, \ddot{\alpha}_p(t)\right] \quad \text{(A3.34)}$$

Acoustic pressure in the enclosure is then given by (A3.24):

$$p(\mathbf{r},t) = \sum_{n=0}^{\infty} a_n(t)\psi_n(\mathbf{r})$$

APPENDIX 3.2 Acoustic potential energy spectrum

The total acoustic potential energy in the enclosure depends on the mean squared pressure at each point. This Appendix expresses the mean squared pressure in terms of the pressure spectrum at each point and hence defines an acoustic potential energy spectrum. This spectrum can be stated in terms of the frequency response functions given in Section 3.3.3. The acoustic potential energy spectrum defined here is equivalent to that defined in [Joplin *et al*,1990].

The autocorrelation function of acoustic pressure in the enclosure at a point $\mathbf{r}$ is given by

$$R_{pp}(\mathbf{r},t) = E[p(\mathbf{r},t)\, p(\mathbf{r},t+\tau)] \qquad \text{(A3.35)}$$

where E[...] denotes expected value. This is related by the Wiener Khinchine relation [Bendat *et al*,1986] to the spectrum of pressure at $\mathbf{r}$, $S_{pp}(\mathbf{r},\omega)$:

$$E[p(\mathbf{r},t)\, p(\mathbf{r},t+\tau)] = \frac{1}{2\pi}\int_{-\infty}^{\infty} S_{pp}(\mathbf{r},\omega)\, e^{j\omega t}\, d\omega \qquad \text{(A3.36)}$$

The mean squared pressure at $\mathbf{r}$ is given when $\tau = 0$:

$$E[p^2(\mathbf{r},t)] = \frac{1}{2\pi}\int_{-\infty}^{\infty} S_{pp}(\mathbf{r},\omega)\, d\omega \qquad \text{(A3.37)}$$

The total acoustic potential energy in the enclosure is given by

$$E_p = \frac{1}{2\rho_0 c_0^2}\int_V E[p^2(\mathbf{r},t)] \qquad \text{(A3.38)}$$

$$= \frac{1}{2\pi}\int_{-\infty}^{\infty} \left\{ \frac{1}{2\rho_0 c_0^2}\int_V S_{pp}(\mathbf{r},\omega)\, dv \right\} d\omega \qquad \text{(A3.39)}$$

The term in curly brackets is defined to be the *potential energy spectrum* $E_p(\omega)$:

$$E_p(\omega) = \frac{1}{2\rho_0 c_0^2}\int_V S_{pp}(\mathbf{r},\omega)\, dv \qquad \text{(A3.40)}$$

The total potential energy E_p is thus the area under the curve $E_p(\omega)$.

The potential energy spectrum can be expressed as a sum of modal amplitudes. Using the frequency-domain expression for acoustic pressure,

$$p(\mathbf{r},\omega) = \sum_{n=0}^{\infty} a_n(\omega)\, \psi_n(\mathbf{r}) \tag{A3.41}$$

The pressure spectrum is:

$$S_{pp}(\mathbf{r},\omega) = \lim_{T\to\infty} E[\frac{1}{T}\, p^*(\mathbf{r},\omega)\, p(\mathbf{r},\omega)] \tag{A3.42}$$

Combining equations (A3.40), (A3.41), (A3.42) and carrying out the integration over volume (using the orthogonality property of the modeshapes) we obtain:

$$E_p(\omega) = \frac{V}{2\rho_0 c_0^2} \sum_{n=0}^{\infty} \lim_{T\to\infty} E[\frac{1}{T}\, a_n^*(\omega)\, a_n(\omega)] \tag{A3.43}$$

The potential energy spectrum has thus been expressed as a sum of modal spectra:

$$E_p(\omega) = \frac{V}{2\rho_0 c_0^2} \sum_{n=0}^{\infty} S_{aan}(\omega) \approx \frac{V}{2\rho_0 c_0^2} \sum_{n=0}^{N-1} S_{aan}(\omega) \tag{A3.44}$$

where N is the number of acoustic modes used in the computer simulation, and

$$S_{aan}(\omega) = \lim_{T\to\infty} E[\frac{1}{T}\, a_n^*(\omega)\, a_n(\omega)] \tag{A3.45}$$

The applied forces $f_1(\omega)$, ... $f_J(\omega)$ are defined to be independent white noise sources with constant power spectral densities A_1, ...A_J. Using the frequency response functions derived in Section 3.3.3 it is now possible to write down the modal spectrum $S_{aan}(\omega)$ either with or without active control. Without control, for example, the modal spectrum is

$$\begin{aligned} S_{aan}(w) &= \lim_{T\to\infty} E[\frac{2}{T}\, a_{0n}^*(\omega)\, a_{0n}(\omega)] \\ &= \lim_{T\to\infty} E[\frac{2}{T}\,(\sum_{i=1}^{J} H_{Ani}^* f_i^*(\omega))(\sum_{j=1}^{J} H_{Anj}\, f_j(\omega))] \\ &= \sum_{j=1}^{J} A_j H_{Anj}^* H_{Anj} \end{aligned} \tag{A3.46}$$

since

$$\lim_{T\to\infty} E[\frac{1}{T} f_i^* f_j] = \begin{cases} A_j & i=j \\ 0 & i\neq j \end{cases}$$

The potential energy spectrum without control is therefore

$$E_{p0}(\omega) = \frac{V}{2\rho_0 c_0^2}\sum_{n=0}^{N-1}\sum_{j=1}^{J} A_j H_{Anj}^* H_{Anj} \tag{A3.47}$$

We could also express $E_p(\omega)$ as

$$E_p(\omega) = \frac{V}{2\rho_0 c_0^2}\sum_{n=0}^{N-1}\sum_{j=1}^{J} E[\frac{1}{T}\mathbf{a}^H(\omega)\,\mathbf{a}(\omega)] \tag{A3.48}$$

where a(w) is the vector of N acoustic mode amplitudes, which may itself be expressed as

$$\mathbf{a}(\omega) = \mathbf{a}_p(\omega) + \mathbf{B}(\omega)\,\mathbf{y}(\omega) \tag{A3.49}$$

where $\mathbf{a}_p(\omega)$ is the contribution from the primary source, $\mathbf{y}(\omega)$ the spectrum of the secondary source signals and $\mathbf{B}(\omega)$ the matrix of coupling coefficients. For random excitation $E_p(\omega)$ may thus be minimised using a procedure exactly analogous to that considered in Section 2.2.3 to yield the optimum unconstrained controller.

APPENDIX 3.3 Direct calculation of multiple coherence in a simple case

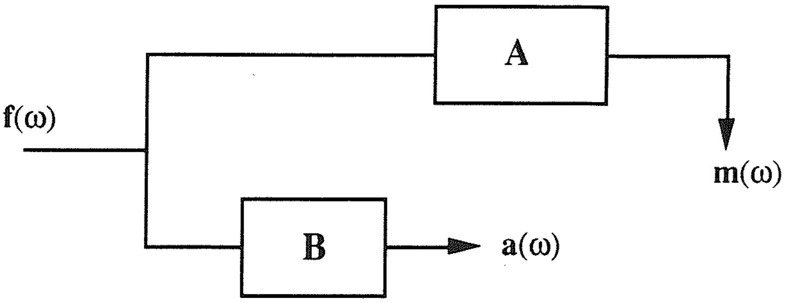

Figure A3.2: Accelerometer (**a**(ω)) and microphone (**m**(ω)) signals as functions of input force

Figure A3.2 shows a schematic diagram of the plate and enclosure calculation in which **f**(ω) is a vector of two applied forces, **a**(ω) is a vector of two accelerometer signals and m(ω) is a microphone signal, representing acoustic pressure at a point in the enclosure. [B] is the matrix of transfer functions relating acceleration to force; A is the vector of transfer functions relating the microphone signal to the input forces.

The relationships are:

$$\mathbf{a}(\omega) = [B]\mathbf{f}(\omega) \qquad (1)$$

$$m(\omega) = \mathbf{A}^T\mathbf{f}(\omega) \qquad (2)$$

The multiple coherence of the microphone signal with respect to the accelerometers is given by:

$$\eta^2_{ma} = \frac{\mathbf{G}_{am}{}^H[G_{aa}]^{-1}\mathbf{G}_{am}}{G_{mm}} \qquad (3)$$

from Section 2.3.2. The auto- and cross-spectral density functions $[G_{aa}]$ and G_{am} are given by:

$$[G_{aa}] = \begin{bmatrix} G_{11} & G_{12} \\ G_{21} & G_{22} \end{bmatrix} \qquad (4)$$

where

$$G_{ij} = \lim_{T\to\infty} E[\tfrac{2}{T} a_i^* a_j] \qquad i=1,2 \;\; j=1,2 \tag{5}$$

a_i is the ith element of **a**. Also:

$$G_{am} = \begin{bmatrix} G_{1m} \\ G_{2m} \end{bmatrix} \tag{6}$$

where

$$G_{jm} = \lim_{T\to\infty} E[\tfrac{2}{T} a_j^* m] \tag{7}$$

and finally

$$G_{mm} = \lim_{T\to\infty} E[\tfrac{2}{T} m^* m] \tag{8}$$

It is possible to evaluate the multiple coherence $\eta^2_{m\mathbf{a}}$ analytically in simple cases. Suppose that the transfer function arrays **A** and [B] consist of sets of real constants (*ie* pure gain terms):

$$\mathbf{A} = \begin{bmatrix} \alpha_1 \\ \alpha_2 \end{bmatrix} \tag{9}$$

$$[B] = \begin{bmatrix} \beta_{11} & \beta_{12} \\ \beta_{21} & \beta_{22} \end{bmatrix} \tag{10}$$

Assume also that the two applied forces making up **f** are independent white noise sources, such that:

$$E\{\tfrac{2}{T} f_i^* f_j\} = \begin{cases} 1 & i=j \\ 0 & i\neq j \end{cases} \tag{11}$$

The auto- and cross-spectral density terms can then be evaluated as:

$$G_{ij} = \beta_{i1}\beta_{j1} + \beta_{i2}\beta_{j2} \tag{12}$$
$$G_{jm} = \beta_{j1}\alpha_1 + \beta_{j2}\alpha_2 \tag{13}$$
$$G_{mm} = |\alpha_1|^2 + |\alpha_2|^2 \tag{14}$$

The 2x2 matrix $[G_{aa}]$ can be inverted in textbook fashion be evaluating its adjoint and dividing by its determinant, provided this determinant is not zero. When the whole expression (3) for η^2_{ma} is multiplied out, the numerator and denominator turn out to be identical so that

$$\eta^2_{ma} \quad = \quad 1 \qquad\qquad \text{provided } |G_{aa}| \neq 0$$

The determinant $|G_{aa}|$ is given from (4) and (12):

$$\begin{aligned} |G_{aa}| &= (\beta_{11}{}^2 + \beta_{12}{}^2)(\beta_{21}{}^2 + \beta_{22}{}^2) - (\beta_{11}\beta_{21} + \beta_{21}\beta_{22})(\beta_{21}\beta_{11} + \beta_{22}\beta_{12}) \\ &= (\beta_{11}\beta_{22} - \beta_{12}\beta_{21})2 \\ &= |B|^2 \qquad\qquad (15) \end{aligned}$$

Thus $|G_{aa}|$ is zero if the transfer function matrix [B] is singular, ie $|B| = 0$. So in this example where there are two forces and two accelerometers, the multiple coherence of the two accelerometers with respect to the microphone is unity unless array [B] is singular (*eg* if both the accelerometers are in the same place). Figure 3.19 illustrates this result in the more general case where there are six forces and six accelerometers.

It is interesting to note that this result holds even though the ordinary coherence between individual accelerometers and the microphone may be low. Defining some numerical values to illustrate the point:

$$[B] = \begin{bmatrix} \beta_{11} & \beta_{12} \\ \beta_{21} & \beta_{22} \end{bmatrix} = \begin{bmatrix} 0.1 & 0.9 \\ 0.2 & 0.8 \end{bmatrix}$$

$$A = \begin{bmatrix} \alpha_1 \\ \alpha_2 \end{bmatrix} = \begin{bmatrix} 0.9 \\ 0.1 \end{bmatrix}$$

The ordinary coherences between the individual accelerometers and the microphone are thus given by:

<u>a1 to m</u>

$$\gamma_{1m}{}^2 = \frac{G_{1m}{}^*G_{1m}}{G_{11}G_{mm}}$$

$$= \frac{(\beta_{11}\alpha_1 + \beta_{12}\alpha_2)^2}{(\beta_{11}{}^2 + \beta_{12}{}^2)(\alpha_1{}^2 + \alpha_2{}^2)}$$

$$= 0.048$$

a2 to m

$$\gamma_{2m}^2 = \frac{G_{2m}{}^*G_{2m}}{G_{22}G_{mm}}$$

$$= \frac{(\beta_{21}\alpha_1 + \beta_{22}\alpha_2)^2}{(\beta_{21}{}^2 + \beta_{22}{}^2)(\alpha_1{}^2 + \alpha_2{}^2)}$$

$$= 0.121$$

So for this perhaps rather artificial example the ordinary coherences between the individual accelerometers and the microphone are 4.8% and 12.1% while the multiple coherence of both with respect to the microphone remains 100%. In practice the situation is affected by other uncorrelated noise sources such as measurement noise on the accelerometers and microphone, but it is worth noting that the multiple coherence can be greater than the sum of the individual ordinary coherences in some situations.